A Single-Event Microkinetic Model for Ethylene Hydroformylation on Rh and Co

Nima Navidi

Promotoren: prof. dr. ir. J. W. Thybaut, prof. dr. ir. G. B. Marin
Proefschrift ingediend tot het behalen van de graad van
Doctor in de ingenieurswetenschappen: chemische technologie

UNIVERSITEIT
GENT

Vakgroep Chemische Proceskunde en Technische Chemie
Voorzitter: prof. dr. ir. G. B. Marin
Faculteit Ingenieurswetenschappen en Architectuur
Academiejaar 2016 - 2017

ISBN 978-90-8578-944-4
NUR 913, 952
Wettelijk depot: D/2016/10.500/76

Examination Committee

Promoters:

Prof. Dr. Ir. Joris Thybaut	Ghent University, Belgium
Prof. Dr. Ir. Guy Marin	Ghent University, Belgium

Other members of the examination committee:

Dr. Peter Bishop	Johnson Matthey, United Kingdom
Prof. Dr. Ir. Claude Mirodatos*	IRCELYON, France
Prof. Dr. Ir. Christian Stevens*	Ghent University, Belgium
Dr. Hilde Poelman	Ghent University, Belgium
Prof. Dr. Ir. Maarten Sabbe*	Ghent University, Belgium (Secretary)
Prof. Dr. Ir. Gert De Cooman	Ghent University, Belgium (Chairman)

*Reading committee

The research leading to these results has received funding from the European community's Sixth Framework Programme (contract nr. 515792-2) and the European Research Council under the European Union's Seventh Framework Programme (FP7/2007-2013) / ERC grant agreement n° 615456." and the Long Term Structural Methusalem Funding by the Flemish Government.

Laboratory for Chemical Technology
Department of Chemical Engineering and Technical Chemistry
Ghent University
Technologiepark 914, B-9052 Ghent, Belgium

UNIVERSITEIT GENT

Acknowledgments

When I started my PhD with lots of enthusiasm, the point where I am standing now seemed to be so distant. Although not that easily achieved, I am finally here, at the end-point of this PhD marathon. I am now writing these lines, not just as a tradition to acknowledge the people involved with this project in different ways, but also to let them know that it could only be done on the grounds of their contribution and helps.

First of all, I am sincerely and deeply grateful of my promoters, Professor Guy Marin and Professor Joris Thybaut, who gave me the opportunity to start my PhD as a member of LCT. Thank you Joris for sharing your experiences and knowledge with me, for all the scientific discussions we have had and for your patient approach towards solving technical problems. I have learnt a lot from you in this aspect.

I would like to thank Prof. Guy Marin further for his valuable scientific guidance from which I have constantly learnt. Your vast knowledge and experience within the field of reactor and reaction engineering has provided great insight into this work.

I am sincerely grateful to all members of my examination committee for their advices, thoughtful comments, corrections and remarks which helped to improve the quality of this thesis.

I also would like to thank Dr. Hilde Poelman, Dr. Ir. Vladimir Galvita and Dr. Ir. Vitaliy Bliznuk for assisting in XRD and TEM analysis.

Besides, I would like to take this opportunity to thank all my colleagues in LCT and especially in CaRE group. Thanks to you all not only for your kind helps and supports, but also for being so nice from the first moment that I met you.

I would also like to mention that I have not forgotten the master students whom I had the pleasure to supervise with their Master's theses. Michaël and Yolanda, I appreciate your hard work and your contribution to this research.

During this work I was fortunate enough to work with very knowledgeable and friendly technical and administration colleagues in LCT. Bedankt allemaal!

Living in Belgium is more joyful with the presence of my good Iranian friends. I want to thank them all. It is excellent to have such wonderful friends when you are far from your country.

Gisela, Carlos and Unmesh, I cannot forget all your help and friendship, especially in my first days in Ghent. I will always remember your supports and the good times that we have had together.

Above all, I would like to mention that I would not be here without the support of my beloved family. My precious parents, my lovely sisters, Sara and Nasim, my parents-in-law, my sisters-in-law, Zari and Mitra and my brother-in-law, Amir, I cannot say how fortunate I am to have you all.

And finally, I have my most special and hurtful thanks to Maryam, as my wife, my friend, my partner and my love. My dearest Maryam, thanks for having a helping hand for me, whenever I was in need of one and thanks for giving me the hope and courage, whenever I lacked some. I dedicate this thesis to you.

Table of Contents

List of Figures

List of Tables

Nomenclature

Roman Symbols

$\Delta_r H$	*reaction enthalpy (kJ mol^{-1})*
ΔS	*entropy change (J mol^{-1} K^{-1})*
A	*pre-exponential factor (s^{-1} or (MPa s)$^{-1}$)*
A	*peak surface area*
$a_{t,\,j}$	*number of t atoms in component j*
a_v	*external surface area per unit catalyst volume (m^2 m^{-3})*
b	*volume of inert material as fraction of total solids (m^3 m^{-3})*
$\boldsymbol{b}$	*vector of parameter estimates*
B_i	*Biot number (-)*
B_o	*Bodenstein number (-)*
C	*concentration (mol m^{-3})*
Ca	*Carberry number (-)*
C_p	*specific heat capacity (J kg^{-1} K^{-1})*
CF	*calibration factor*
C_f	*conversion factor (-)*
d_n	*normal density (kg m^{-3})*
$D_{A,eff}$	*effective diffusivity of component A in the pellet (m^2 s^{-1})*
$D_{A,\,ax}$	*axial dispersion coefficient (m^2 s^{-1})*
d_{at}	*atomic diameter (m)*
d_p	*catalyst particle diameter (m)*
d_{pe}	*equivalent pellet diameter (m)*
$d_{rel(VS)}$	*mean relative size of metallic crystallite (m)*
d_t	*catalyst bed diameter (m)*
d_{VS}	*the mean size of metal crystallite (m)*
E_a	*activation energy (kJ mol^{-1})*
f_m	*friction factor (-)*
F_v	*volumetric flow rate (Nl s^{-1})*
F	*molar flow rate (mol s^{-1})*
F_p	*molar outlet flow rate of P (mol s^{-1})*
h	*Planck constant (6.626068×10^{-34} m^2 kg s^{-1})*
H	*enthalpy (kJ mol^{-1})*

J	*Jacobian matrix*
k	*kinetic coefficient of an elementary step (s^{-1} or $(MPa\ s)^{-1}$)*
k_B	*Boltzmann constant ($1.3806503\times10^{-23}\ m^2\ kg/s\ K$)*
k_f	*mass transfer coefficient ($m\ s^{-1}$)*
L	*bed length or height (m)*
M	*metal atom*
ME	*empty metal site*
M_j	*molecular mass of component j ($g\ mol^{-1}$)*
M_M	*standard atomic weight ($kg\ mol^{-1}$)*
N_A	*Avogadro constant ($6.02214086\times10^{23}\ mol^{-1}$)*
$\dot{m}$	*mass flow rate ($g\ s^{-1}$)*
n	*reaction order (-)*
n_e	*number of single events*
n_{ob}	*number of observations*
n_{comp}	*number of components*
n_{resp}	*number of responses*
n_{par}	*number of parameters*
P	*pressure (MPa)*
Pe_p	*Péclet number (-)*
Q	*chemisorption enthalpy ($kJ\ mol^{-1}$)*
R	*universal gas constant ($8.3144\ J\ (mol\ K)^{-1}$)*
R_i	*net production rate ($mol\ (kg\ s)^{-1}$)*
$R_{v,A}$	*observed volumetric reaction rate ($mol\ m^{-3}\ s^{-1}$)*
Re	*Reynolds number (-)*
r_i	*reaction rate (of reaction i) with reaction order n ($mol\ (kg\ s)^{-1}$)*
S_P	*selectivity towards product P ($mol\ mol^{-1}$)*
T	*absolute temperature (K)*
t	*time (s)*
t_c	*Student t-test calculated value*
TOF	*turnover frequency (s^{-1})*
u	*fluid velocity ($m\ s^{-1}$)*
$V(b)$	*variance-covariance matrix of parameter estimates b*
W	*catalyst mass (kg_{cat})*

Y_P	*molar yield of product P (mol mol^{-1})*
X_A	*conversion of component A (mol mol^{-1})*
z	*number of nearest neighbor atoms*

Greek symbols

α_p	*heat transfer coefficient (W m^{-2} K^{-1})*
β	*parameter vector*
ε_b	*bed porosity (-)*
Δ	*difference*
θ	*degree of coverage (mol mol^{-1})*
λ_{er}	*effective radial bed thermal conductivity (W m^{-1} K^{-1})*
λ_p	*catalyst pellet heat conductivity (W m^{-1} K^{-1})*
μ	*viscosity (kg m^{-1} s^{-1})*
ρ	*density (kg m^{-3})*
ρ_{jk}	*binary correlation coefficient between parameter estimates j and k*
σ^{jk}	*Inverse of the covariance between the experimental errors associated with measurements of the jth and kth response*
$\sigma_{gl,r}$	*global symmetry number of reactant(s)*
$\sigma_{gl,\neq}$	*global symmetry number of transition state*
Φ	*Weisz modulus (-)*
$^{\varphi}_{m}$	*mass balance*
$^{\varphi}_{e}$	*element balance*

Superscripts

^	*model calculated value*
~	*single-event*
$\neq$	*activated complex*
0	*initial or standard state*
for	*forward reaction*
M	*metal site*
rev	*reverse reaction*

Subscripts

$\rightarrow$	*forward reaction*
$\leftarrow$	*reverse reaction*

$\neq$	*activated complex*
Cat.	*catalyst*
chem	*chemisorption*
e_t	*element t*
gl	*global*
in	*inlet*
tot	*total*

Abbreviations

BET	Brunauer–Emmett–Teller
BoM	Bill of Materials
EDX	Energy Dispersive X-ray
FE	Fraction of Exposed metal atoms (%)
FID	Flame Ionization Detector
FTS	Fischer-Tropsch Synthesis
GC	Gas Chromatograph
HTK-MI	High-Throughput Kinetic Mechanistic Investigation
ID	Internal Diameter
LCT	Laboratory for Chemical Technology
PFR	Plug Flow Reactor
P&ID	Piping and Instrument Diagram
PSSA	Pseudo Steady State Approximation
PVC	Polyvinyl Chloride
ReNGeP	Reaction Network Generation Program
SEMK	Single-Event Micro Kinetic
SSITKA	Steady State Isotopic Transient Kinetic Analysis
SSQ	Sum of squares of residuals between observed and calculated response values
Stat. TD	Statistical Thermodynamics
STEM	Scanning Transmission Electron Microscopy
TCD	Thermal Conductivity Detector
TEM	Transmission Electron Microscopy
TPD	Temperature Programmed Desorption

TPR	Temperature Programmed Reduction
UBI-QEP	Unity Bond Index/Quadratic Exponential Potential
XRD	X-ray Diffraction

Glossary of terms

Activation energy (E_a)	For an elementary-step, it is the difference in internal energy between transition state and reactants. A measure for the temperature dependence of the rate coefficient $k=A \exp(E_a/RT)$ with R is the universal gas constant, T the temperature, A the pre-exponential factor and E_a the activation energy.
Active site	Also called active centre. Those sites for adsorption which are responsible for adsorption and subsequent reaction.
Acyl	It refers to a moiety consisting of a carbonyl group bonded to a carbon group.
Adatom	It refers to an adsorbed atom. Single atoms lying on surfaces and surface roughness.
Adsorption	The preferential concentration of a species at the interface between two phases. Adherence of the atoms, ions or molecules of a gas or liquid to the surface of another substance.
Alloy	A material made of two or more metals. A mixture of metals or a mixture of a metal and another element.
Arrhenius relation	Expresses the dependence of a rate coefficient, k, corresponding with a chemical reaction on the temperature T and activation energy, E_a: $k=A \exp(E_a/RT)$ with R is the universal gas constant, T the temperature, A the pre-exponential factor and E_a the activation energy.
Back mixing	Is defined as the axial diffusion-like movement of reactants and/or product molecules in the reactor superimposed on the convective flow.
BET	Analysis technique used for the measurement of the specific surface area of a material.
Catalyst	A source of active sites, which augments the rate of a chemical reaction and is regenerated at the end of a closed reaction sequence.
Catalyst support	Refers to a material, usually a solid with a high surface area, on which a catalytically active material is deposited.
Chemisorption	Also known as chemical adsorption. Adsorption in which the forces

	involved are valence forces of the same kind as those operating in the formation of chemical compounds. Chemisorption strongly depends on the surface and the sorptive, and only one layer of chemisorbed molecules is formed. Its energy of adsorption is the same order of magnitude as in chemical reactions, and the adsorption may be activated.
Chiral	A chiral molecule is a type of molecule that lacks an internal plane of symmetry and thus has a non-super imposable mirror image. Achiral (not chiral) objects are objects that are identical to their mirror image. Human hands are perhaps the most universally recognized example of chirality.
Conversion	Measure for the amount of a reactant that has been transformed into products as a result of a chemical reaction.
Cluster	In chemistry refers to a small group of atoms or molecules, such as metal cluster.
Deactivation	The decrease in conversion in a catalytic reaction with time of run under constant reaction conditions.
Degree of freedom	It defines number of adjustable physical variables/parameters that give a particular system its characteristics. Each degree of freedom lends a particular trait to a system, the number of independent co-ordinates required to completely specify the state of a system.
Desorption	The release of one substance from another, either from the surface or through the surface.
Diffusion	Movement of a fluid from an area of higher concentration to an area of lower concentration.
Dissociative chemisorption	Adsorption of a molecule with dissociation into two or more fragments, both or all of which are bound to the surface of adsorbent.
DNSQE	Subroutine used to solve the algebraic equations which are a result of the reactor mass balance. This subroutine is used to find a zero of a system of N nonlinear functions in N variables by a modification of the Powell hybrid method.
Elementary step	The irreducible act of reaction in which reactants are transformed

	into products directly, i.e. without passing through an intermediate that is susceptible to isolation.
Endothermic reactions	A chemical reaction accompanied by the absorption of heat. It is the opposite of an exothermic reaction.
Entropy change	The difference in entropy in any process, chemical or physical, is the entropy of the final situation minus the entropy of the initial situation. For a chemical reaction this is the difference between the products entropy and the reactants entropy, called the entropy change. The entropy change is symbolised by ΔS, delta S. When the entropy increases, ΔS is positive.
Exothermic reaction	A chemical reaction that releases heat. It is the opposite of an endothermic reaction.
External diffusion	Also called interphase diffusion. Diffusion from the fluid phase to the external surface of catalyst.
Fixed bed reactor	It is a vessel that contains catalyst, typically in pellet form, packed in a static bed. The core part of any fixed-bed reactor is the solid catalyst where the reaction takes place.
Gas Chromatography (GC)	The process in which the components of a mixture are separated from one another by injecting the sample into a carrier gas which is passing through a column or over a bed of packing with different affinities for adsorption of the components to be separated.
Heterogeneous catalysis	Refers to the form of catalysis where the phase of the catalyst differs from that of the reactants. This involves the use of a catalyst in a different phase from the reactants. Typical examples involve a solid catalyst with the reactants as either liquids or gases.
Homogenous catalysis	Catalytic reactions where the catalyst is in the same phase as the reactants.
Hydrogenation	Reduction reaction which results in an addition of hydrogen, The addition of hydrogen to another compound.
Intermediate	Is formed from a reactant and transforms into a product during a chemical reaction. The intermediate is often a short-lived and unstable species that cannot directly be detected during a reaction.
Internal diffusion	Also called intra-particle diffusion. Motion of atoms within the

	particles of a solid phase that has a sufficiently large porosity to allow this motion.
Langmuir-Hinshelwood-Hougen-Watson (LHHW) mechanism	It is assumed that both reactants must be adsorbed on the catalyst in order to react in Langmuir-Hinshelwood-Hougen-Watson (LHHW) mechanism. Normally adsorption-desorption steps are essentially at equilibrium and a surface step is rate-determining. Adsorption steps can also be rate-determining.
Levenberg-Marquardt algorithm	It is a method of finding the minimum of a function that is a sum of squares of nonlinear functions, It is used to solve non-linear least squares problems. These minimization problems arise especially in least squares curve fitting.
Mechanism	A sequence of elementary steps in which reactants are converted into products, through the formation of intermediates.
Metal carbide	Refers to a carbon atom that is compounded with a metal.
Metal dispersion	The ratio of the number of surface metal atoms to the total number of metal atoms, also denoted as fraction exposed.
Microscopic reversibility	The mechanism of a reversible reaction is exactly the same (but reversed) for both the forward and backward version of the reaction. The transition states for each mechanism step are identical regardless of reaction direction. The forward and reverse of a particular pathway are related as mirror images.
Most abundant surface intermediate (MASI)	Reaction intermediate on a catalyst surface whose concentration is much greater than that all of the other intermediates.
Netlib	It is a repository of software for scientific computing maintained by AT&T, Bell Laboratories, the University of Tennessee and Oak Ridge National Laboratory. Netlib comprises a large number of separate programs and libraries.
Network	When several single reactions take place in a system, these parallel and consecutive reactions constitute a network.
Objective function	It is a function used during optimization problems which have to be minimized or maximized by choosing the best set of variables which determines the values of this function.

ODRPACK	It is a software package for weighted orthogonal distance regression, i.e., for finding the parameters that minimize the sum of the squared weighted orthogonal distances from a set of observations to the curve or surface determined by the parameters.
Parameter estimation	Process of estimating the parameters of a relation between independent and dependent variables as to describe a chemical reaction as good as possible.
Parity diagram	Diagram representing the model calculated values as a function of the experimentally observed values. The better the correspondence with the first bissectrice, the better the model.
Physisorption	Also called physical adsorption, is the physical bonding of gas molecules to the surface of a solid or liquid that the gas comes into contact with at low temperatures. This occurs due to Van der Waals forces.
Plug Flow Reactor (PFR)	A tubular reactor where the feed is continuously introduced at one end and the products continuously removed from the other end. The concentration/temperature in the reactor is not uniform.
Porosity	A measure of the void spaces in a material, expressed as the ratio of the volume of voids to the total volume of the material.
Pre-exponential factor	The temperature-independent factor of a rate coefficient $k=A \exp(E_a/RT)$ also called the frequency factor.
Pseudo-steady state	Its mathematical expression is that the time rate of change of the concentration of all active centers in a reaction sequence is equal to zero.
Reaction family	Classification of elementary reaction steps on the basis of same features.
Reaction rate	The number of moles of a component created by a chemical reaction per unit of time, volume or catalyst weight.
Rate-Determining Step (RDS)	If, in a reaction sequence, consisting of *n* steps, *(n-1)* steps are reversible and if the rate of each of these *(n-1)* steps is potentially larger than the rate of the *n*th step, the latter is said to be rate-determining. The rate-determining step need not be reversible.
Rosenbrock algorithm	It is an automatic method for finding the greatest or least value of a

	function.
Selectivity	The total amount of reactant to form a product per total amount of reactant consumed.
Site time	The equivalent of the space time which has been corrected for the metal loading on the catalyst and the fraction of exposed metal atoms.
Space time	Ratio of catalyst mass to the feed flow rate. Typically has the units of kg_{cat} s mol^{-1}
Statistical thermodynamics	The science that deals with average properties of the molecules, atoms, or elementary particles in random motion in a system of many such particles and relates these properties to the thermodynamic and other macroscopic properties of the system.
Steady state	A system in steady state has certain properties that are time-independent.
Syngas	Also called synthesis gas, is a mixture of hydrogen and carbon monoxide**.**
Turnover Frequency (TOF)	It quantifies the specific activity of a catalytic site for a special reaction under defined reaction conditions by the number of molecular reactions or catalytic cycles occurring at the site per unit time.
Transition state	Also called activated complex. The configuration of highest potential energy along the path of lowest energy between reactants and products.
Yield	Refers to the amount of a specific product formed per mole of reactant fed.

Summary

The ever increasing search for more sustainable and environmentally friendly chemical processes as well as historical oil price fluctuations have led to the exploration of alternative feeds such as natural gas, and correspondingly new processes, for the production of the same or similar hydrocarbon products. Hydroformylation, or oxo synthesis, is an important process for the production of aldehydes from alkenes. Simultaneously, double bound hydrogenation may occur as an undesired parallel and/or consecutive reaction, converting the reactant alkene into the corresponding alkane as well as the product aldehyde into alcohol. Although all transition metals capable of forming carbonyls are potential hydroformylation catalysts, rhodium and cobalt complexes are used most frequently in industrial, homogeneous hydroformylation [1]. The reaction products constitute a basis for a wide variety of chemicals, mainly for plasticizers and detergents [2, 3]. The homogeneous nature of typical, present-day, industrial process configurations leads to some inherent problems related to catalyst product separation and equipment corrosion [4]. The successful implementation of an active and stable heterogeneous hydroformylation catalyst would allow avoiding these drawbacks.

In this work, intrinsic hydroformylation kinetics data have been acquired in a high-throughput kinetics mechanistic investigation (HTK-MI) set up at temperatures varying from 448 to 498 K, with the total pressure ranging from 1 to 3MPa. A gaseous feed containing CO, C_2H_4 and H_2 was used with space times varying from 2.7 kg_{cat} s/$mol_{C2H4,in}$ to 149 kg_{cat} s/$mol_{C2H4,in}$. Three catalysts, i.e., 5%Rh on Al_2O_3, 1%Co on Al_2O_3 and 0.5%Co-0.5%Rh on Al_2O_3 have been investigated. At these conditions the observations are not affected by mass or heat transfer limitations [5]. Catalyst characterisation has been performed to independently determine essential information about the catalysts, such as their BET surface area and the metal particle size.

Ethane, propanal and propanol were the main products observed. The Rh catalyst exhibited the highest hydroformylation and hydrogenation rates over the entire range of operating conditions. It was observed that a small particle size specifically enhances the CO site time conversion and, hence, the oxo-selectivity. This effect, also denoted as structure sensitivity, has already been reported in hydroformylation [6, 7]. Moreover it was found on all investigated catalysts that a temperature increase has a more pronounced effect on the hydrogenation than on the hydroformylation rate. Hence, a temperature increase has a negative effect on the desired oxygenates selectivity. More quantitatively, the apparent

activation energy for ethane formation exceeds that for propanal formation on the tested catalysts by 15 to 20 kJ mol^{-1}. This can be related to the expected evolution in the hydrogen and CO surface concentrations. The chemisorption heat of CO is typically about the double of that of hydrogen [8] and as a result, the CO concentration on the catalyst surface, will decrease more pronouncedly with increasing temperature than that of hydrogen. On the Rh catalyst, higher ethylene feed concentrations have a higher impact on CO conversion and production of propanal and propanol compared with an increase in the inlet concentration of the other reactants.

A Single-Event MicroKinetic (SEMK) model, originally developed for Fischer-Tropsch Synthesis (FTS) [8], has been extended towards ethylene hydroformylation. The SEMK modelling methodology, first introduced by Froment et al. [9], has recently been reviewed by Thybaut and Marin [10]. Its key feature is that it accounts for the rate of every elementary step in a complex reaction network. More in particular, symmetry effects are explicitly accounted for to reduce the number of adjustable parameters in the model, essentially to the double of the number of reaction families which is considered. The forward and reverse elementary steps in the proposed reaction network were generated using the Reaction Network Generation Program (ReNGeP) in which the molecules are represented numerically using standardized labels and Boolean matrices as it was originally implemented for FT synthesis [11]. The generated reaction network is in accordance with the Wilkinson reaction mechanism for hydroformylation, which is the most popular one today [2, 12].

Per reaction family, a pre-exponential factor and activation energy are required. While the former was obtained from statistical thermodynamics, the latter has been estimated via regression to experimental data. The relevant thermodynamics have been calculated according to the UBI-QEP method [8, 13]. The correspondingly required atomic chemisorption enthalpies, i.e., Q_C, Q_H and Q_O, also denoted as the catalyst descriptors, have also been determined as adjustable parameters. When assessing kinetic data acquired on alternative catalysts only the latter parameters need to be redetermined to simulate the observed behaviour. The catalyst descriptors_can also be manipulated to identify an optimal catalyst. Using the SEMK model, detailed product profiles can be obtained which makes it a potential tool to propose better performing catalysts. Detailed reactant conversions as well as product molar yields over a wide range of operating conditions can be predicted by implementing a SEMK model.

This consists of writing the proper rate equations according to the mechanism implemented in the reaction network generation program. Among other things, this means that the rate coefficient is written as the product of a single event coefficient and the number of single events, i.e., the number of indistinguishable ways an elementary step can proceed. A 1D pseudo-homogeneous plug-flow reactor model is applied to calculate the conversions and molar yields. In total 95 forward and reverse elementary steps were accounted for in the corresponding reaction network.

The validation of the SEMK model for the ethylene hydroformylation is performed by regression against experimental data as acquired on 5%Rh/Al_2O_3 and 1%Co/Al_2O_3. The SEMK model well describes the product distribution over a wide range of operating conditions on both investigated catalysts. It also quantitatively describes the experimentally observed temperature and pressure variations. The estimated activation energies and atomic chemisorption enthalpies for both catalysts are statistically significant and physically sound i.e., in line with literature reported values. The carbon atomic chemisorption enthalpy on Rh (591 kJ/mol) exceeds the corresponding value on Co (575 kJ/mol), while the oxygen atomic chemisorption enthalpy is higher on Co compared to Rh, which is in agreement with the trends reported in literature [14]. Apart from that, the metal-hydrogen binding energies are rather uniform with an average value of 251 kJ/mol [15] that also agrees with the values obtained in the present work. CO insertion into a metal alkyl species was identified as the kinetically relevant surface elementary step in hydroformylation product formation. Metal carbide and metal oxide surface concentrations were found to be negligible.

Catalyst descriptor values, i.e., the atomic chemisorption enthalpies in the developed SEMK model in this work, can be determined to identify the ideal catalyst for the ethylene hydroformylation. Within the allowed operating conditions, a maximum propanal to ethane yield ratio was observed at Q_c=597, Q_O=494 and Q_H=250 kJ/mol for carbon, oxygen and hydrogen atomic chemisorption, in which the average propanal yield and selectivity increased by 80% and 35% respectively compared with the reported experimental results for Rh in this work. Hence, a highly dispersed catalyst with the above-mentioned characteristics, can be expected to exhibit the best behavior in heterogeneous ethylene hydroformylation.

References:

[1] Cornils B., H.W.A., Applied Homogeneous Catalysis with Organometallic Compounds. VCH, Weinheim, 1996.

[2] B. Breit, W. Seiche, Synth. (2001) 1–36.

[3] P. W. Van Leeuwen, Rhodium catalysed hydroformylation, Springer, New York, 2002.

[4] T.A. Zeelie, A. Root, A.O.I. Krause, Appl. Catal. A. 285 (2005) 96-109.

[5] R.J. Berger, E. H. Stitt, G. B. Marin, F. Kapteijn, J. Moulijn, CATTECH. Vol. 5 (2001) 30-60.

[6] T. A. Zeelie, Rhodium and cobalt catalysts in the heterogeneous hydroformylation of ethane, propene and 1-hexene. PhD thesis, Helsinki, 2007.

[7] T. Hanaoka, H. Arakawa, T. Matsuzaki, Y. Sugi, K. Kanno, Y. Abe, Catal. Today. 58 (2000) 271-280.

[8] G. Lozano-Blanco, J. W. Thybaut, K. Surla, P. Galtier, G. B. Marin, Ind. Eng. Chem. Res. 47(2008) 5879-5891.

[9] G.F. Froment, Catal. Today. 52 (1999) 153-163.

[10] J.W. Thybaut, G.B. Marin, J. Catal. 308 (2013) 352-362.

[11] G. Lozano-Blanco, J. W. Thybaut, K. Surla, P. Galtier, G. B. Marin, Oil Gas Sci. Technol. 6I (2006) 489-496.

[12] M. A. Brundage, S.S.C. Chaung, J. Catal. 164 (1996) 94-108.

[13] E. Schustorovich, H. Sellers, Surf. Sci. Rep. 31 (1998) 5-119.

[14] R. A. Van Santen, M. Neurock., Molecular Heterogeneous catalysis: A conceptual and computational approach, Wiley-VCH, 2006.

[15] M. L. Burke, R. J. Madix, J. Am. Chem. Soc. 114 (8) (1992) 2780-2783.

Samenvatting

De steeds groeiende zoektocht naar meer duurzame en milieuvriendelijke chemische processen alsook de historische schommelingen in de olieprijs, hebben geleid tot de exploratie van alternatieve voedingen, zoals aardgas, en overeenkomstige nieuwe processen, voor de productie van dezelfde of soortgelijke koolwaterstofproducten. Hydroformylering of oxosynthese is een belangrijk proces voor het verkrijgen van aldehyden uit alkenen. Tegelijkertijd, kan de hydrogenering van een dubbele binding plaatsvinden als een ongewenste parallelle en/of opeenvolgende reactie, waarbij het reagerende alkeen wordt omgezet in een overeenkomstig alkaan alsook het aldehydeproduct wordt omgezet in een alcohol. Hoewel alle overgangsmetalen die in staat zijn tot het vormen van carbonylverbindingen potentiële hydroformyleringskatalysatoren zijn, worden rhodium en kobalt complexen het meest frequent gebruikt in industriële, homogene hydroformylering [1]. De reactieproducten vormen een basis voor een groot aantal chemische producten, namelijk voor weekmakers en detergenten [2, 3]. De homogene aard van de typische, hedendaagse, industriële procesconfiguraties leidt tot een aantal inherente problemen met betrekking tot katalysator-product scheiding en corrosie van de apparatuur [4]. De succesvolle implementatie van een actieve en stabiele, heterogene hydroformyleringskatalysator laat toe deze nadelen vermijden.

In het kader van dit doctoraat werd intrinsieke hydroformyleringskinetiek verkregen in een hoge doorvoer kinetische opstelling (HTK-MI) bij temperaturen variërend tussen 448 en 498 K, met de totale druk variërend van 1 tot 3 MPa. Een gasvormige voeding bestaande uit CO, C_2H_4 en H_2 werd gebruikt met ruimtetijden variërend tussen 2.7 kg_{cat} $s/mol_{C2H4,in}$ en 149 kg_{cat} $s/mol_{C2H4,in}$. Drie katalysatoren, nl., 5%Rh op Al_2O_3, 1%Co op Al_2O_3 en 0.5%Co-0.5%Rh op Al_2O_3 werden onderzocht. Bij deze omstandigheden worden de waarnemingen niet beïnvloed door massa- of warmteoverdrachtbeperkingen [5]. Katalysatorkarakterisering is uitgevoerd om essentiële informatie van de katalysatoren te bepalen, zoals de BET oppervlakte en de metaaldeeltjesgrootte.

Ethaan, propanal en propanol werden als belangrijkste producten waargenomen. De Rh katalysator vertoonde de hoogste hydroformylering- en hydrogeneringssnelheid in het gehele bereik van reactiecondities. Er werd waargenomen dat, in het bijzonder, een kleine deeltjesgrootte de hydroformyleringssnelheid verhoogt, eerder dan de hydrogeneringssnelheid, en bijgevolg dus tevens de oxo-selectiviteit verhoogt. Dit effect, ook

wel structuur-gevoeligheid genoemd, werd reeds gerapporteerd voor hydroformylering [6, 7]. Bovendien, werd op alle onderzochte katalysatoren vastgesteld dat een temperatuursverhoging een meer uitgesproken effect heeft op de hydrogeneringssnelheid dan op de hydroformyleringssnelheid. Bijgevolg heeft een temperatuurstijging een negatief effect op de gewenste selectiviteit van de zuurstofbevattende componenten. Meer kwantitatief is de schijnbare activeringsenergie op de geteste katalysatoren 15 tot 20 kJ mol^{-1} hoger voor ethaanvorming dan voor propanalvorming. Dit kan worden gerelateerd aan de verwachte evolutie van de waterstof en CO oppervlakconcentratie. De chemisorptiewarmte van CO is typisch het dubbele van die van waterstof [8]. Als gevolg hiervan daalt de CO concentratie op het katalysatoroppervlak meer uitgesproken bij een toenemende temperatuur dan die van waterstof. Op de Rh katalysator, hebben hogere ethyleenvoedingsconcentraties een grotere impact op de CO conversie en de vorming van propanal en propanol, in vergelijking met de inlaatconcentraties van de andere reactanten.

Een Single-Event MicroKinetisch (SEMK) model, oorspronkelijk ontwikkeld voor Fischer-Tropsch Synthese (FTS) [8], werd uitgebreid met ethyleen hydroformylering. De SEMK modelleringsmethode, eerst geïntroduceerd door Froment et al. [9], werd onlangs gereviseerd door Thybaut en Marin [10], rekening houdend met de snelheid van elke elementaire reactiestap in een complex reactienetwerk. In het bijzonder, zijn symmetrie-effecten expliciet opgenomen om het aantal instelbare parameters in het model te beperken tot het dubbele van het aantal beschouwde reactiefamilies. De voorwaartse en terugwaartse elementaire stappen in het voorgestelde reactienetwerk werden gegenereerd met het Reactie Netwerk GenereringsProgramma (ReNGeP), waarin de moleculen numeriek worden voorgesteld gebruikmakend van gestandaardiseerde labels en Booleaanse matrices zoals het oorspronkelijk werd geïmplementeerd voor FTS [11]. Het gegenereerde reactienetwerk stemt overeen met het Wilkinson reactiemechanisme voor de hydroformylering, welke vandaag het meest populaire is [2, 12].

Per reactiefamilie, is er een pre-exponentiële factor en een activeringsenergie vereist. Terwijl de eerstgenoemde wordt verkregen via statische thermodynamica, wordt de laatstgenoemende bepaald door regressie van experimentele gegevens. De relevante thermodynamica werd berekend volgens de UBI-QEP methode [8, 13]. De overeenkomstige gewenste atomaire chemisorptie-enthalpieën, nl., Q_C, Q_H en Q_O, ook wel katalysatordescriptoren genoemd, werden eveneens bepaald als aanpasbare parameters. Bij de beoordeling van de kinetische data verkregen op alternatieve katalysatoren, moeten alleen de laatste parameters opnieuw

worden bepaald om het geobserveerde gedrag te simuleren. De katalysatordescriptoren kunnen ook worden gebruikt om een optimale katalysator te identificeren. Met behulp van het SEMK model kunnen gedetailleerde productprofielen worden verkregen, wat dit een potentieel hulpmiddel maakt voor het bepalen van beter presterende katalysatoren. Gedetailleerde reactantconversie alsook de molaire productopbrengsten kunnen worden voorspeld over een wijd bereik van reactiecondities door het implementeren van een SEMK model.

Dit bestaat uit het schrijven van de juiste snelheidsvergelijkingen voor het geïmplementeerde mechanisme in het reactienetwerkgenereringsprogramma. Onder andere, betekent dit dat de coëfficiënt wordt geschreven als het product van een single-event coëfficiënt en het aantal enkelvoudige gebeurtenissen, nl. het aantal onderscheiden manieren waarop een elementaire stap kan doorgaan. Een 1D pseudo-homogeen propstroomreactormodel wordt toegepast voor de berekening van de conversie en de molaire productopbrengsten. In totaal werden 95 voorwaartse en terugwaartse reacties in rekening gebracht in het overeenkomstig reactienetwerk.

De validatie van het SEMK model voor ethyleen hydroformylering wordt uitgevoerd door regressie naar experimentele gegevens verkregen op de 5%Rh/Al_2O_3 en 1%Co/Al_2O_3 katalysator. Het SEMK model is goed in staat om de productdistributie over een wijd bereik van reactiecondities te beschrijven op de beide bestudeerde katalysatoren. Het beschrijft ook kwantitatief de experimenteel waargenomen temperatuur- en drukvariaties. De geschatte activeringsenergieën en atomaire chemisorptie-enthalpiën voor de beide katalysatoren zijn statistisch significant en fysisch relevant, nl., in overeenstemming met waarden gerapporteerd in de literatuur. De atomaire chemisorptie-enthalpie voor koolstof op Rh (590 kJ/mol) is groter dan deze op Co (575 kJ/mol), terwijl de atomaire chemisorptie-enthalpie voor zuurstof hoger is op Co dan op Rh. Beide trends komen overeen met waarnemingen uit de literatuur [14]. Daarnaast, zijn de metaal-waterstof bindingsenergieën eerder uniform met een gemiddelde waarde van 251 kJ/mol [15] wat ook overeenkomt met de waarde verkregen in dit werk. CO insertie in een metaal-alkyl species is geïdentificeerd als een kinetisch relevante, elementaire reactiestap op het oppervlak bij de vorming van hydroformyleringsproducten. De oppervlakconcentraties van de metaalcarbiden en de metaaloxiden zijn verwaarloosbaar.

Waarden voor katalysatordescriptoren, nl., de atomaire chemisorptie-enthalpiën in het ontwikkelde SEMK model, kunnen worden bepaald om een ideale katalysator te identificeren voor ethyleen hydroformylering. Binnen de onderzochte reactiecondities werd een maximum propanal tot ethyleen opbrengst verhouding verkregen bij Q_c=597, Q_O=494 en Q_H=250

kJ/mol voor respectievelijk koolstof, zuurstof en waterstof atomaire chemisorptie, waarbij een gemiddelde propanal opbrengst en selectiviteit stijgen met 80% en 35%, ten opzichte van de gerapporteerde experimentele resultaten voor Rh. Vandaar dat van een sterk gedispergeerde katalysator met de hierboven genoemde kenmerken kan worden verwacht dat deze het beste gedrag zal vertonen in heterogene ethyleen hydroformylering.

References:

[1] Cornils B., H.W.A., Applied Homogeneous Catalysis with Organometallic Compounds. VCH, Weinheim, 1996.

[2] B. Breit, W. Seiche, Synth. (2001) 1–36.

[3] P. W. Van Leeuwen, Rhodium catalysed hydroformylation, Springer, New York, 2002.

[4] T.A. Zeelie, A. Root, A.O.I. Krause, Appl. Catal. A. 285 (2005) 96-109.

[5] R.J. Berger, E. H. Stitt, G. B. Marin, F. Kapteijn, J. Moulijn, CATTECH. Vol. 5 (2001) 30-60.

[6] T. A. Zeelie, Rhodium and cobalt catalysts in the heterogeneous hydroformylation of ethane, propene and 1-hexene. PhD thesis, Helsinki, 2007.

[7] T. Hanaoka, H. Arakawa, T. Matsuzaki, Y. Sugi, K. Kanno, Y. Abe, Catal. Today. 58 (2000) 271-280.

[8] G. Lozano-Blanco, J. W. Thybaut, K. Surla, P. Galtier, G. B. Marin, Ind. Eng. Chem. Res. 47(2008) 5879-5891.

[9] G.F. Froment, Catal. Today. 52 (1999) 153-163.

[10] J.W. Thybaut, G.B. Marin, J. Catal. 308 (2013) 352-362.

[11] G. Lozano-Blanco, J. W. Thybaut, K. Surla, P. Galtier, G. B. Marin, Oil Gas Sci. Technol. 6I (2006) 489-496.

[12] M. A. Brundage, S.S.C. Chaung, J. Catal. 164 (1996) 94-108.

[13] E. Schustorovich, H. Sellers, Surf. Sci. Rep. 31 (1998) 5-119.

[14] R. A. Van Santen, M. Neurock., Molecular Heterogeneous catalysis: A conceptual and computational approach, Wiley-VCH, 2006.

[15] M. L. Burke, R. J. Madix, J. Am. Chem. Soc. 114 (8) (1992) 2780-2783.

Chapter 1:

Hydroformylation

History, products, industrial processes and reaction mechanism

Abstract: *Hydroformylation, or oxo synthesis, is an important process for the production of aldehydes from alkenes. Alkene and aldehyde hydrogenation are undesired parallel and consecutive reactions. Hydroformylation products have applications in a variety of chemicals, mainly for plasticizers and detergents. Whereas present-day industrial process configurations typically operate in a homogenous mode, the development of a heterogeneous hydroformylation catalyst is aimed at to avoid the well-known drawbacks of homogenous catalysis such as catalyst recovery and corrosiveness. Rhodium and cobalt are reported as the most active catalysts for this reaction. It is generally accepted that the Wilkinson mechanism, resembling a typical Fischer-Tropsch synthesis mechanism but not considering carbon-oxygen bond dissociation, is the most likely one for hydroformylation.*

1.1 Introduction

The search for more sustainable and environmentally friendly processes as well as historical oil price fluctuations have led to the exploration of alternative feeds such as natural gas, and correspondingly new processes, for the production of hydrocarbon chemicals. Hydroformylation, or oxo synthesis, is an important process for production of aldehydes that may play a key role in the upgrading of alkenes produced from alternative routes such as oxidative coupling of methane or methanol to olefins [1, 2]. Hydroformylation catalysts are also active in double bound hydrogenation which may convert the reactant alkene into the corresponding alkane as well as the product aldehyde into alcohol [3]. While the double bond hydrogenation in the reactant alkene is, per definition, undesired, the consecutive hydrogenation of the product aldehyde into the corresponding alcohol may be advantageous. Typical hydroformylation products are in the carbon number range from 3 to 19. The reactant alkene is selected based on the desired product aldehyde.

Aldehydes are useful intermediates in the production of valuable products such as alcohols, carboxylic acids, amines, etc. More recently, hydroformylation has also been widely applied in the pharmaceuticals and fine chemicals industry for the production of drugs, detergents, cosmetics, surfactants, lubricants, vitamins, herbicides and perfumes [4, 5]. Alcohols can also be used to produce dialkyl phthalate plasticizers which, in turn, are employed in polyvinyl chloride plastics that are broadly used in several industries such as clothing, electric wires and pipes.

The present work concentrates on ethylene hydroformylation on a series of Rh and Co based heterogeneous catalysts. Gas phase experiments are performed using a High-Throughput Kinetics Mechanistic Investigation set up [6] to investigate the effect of the operation conditions on the main and by products formation rates on these catalysts. Subsequently a Fischer-Tropsch Synthesis based Single-Event MicroKinetic (SEMK) model is extended towards ethene hydroformylation. Starting from the available FTS model [7] a mechanism based upon elementary steps is implemented and used in the simulation of data acquired on a Rh and a Co catalyst. This will allow gaining deeper insight in the determining factors for the catalyst activity and selectivity.

1.2 Definition and history

Hydroformylation, or oxo–synthesis, is a chemical process that was discovered by the German scientist Otto Roelen in 1938 during his investigation of the origin of oxygenated products observed during cobalt catalysed Fischer – Tropsch (FT) synthesis. Roelen noticed that ethylene, hydrogen and carbon monoxide were converted into propanal and, at higher pressures, also into diethyl ketone [3]. A key consideration of hydroformylation in general is the linear versus branched product selectivity. Depending on the reaction conditions, a specific mixture of *iso* and *normal* aldehyde isomers is obtained. Both products are not equally desirable and a lot of research has been dedicated over the years to the quest for catalysts based on the transition metals cobalt and rhodium that favoured the linear isomer [8]. The overall reaction is depicted in Figure 1-1.

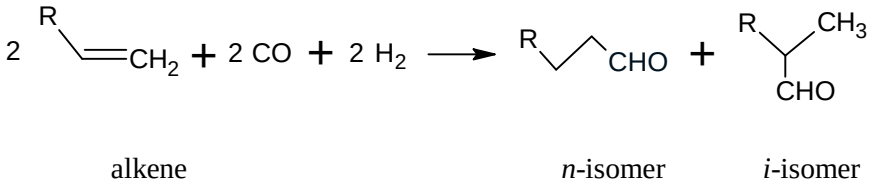

Figure 1- 1. Hydroformylation reaction

The name hydroformylation becomes clear when looking at the nature of the products that are formed. The reaction entails the addition of a formyl group (CHO) and a hydrogen atom to a carbon – carbon double bond. Depending on the catalyst used, the aldehyde is prone to further hydrogenation to the corresponding alcohol.

The hydroformylation of ethylene, as shown in Eq. 1-1, is a spontaneous, exothermic reaction (ΔG^o = -56.9 kJ mol^{-1} at 373 K, ΔH^o = -129.0 kJ mol^{-1}) [9]. Due to significant energy barriers, the reaction rate remains low, however.

$$H_2C = CH_2 + CO + H_2 \rightarrow C_2H_5CHO \qquad \text{Eq.1-1}$$

In principle, all the transition metals capable of forming carbonyls such as Rh, Co, Ir, Ru, ... are potential hydroformylation catalysts. The order of activity from the most to the least active metal, is as follows: Rh >> Co > Ir, Ru > Os > Pt > Pd > Fe > Ni [10, 11].

Industrial process configurations typically make use of homogenous catalysis, which leads to some inherent problems such as difficulties in catalyst separation from products, expensive metal losses and, corrosivity of catalytic solutions. This justifies the investigation of

heterogeneously catalysed counterparts of sufficiently high activity and stability. Heterogeneous process implementations inherently do not require a specific catalyst separation step from the products that are formed. Depending on the catalyst activity, stability and selectivity, cheaper catalyst formulations and milder reaction conditions may constitute possible additional benefits.

A wide range of research activities has been performed on this reaction with various reactants, catalysts and operation conditions. Table 1-1 gives an overview of the reactants, catalysts and operation conditions used in some experimental heterogeneous hydroformylation till present.

Table 1- 1. Examples of experimental heterogeneous hydroformylation

Reactant	Catalyst	Temperature (K)	Pressure (MPa)	Aldehyde TOF (min^{-1})	Aldehyde selectivity	Reference
Ethylene	Rh/SiO_2	483-573	0.1	$24.8\ 10^3$ - $229\ 10^3$	0.136 to 0.039 [a]	[12]
"	Various fibre-supported Rh-phosphine catalysts	373	0.5	---	0.58 to 0.61 [b]	[13]
"	Mo-Rh/SiO_2 Rh/SiO_2	388	0.1	$4.8\ 10^{-2}$ $6.9\ 10^{-2}$	0.15 0.38 [a]	[14]
"	Mn–Rh/SiO_2 (Mn:Rh=0.1:1)	483-573	0.1	$154\ 10^3$ to $269\ 10^3$	0.26 to 0.017[a]	[15]
"	$RhCl(PPh_3)_3$ and $RhCl(CO)(PPh_3)_2$	458	0.1 0.3	$1.8\ 10^{-6}$ $227\ 10^{-6}$	0.16 to 0.30 0.38 to 0.76 [b]	[16]
"	Various types of Rh/SiO_2	413 – 533	2	$0,4\ 10^{-6}$ to $2\ 10^{-6}$	0.056 to 39 [b]	[17]
"	SiO_2, MgO and carbon-supported Co, Ru, Ru-Co, Ru-Mn and Ru-Cr	345 – 473	0.1	$2.9\ 10^{-3}$ to $110\ 10^{-3}$	0.10 to 0.17 [a]	[18]
Propylene	Mo-Rh/SiO_2 Rh/SiO_2	403-448	0.1	$0.6\ 10^{-2}$ to $1.0\ 10^{-2}$	---	[14]
1-Pentene	$[Ru(CO)_3(PPh)_3]_2$	413	7	---	0,2 to 0.45 [b]	[19]
1-Hexene	$[Rh(CO)_2Cl]_2$	363-493	3 - 6	---	0.2 to 0,9 [b]	[20]
1-Octene	[Rh2(*í*-$StBu)_2(CO)_2(TPPTS)_2$]	353 - 373	0.05 - 0.1	0.5 to 8	---	[21]

a) $TOF_{aldehyde}/TOF_{Alkane}$ b) molar selectivity

1.3 Products and derivatives

In Table 1-2 an overview of production capacity of aldehydes by hydroformylation process is presented [22].

Table 1- 2. Production capacity of aldehydes via hydroformylation process

Region	Aldehydes (10^3 tonnes/year)			
	C_3	C_4	$C_5 - C_{13}$	C_{13+}
Europe	25	2385	535	85
North America	75	970	450	270
Latin America	-	120	55	-
Far East	-	1040	140	30
Total	100	4515	1180	385
Fraction (%)	2	73	19	6

Since the mid-50s of the last century, hydroformylation has been used on an industrial and commercial scale. Until recently, the capacity of aldehyde production has constantly increased. Some industrial applications of the most important aldehydes are briefly described in what follows.

1.3.1 Propanal (C_3H_5OH)

Propanal derived products are schematically represented in Figure 1-2. In the first instance propanal can either be hydrogenated into propanol or oxidized into propionic acid. n-Propanol has a direct application as an ink solvent but can also further be converted into propyl acetate, *n*-propylamines and glycol ethers. Propyl acetate has applications in fragrances and as a flavour additive, while glycol ethers have applications as ink solvents. Some pesticides and zeolites require *n*-propylamine in their production or synthesis. The most important direct application of propionic acid occurs as a grain and animal feed preservative. Propionic acid can be also used as an intermediate in the production of other chemicals, especially polymers. It is also useful as an intermediate for herbicides and some pharmaceuticals. Cellulose acetate propionate, as produced from propionic acid, is a low cost plastic that can be used to produce useful thermoplastics such as toothbrush handles, some plastic toys and packaging materials. Propionate salts are also used as a food preservative and additive [22-24].

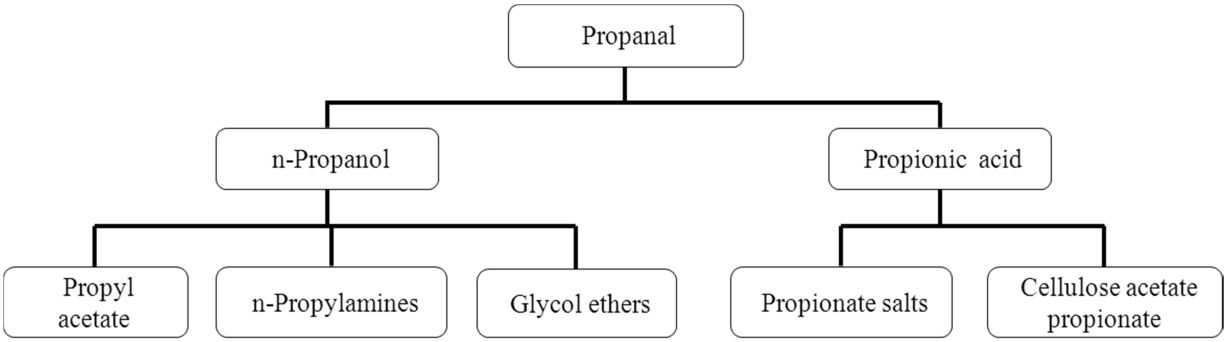

Figure 1- 2. Propanal derived products, after [24]

1.3.2 n-Butanal (C_3H_7CHO)

Also butanal or *n*-butyraldehyde and its derivatives, have a wide range of industrial applications. The chemicals produced from this aldehyde are schematically indicated in Figure 1-3. The *n*-butanol, which is produced by hydrogenation of butanal, has applications in the food industry. It can also be used for the manufacturing of pharmaceuticals, polymers, herbicide esters and printing ink. The eight carbon number alcohol, 2-Ethylhexanol, that is produced industrially by the aldol condensation of butanal, followed by hydrogenation of the resulting hydroxy aldehyde [25], can be applied as a solvent in acrylic-based paints, as an additive for diesel lubricants, as a component in surfactants, and as a precursor for commonly used phthalate esters. The phthalate esters have a wide range of industrial applications such as pharmaceutical, nutritional supplements, stabilizers and lubricants. 2-ethylhexenal has applications as a paint drying agent and a heat stabilizer for PVC processing. Polyvinyl butyral (PVB), which is produced by reaction of n-butyraldehyde with polyvinyl alcohol (PVOH), can be implemented for the manufacturing of specific safety glasses as used in cars and buildings. The reaction of formaldehyde with *n*-butanal produces trimethylolpropane (TMP) that has applications for producing urethanes, unsaturated polyesters, and as an additive in synthetic lubricants. Reaction with acetone yields methyl amyl ketone which has application as a solvent for coatings. Butyric acid can be used in the production of various butyrate esters, which have generally nice aromas or tastes. Hence, they have applications as food and perfume additives [22-24].

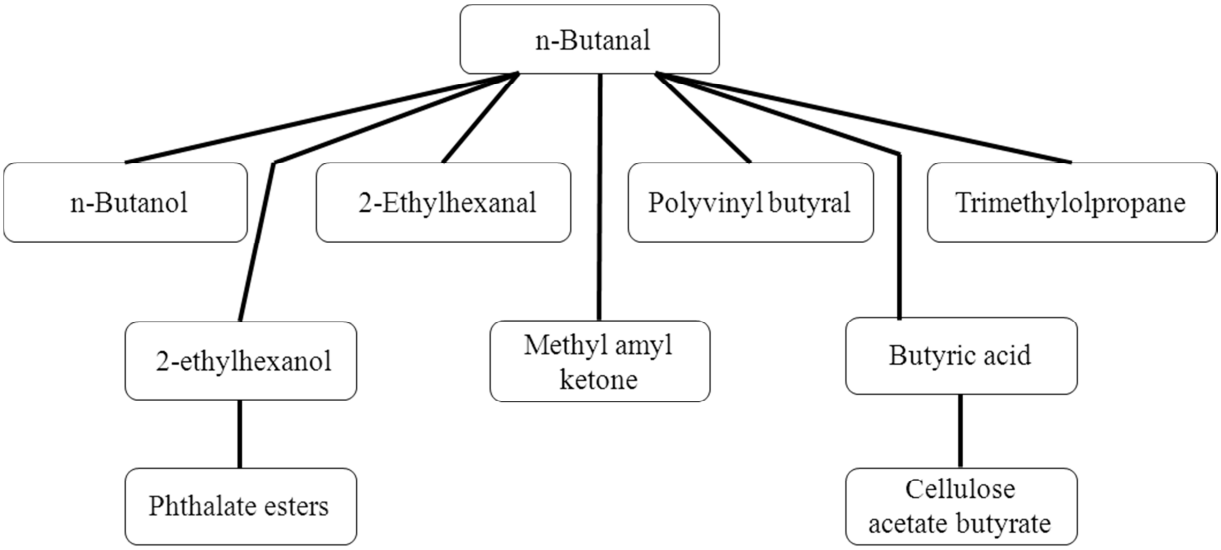

Figure 1- 3. *n*-butanal derived products, after [24]

1.3.3 Iso-butanal ($(CH_3)_2CHCHO$)

Iso-butyraldehyde or *iso*-butanal derived products are schematically presented in Figure 1-4. *Iso*-butanol used to be an undesired byproduct in *n*-butanol production until Eastman recognized its potential and correspondingly developed applications for it. It can be used industrially in some similar applications as n-butanol, e.g., in printing inks. It additionally has applications in lube oil additives, paint additives, and as a precursor for herbicides and isobutyl acetate. Isobutyl acetate that is produced from the esterification of *iso*-butanol with acetic acid, can be used as a solvent for nitrocellulose coatings which have applications as a plastic film, in inks and wood coatings. Neopentylglycol, another specialty chemical produced from *iso*-butanal, is industrially used in production of polyesters, paints, lubricants and pelastisizers.

Isobutyric acid has applications in the food industry. *Iso*-butylidenediurea is used for the production of fertilizers and methyl *iso*-amyl ketone can be used as a solvent for nitrocellulose, lacquers, as well as in the production of some polymers and resins materials [22-24].

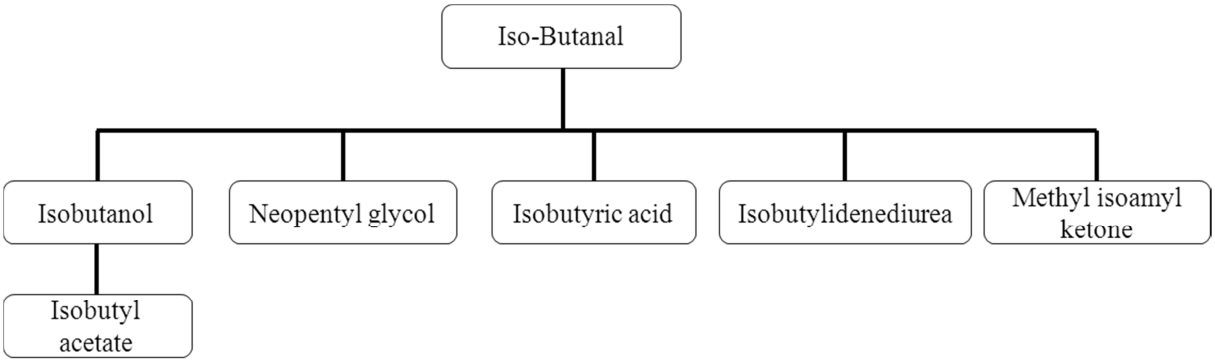

Figure 1- 4. *Iso*-butanal derived products, after [24]

1.3.4 C_5 aldehydes

These aldehydes are mostly used in the production of synthetic lubricants, amyl alcohol, valeric acid, and isopentanoic acid. Union Carbide is one of the largest producers of these chemicals [22-24]. The C_3 to C_5 aldehydes are also used as solvents and intermediates for specialty products [22-24].

1.3.5 C_{5+} aldehydes

Heavier aldehydes are mostly converted to alcohols and acids. The C_7 to C_9 fatty acids can be implemented as intermediates for specialty synthetic lubricants. The C_{10} through C_{l3} plasticizer alcohols are used to improve the quality of some polymers such as PVC [22-24].
The C_{11} to C_{18} alcohols are used for surfactants in detergents. They also have applications in herbicides, pesticides, pharmaceuticals, lube oil additives, and cosmetic formulations [22-24]. The C_{12} to C_{15} as well as higher alcohols are mainly used for biodegradable detergents [22-24].

1.4 Industrial processes

Cobalt carbonyls were the first catalysts to be implemented for commercial hydroformylation processes. Since their activity is rather limited, more extreme reaction conditions, i.e., 20 to 35 MPa and 433 to 453K, had to be used [26, 27]. The next generation of cobalt catalysts had been modified with alkylphosphine ligands that increased the yield and selectivity to linear aldehydes. While alkylphosphines ligands have a positive effect on the performance of cobalt based catalysts, they tend to slow down the catalytic behaviour exhibited by rhodium. Wilkinson demonstrated that arylphosphine ligands are a better alternative to tune rhodium based catalysts [28].

Cobalt complexes had been the main industrial hydroformylation catalysts until the early 1970's when rhodium catalysts were commercialized. In 1974-1975 Union Carbide and Celanese, independently of one another, introduced rhodium based catalysts on an industrial scale. Since then, cobalt catalysts have been replaced by rhodium in almost all major hydroformylation processes. The expensive nature of rhodium was compensated by cheaper equipment as well as increased catalyst activity and selectivity to desired products. Almost 75% of all hydroformylation processes in 2004 were based on rhodium triarylphosphine catalysts.

In 1984 scientists introduced a biphasic system, allowing a more easy separation between the water soluble catalyst and the organic product [4, 28]. Commercially, homogeneous Co or Rh complexes are typically applied at temperatures ranging from as low as 360 K up to 573 K [13, 22]. The homogenous reaction shows higher selectivity towards aldehydes and alcohols compared to the heterogeneous hydroformylation reaction [10, 29]. The selectivity of 80% towards aldehydes and a 90% conversion of CO/H_2 mixture is reported for an industrial homogenous propene hydroformylation reaction [30]. Besides, a high selectivity can be achieved when the propene conversion is decreased [30]. Later investigations focused on alternative noble metals, heterogeneous catalysts and improvement of the catalytic activity for specific feed olefins and selectivity for desired products such as chiral aldehydes [31]. The important industrial processes can be divided into five main types regarding their catalyst used and operation conditions of these processes [3]. Table 1-3 gives a brief overview of their corresponding catalysts and reaction conditions.

Table 1- 3. Industrial hydroformylation processes

Process	Alkene	Company	Catalyst	P (MPa)	T (°C)	Aldehyde selectivity	*n/i* ratio	Water solubility
Low-Pressure Oxo (LPO)	Propylene	Union Carbide & Johnson Matthey	$[RhH(CO)(PR_3)_3]$[1]	1.5-2	85-115	High	92:8	No
RCH-RP	Propylene	Ruhrchemie	$[RhH(CO)(PR_3)_3]$[2]	1-10	50-130	High	96:4	Yes
Unmodified cobalt carbonyl	$C_6 - C_{12}$ alkenes	Exxon	$[CoH(CO)_4]$	20-35	110-180	Medium	80:20	No
Modified catalysts	$C_7 - C_{14}$ alkenes	Shell	$[CoH(CO)_3PR_3]$[3]	5–10	160–200	Low	88:12	No
BASF-Oxo process	Ethylene, Propylene	BASF	$[Co_2(CO)_8]$	30	150-170	High	80:20	Yes

[1]R=C_6H_5 [2]R=3-$C_6H_4SO_3Na$ [3]R=C_4H_9

As shown in Table 1-3, rhodium based processes can be classified into two types, accounting for the operating conditions used. The most important of them on an industrial scale uses the so-called phosphine-modified catalyst complex. The first process is the Low Pressure Oxo (LPO) process that was jointly developed by Union Carbide, Davy McKee, and Johnson Matthey [24]. The Ruhrchemie - Rhône-Poulenc (RCH-RP process) is another industrial low pressure process for alkene hydroformylation. This process has found its greatest importance in the hydroformylation of propylene. Apart from some differences in operation conditions and equipment, the major difference between this RCH-RP and the LPO process is the use of a water soluble catalyst. Such a catalyst has as advantage that is insoluble in the organic product phase and, hence, separation of the aqueous catalyst phase and the produced butanal is considerably simplified. As a result, catalyst metal losses via the aldehyde product stream are significantly reduced.

In the LPO process, a stirred back-mixed reactor together with a stripping column are used to separate the product and by-products from the catalyst. The high molecular weight of the rhodium catalyst complex leads to an adequate separation of the catalyst mixture from the products [32].

The cobalt based processes are divided into three groups, depending on the modifying ligands used and the corresponding operation conditions. The first one and, for a long time, the most important industrial hydroformylation process was based on an unmodified cobalt carbonyl hydride catalyst as developed by Roelen. This process operates at high pressures and temperatures. A high temperature is required to achieve a sufficiently high reaction rate due to the low catalyst activity. As a consequence of the increased reaction temperature, also higher CO partial pressures are required to guarantee the (thermal) stability of this catalyst, see Figure 1-5 [4].

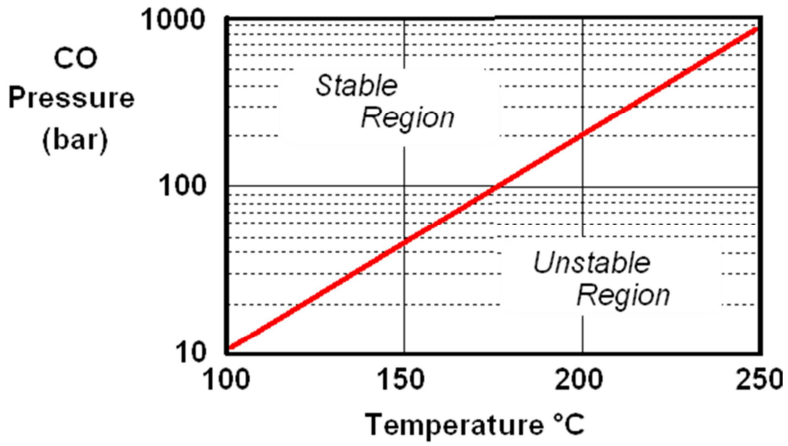

Figure 1- 5. Stability of $HCo(CO)_4/Co_2(CO)_8$ with respect to precipitation of cobalt metal [4]

The second process, i.e., the Shell process can be implemented in the case that the alcohol is the desired product rather than the aldehyde. A phosphine-modified cobalt catalyst with a strong hydrogenation activity is used in this process and gives a good *normal/iso* ratio (88:12) in the initially formed aldehyde product mixture [24].

The third process, i.e., the BASF-oxo process, has mainly been developed for higher carbon number alkenes as reactant and cobalt carbonyl-based catalyst. The operating pressure amounts to 30 MPa approximatively in temperature range from 150 to 170 °C. By using this process an aqueous cobalt catalyst phase is produced, which can be easily recycled afterwards [29].

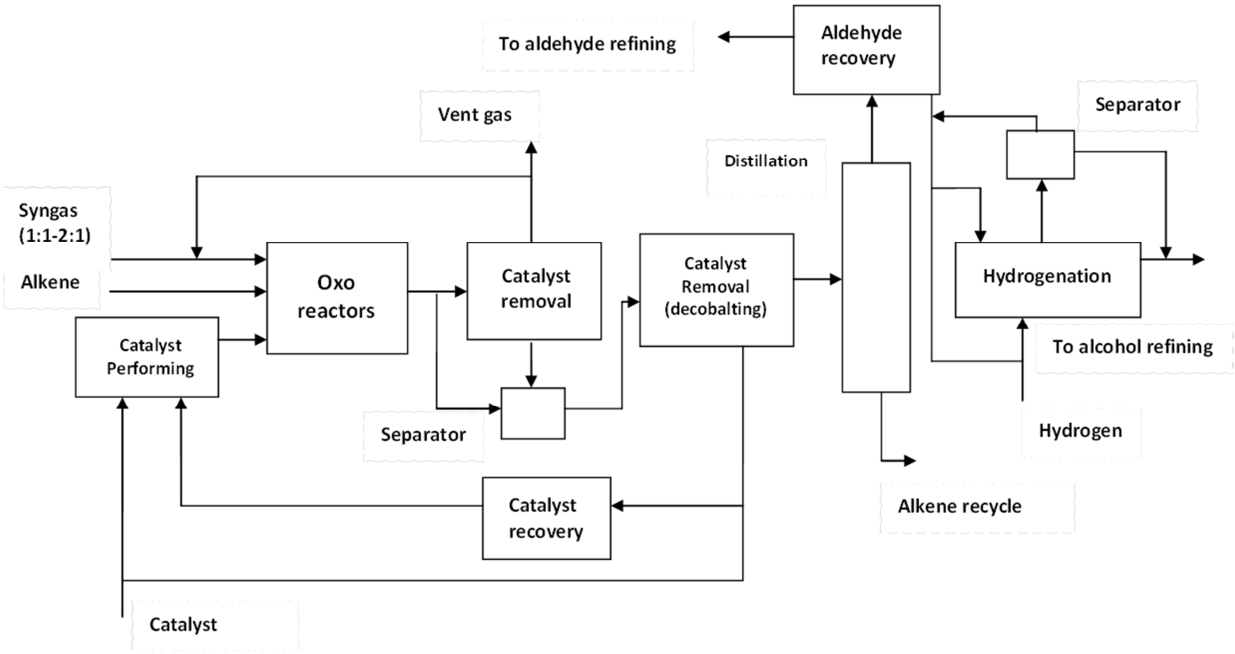

Figure 1- 6. Flow diagram of a typical hydroformylation process, after [24]

Despite some differences, all these processes have some common features. A simplified flow diagram of an industrial hydroformylation is shown in Figure 1-6 [24]. As it can be seen in this figure a gas mixture of carbon monoxide and hydrogen, i.e., syngas, together with the alkene stream are fed to the oxo reactors where both new and recovered catalysts after preparation in a catalyst performing unit are added. The reactors operate over a temperature range from 373 to 473K and at total pressures between 10 to 45 MPa. The products flow to catalyst removal and separation units where the catalyst is separated from the products and unreacted feed. After the recovery, the separated catalysts are added to the fresh catalysts and can be recycled to the reactors. The catalyst free product first enters the distillation unit where the unreacted alkenes are removed, and is subsequently sent to the aldehyde recovery unit to recover the aldehydes. Part of these aldehydes are then sent to the aldehyde refining unit. Another part of the process, as it is shown in Figure 1-6, can be used to produce alcohols in the hydrogenation reactor(s). The hydrogenation is typically performed over a temperature range from 323 to 473K and at total pressures between 0.3 to 24 MPa.

1.5 Homogeneous and heterogeneous reaction mechanisms

This section starts with an overview of the generally accepted mechanism for the homogeneous hydroformylation reaction and subsequently extends towards the heterogeneous variant. Because of the mechanistic similarity of the heterogeneously catalysed hydroformylation with Fischer-Tropsch synthesis, some attention will be devoted to this latter mechanism as well.

1.5.1 Homogenous reaction mechanisms

The first homogeneous hydroformylation reaction mechanism was proposed by Heck and Breslow [33], see Figure 1-7. This mechanism was initially formulated for cobalt based catalysts but it is also accepted for rhodium based ones. It comprises both a monoatomic as well as a biatomic pathway. Especially the former is reported to be more likely to occur [33]. The monoatomic pathway involves the reaction of an acyl intermediate with H_2 and has been reported to be the dominant mechanism for hydroformylation of 1-alkenes [34].
The consecutive steps in this reaction mechanism, starting from the activated catalyst species (at the top of Figure 1-7) and going through the reaction cycle in a clockwise fashion, involve the following elementary phenomena:

1- Carbon monoxide molecular desorption
2- Alkene chemisorption
3- Alkene insertion into the metal – hydrogen (M-H) bond
4- Carbon monoxide molecular chemisorption
5- Carbon monoxide insertion into the metal – carbon (M-C) bond
6- Concerted hydrogen chemisorption
7- Aldehyde elimination
8- CO insertion and regeneration of the active catalyst species

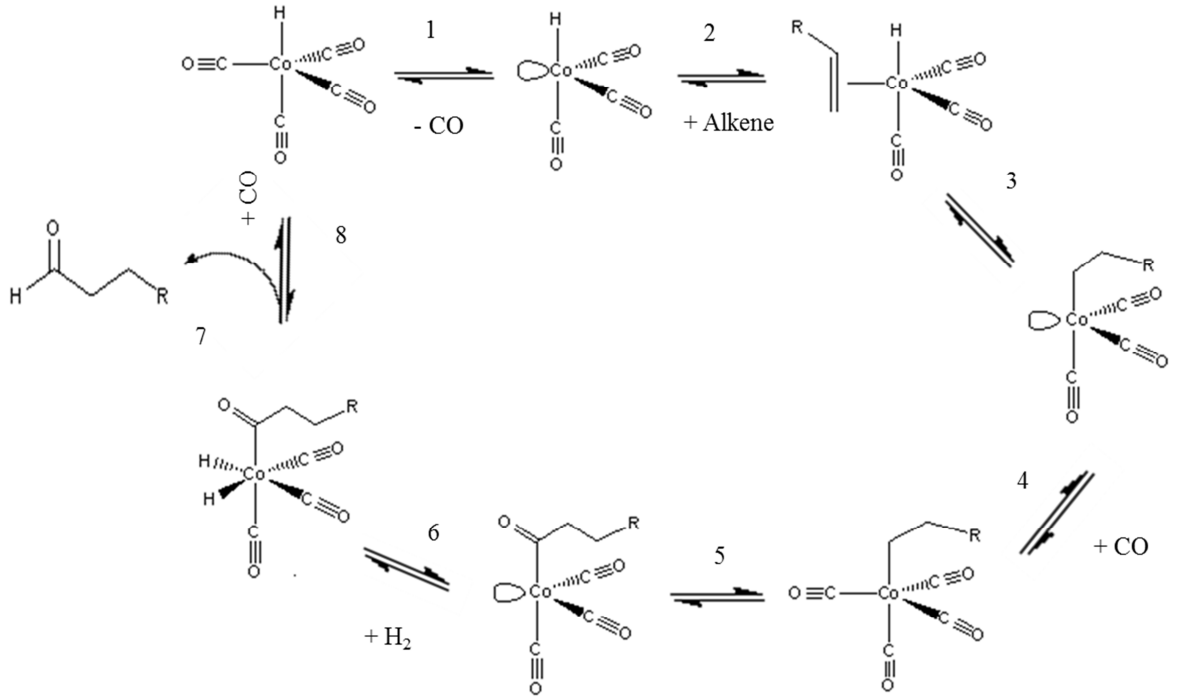

Figure 1- 7. Heck and Breslow mechanism for homogenous hydroformylation, after [33].

In this mechanism, a ligand substitution followed by an insertion reaction in step 1 and 2. In the second elementary step, i.e., alkene molecular chemisorption, the vacant orbital originating from CO desorption serves as an acceptor for the electrons of the carbon-carbon bond of the alkene. In the third elementary step, i.e., the alkene insertion into the metal – hydrogen (M-H) bond, steric effects induced by the presence of ligands are determining the nature of the final product formed. According to the Markovnikov rule, the hydrogen atom should be transferred to the carbon atom bearing the most hydrogen atoms, see step 1 in figure 1-8. Depending on the ligands used, however, the product obtained according to Markovnikov's rule may be sterically less favoured. Bulky ligands, such as tributyl phosphine, can indeed logically be expected to induce such steric effects, resulting in the hydrogen transfer to occur to the bulkier carbon. Such an anti-Markovnikov addition, see step 2 in Figure 1-8 results in enhanced selectivities towards the straight chain products [4]. In the homogeneous variant, the presence of ligands allows tuning the selectivity towards the oxygenated products while simultaneously avoiding alkene hydrogenation.

Almost all catalytic carbonylation reactions rely on the insertion of carbon monoxide into a metal - carbon or a metal - hydrogen bond. In this process a carbonyl ligand participates in a concerted intramolecular attack with another ligand, typically an alkyl or an aryl.

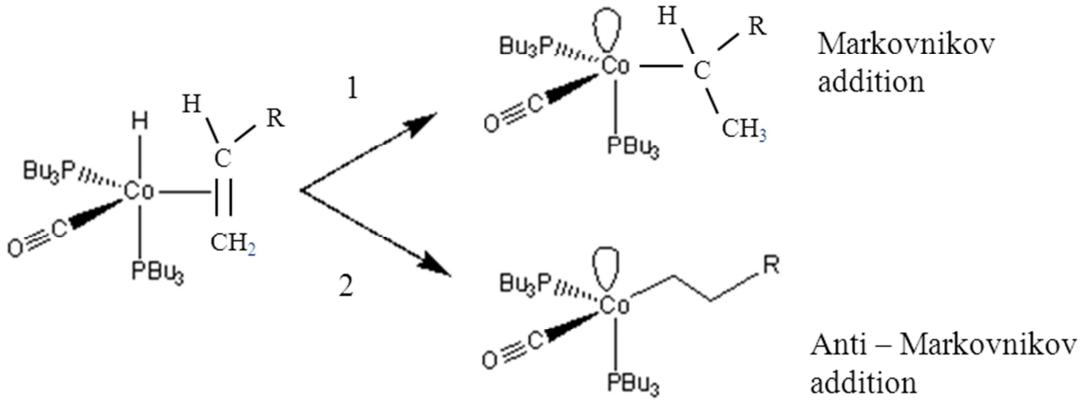

Figure 1- 8. Markovnikov and anti-Markovnikov addition in the hydroformylation reaction mechanism, after [35]

After aldehyde desorption, the active catalyst species can be regenerated as it is shown in step 8 of the Figure 1-7.

1.5.2 From homogeneous to heterogeneous reaction mechanism

The most reported heterogeneous hydroformylation reaction mechanism is based on the homogeneous mechanism as proposed by Wilkinson et al. [36], see Figure 1-9. In essence, this mechanism consists of the same elementary steps as the homogeneous one discussed above. A complementary side reaction, i.e., metal alkyl hydrogenation to the corresponding alkane has now been accounted for. Also, the regeneration of the active site is indicated not to require the (simultaneous) addition of a CO molecule. A more specific heterogeneous ethylene hydroformylation mechanism will be discussed in Section 3.2 in Chapter 3. The elementary steps as occurring in the Wilkinson mechanism can, hence, be summarized as follows:

1- Carbon monoxide desorption
2- Alkene chemisorption
3- Hydride addition towards a metal alkyl
4- Hydrogenation to ethane (side reaction)
5- Carbon monoxide molecular chemisorption
6- Carbon monoxide insertion into the metal alkyl bond
7- Acyl hydrogenation
8- Aldehyde elimination

The side reaction which leads to alkane formation is also included as it cannot be neglected in heterogeneous catalysis. It is generally believed that the addition of hydrogen to the rhodium-acyl complex is the rate-determining step [37, 38].

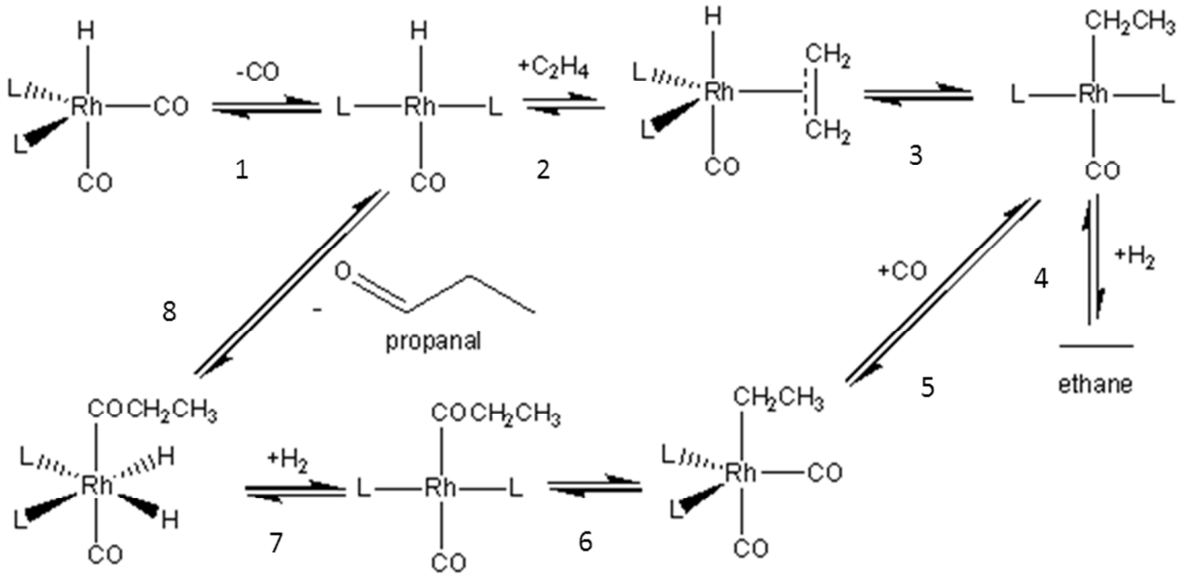

Figure 1- 9. Wilkinson dissociative mechanism for “heterogeneous” ethylene hydroformylation [36]

In this mechanism, it is assumed that once a CO molecule has been inserted in an alkyl fragment, carbon-oxygen bond scission does not occur. Two competitive steps are involved both starting from a metal bound alkyl (MC_nH_{2n+1}) that is obtained after alkene chemisorption on the metal surface, and the addition of a first H atom. The first step, which is the desired one in hydroformylation, involves CO insertion and ultimately leads to aldehyde or alcohol formation. The second one is alkene hydrogenation into alkane.

Some studies show that the CO insertion rate on metal catalysts and, as a consequence, the reaction rate and selectivity for aldehyde production increase in the presence of small Rh particles [39, 40]. Of course apart from the metal, also the dispersion and the reduction extent are main factors determining the CO insertion activity, and thereby, the selectivity towards aldehyde formation. Sachtler and Ichikawa [41], made a distinction between two types of active sites for aldehyde formation: isolated, partially oxidized metal crystallites for the migratory CO insertion into metal alkyl bonds, and fairly large metal ensembles for the dissociation of hydrogen.

Hedrick et al. [42] reported that on a Mn-Rh/SiO_2 catalyst, transferring hydrogen from the metal to the silica surface plays a main role in the hydrogenation of the acyl intermediate.

According to these authors, two different types of hydrogen are involved in the hydrogenation of ethyl species to form ethane and in the hydrogenation of adsorbed acyl species to form propanal. These are, metal adsorbed hydrogen and hydrogen from the carrier Si-OH, respectively.

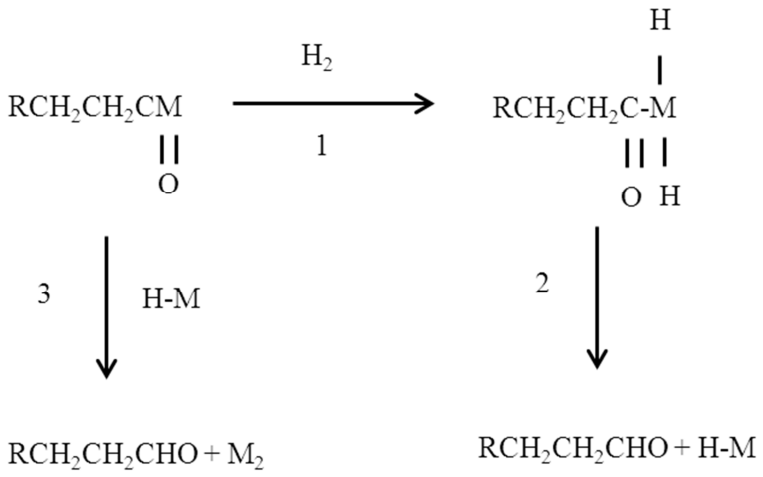

Figure 1- 10. Two possible routes for the transformation of the acyl-metal species to the aldehyde [44].

In the literature two possible routes have been discussed for the transformation of the acyl-metal species to the aldehyde: either a dissociative desorption following a previous hydrogenation and leaving a H on the catalyst surface (steps 1 and 2 in Figure 1-10), or a direct, hydrogen assisted desorption (step 3) [43]. According to Henrici-Olivé and Olivé [44], in the heterogeneous reaction mechanism, the first route (step 1 and 2 in Figure 1-10 and step 7 in Figure 1-9) is the only means to form an aldehyde. Therefore, the main difference between the homogeneous and the heterogeneous mechanisms is the presence of a free, mobile and reactive hydrido-metal species in the solution [44].

1.5.3 Fischer-Tropsch synthesis reaction mechanism

Not only historically, but also mechanistically, heterogeneously catalysed hydroformylation is very closely related to Fischer-Tropsch (FT) synthesis. As a result, a mechanistic investigation of the hydroformylation reaction will benefit from what is already known for FT synthesis. It is a heterogeneously catalyzed reaction in which a mixture of carbon monoxide and hydrogen, better known as synthesis gas or syngas, is converted into a wide variety of higher hydrocarbons and possibly oxygenates. The global reaction is shown in Eq. 1-2.

$$nCO + 2nH_2 \rightarrow -(CH_2)_n - + nH_2$$ Eq. 1-2

The reaction of ethylene with syngas has been used as a probe reaction to study the activity and selectivity in the FT process on supported transition metals [12].

This reaction was first reported in 1925 by Franz Fischer and Hans Tropsch on cobalt and nickel catalysts and has received wide attention since. Recently, with stricter environmental regulations towards emissions and a focus on alternative feeds such as natural gas, FT fuels have become even more interesting.

In FT synthesis, a broad range of alkenes, alkanes and, to some extent, also oxygenates are generally produced. The product distribution depends on the operating conditions used such as temperature, feedstock ratio, pressure, catalyst type, etc. The hydrocarbons are mainly linear and the double bond in the alkenes is mostly terminal. Oxygenated components, i.e., alcohols, aldehydes, ketones and acids, are usually only produced to a lesser extent on transition metal catalysts such as cobalt.

Over the years, various mechanisms have been proposed for FT synthesis. It is believed that FT synthesis is a kind of polymerization reaction comprising CO activation, chain growth and termination. The oxygenates are produced by means of carbon monoxide insertion in the growing chain without a CO bond scission occurring. [45]. The carbene mechanism is the most popular FT mechanism. It accounts for chain growth through methylene insertion into a metal alkyl species. The CO activation reactions and chain growth and termination elementary steps in this mechanism are depicted in Figure 1-11. In this mechanism dissociative carbon monoxide chemisorption occurs on the catalyst surface and the hydrogenation of the resulting carbide species leads to the formation of methyl and methylene species. Alkanes are formed through reductive elimination of metal alkyl species while the alkenes are formed through β-hydride elimination [46].

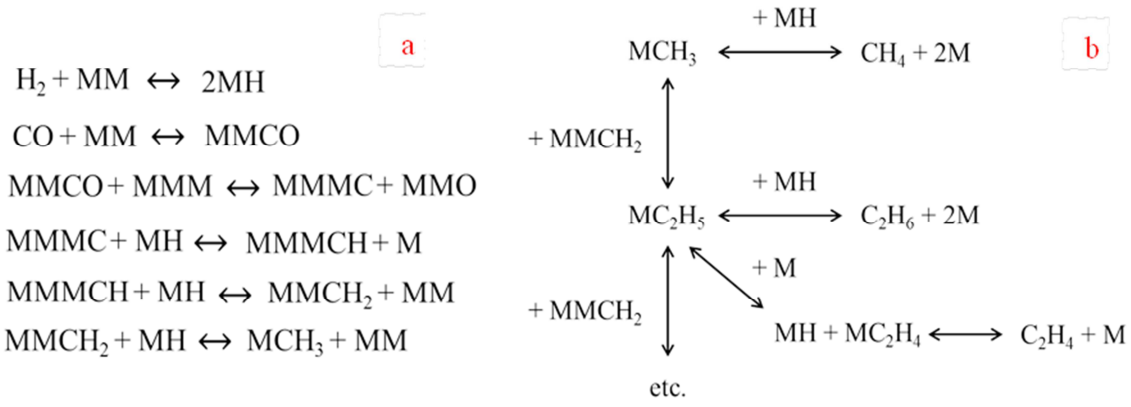

Figure 1- 11. (a) The chain initiation reactions (b) Chain growth and termination elementary steps in the “carbene” mechanism for FT reaction.

According to Iglesia et al. and Schulz and Claeys [47, 48], linear 1-alkenes are primary products in FT synthesis. These species can be re-adsorbed on the metal surface to undergo secondary reactions such as hydrogenation, double bond isomerization, re-insertion, hydrogenolysis and hydroformylation.

Pichler and Schulz [49] proposed an alternative mechanism, based on carbon monoxide insertion, that also received considerable support. It allows explaining both the formation of the typical hydrocarbon FT products as well as the appearance of oxygenates [48-51]. This mechanism is illustrated in Figure 1-12. It includes carbon monoxide insertion into a metal-alkyl bond resulting in an acyl (also termed a metal carbonyl) intermediate that as depicted in Figure 1-12 can lead to linear or branched (step 5 in Figure 1-12) hydrocarbons, linear 1-alkenes (step 4 in Figure 1-12) and the formation of oxygenates such as, alcohols (step 2 in Figure 1-12), aldehydes, ketones (step 7 in Figure 1-12) and acids (step 6 in Figure 1-12).

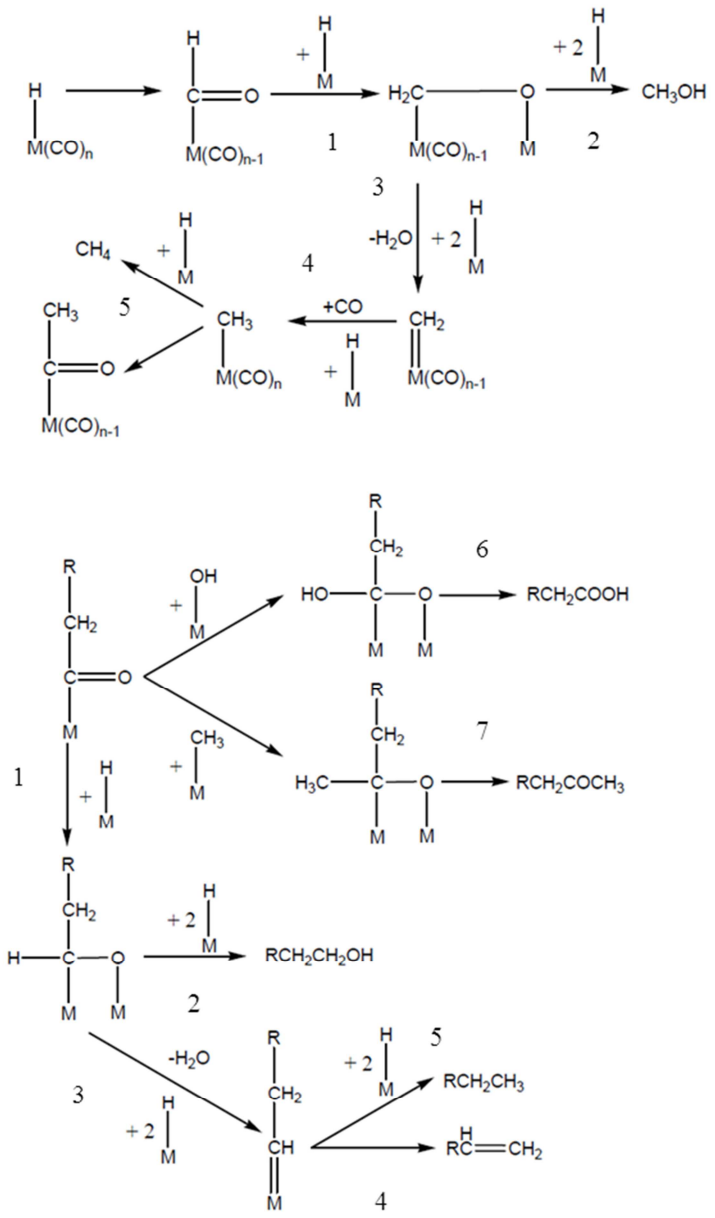

Figure 1- 12. Carbon monoxide insertion mechanism [49]

1.6 Summary and Objectives of the thesis

Hydroformylation or oxo synthesis is an important catalytic process for the production of aldehydes and alcohols from alkenes. This introduction started with a definition for hydroformylation followed by an overview of its history and products, including their applications. Different industrial hydroformylation process implementations and corresponding catalysts, Rh and Co being the most relevant ones, were discussed. Industrial process configurations typically make use of homogenous catalysis, which leads to some inherent problems that justify the investigation of the potential of using an active and stable

heterogeneous hydroformylation catalyst. Homogenous and heterogeneous hydroformylation mechanisms were discussed in this chapter. Fischer-Tropsch (FT) synthesis exhibits a lot of similarities with heterogeneous hydroformylation. The corresponding reaction families and elementary steps in hydroformylation mechanisms also come back in FT mechanisms and the difference between these mechanisms is situated in which elementary steps occur more dominantly. It is generally accepted today that the Wilkinson mechanism is the most likely one for hydroformylation [14, 52]. This mechanism assumes that, once a CO molecule has been inserted in an alkyl fragment, the carbon oxygen bond remains intact.

The ultimate objective of this work is to determine the effect of different catalysts on reactant conversion, product selectivity and yields in ethylene hydroformylation to propanal and subsequently, to explain and interpret its corresponding reaction mechanism in terms of elementary steps and to develop a fundamental kinetic model for this reaction on the selected catalysts. Starting from the model available for FTS [7] a mechanism based upon elementary steps is implemented and used in the simulation of data acquired on a Rh and a Co catalyst. This will allow gaining deeper insight in the determining factors for the catalyst activity and selectivity.

1.7 References

[1] J. W. Thybaut, J. Sun, L. Olivier, A. C. Van Veen, C. Mirodatos, G. B. Marin, Catal. Today. 159 (2011) 29-36.

[2] V.I. Alexiadis, J. W. Thybaut, P. N. Kechagiopoulos, M. Chaar, A. C. Van Veen, M. Muhler, G. B. Marin, Appl. Catal., B. 150 (2014) 496-505.

[3] B. Cornils, M. Rasch, Angew. Chem. Int. Ed. 33 (1994) 2144 - 2163.

[4] P. W. Van Leeuwen, Rhodium catalysed hydroformylation, Springer, New York, 2002.

[5] B. Breit, W. Seiche, Synth. (2001) 1–36.

[6] K. Van der Borght, K. Toch, V. V. Galvita, Y.W. Thybaut, G. B. Marin, Catalysts 5 (2015) 1948-1968.

[7] G. Lozano-Blanco, J.W. Thybaut, K. Surla, P. Galtier, G.B. Marin, Ind. Eng. Chem. Res. 47 (2008) 5879-5891.

[8] R.F. Heck, B.D.S., J. Am. Chem. Soc, (1961)4023 – 4027.

[9] K. Otsuka, T. Ando, I. Yamanaka, J. Catal. 165 (1997) 221-230.

[10] Cornils B., H.W.A., Applied Homogeneous Catalysis with Organometallic Compounds. VCH, Weinheim, 1996.

[11] T. A. Zeelie, Rhodium and cobalt catalysts in the heterogeneous hydroformylation of ethane, propene and 1-hexene. PhD thesis, Helsinki, 2007.

[12] M.W. Balakos, S.S.C. Chuang, J. Catal. 1994. 151 (1994) 266-278.

[13] T. A. Zeelie, A. Root, A.O.I. Krause, Appl. Catal., A. 285 (2005) 96-109.

[14] K. Tomishige, I. Furikado, T. Yamagishi, S. Ito, K. Kunimori, Catal. Lett. 103 (2005) 15-21.

[15] M. A. Brundage, M. W. Balakos, S.S.C. Chaung, J. Catal. 173 (1998) 122-133.

[16] V. I. Zapirtan, B. L. Mojet, J.G.V. Ommen. J. Spitzer, L. Lefferts, Catal. Lett. 101 (1-2) (2005) 43-47.

[17] T. Hanaoka, H. Arakawa, T. Matsuzaki, Y. Sugi, K. Kanno, Y. Abe, Catal. Today. 58 (2000) 271-280.

[18] F.S. Xiao, M. Ichikawa, J. Catal. 147 (1994) 578-593.

[19] C. U. Pittman Jr. G. M. Wilemon, J. Org. Chem. 46 (1981) 1901-1905.

[20] W. Junfan, S. Juntan, L. Hong, H. Binglin, React. Polym. 12 (1990) 177–186.

[21] U. J. Jauregui-Haza, O. Diaz-Abin, A. M. Wilhelm, H. Delmas, Ind. Eng. Chem. Res. 44 (2005) 9636-9641.

[22] Ullmann's Encyclopedia of Industrial Chemistry, sixth ed., John Wiley & Sons, 2002.

[23] Kirk - Othmer Encyclopedia of Chemical Technology. 5 ed. John Wiley & Sons, 2007.

[24] H. Gunardson, Industrial Gasses in Petrochemical Processes, Marcel Dekker, New York, 1998.

[25] R. Miller, G. Bennett, Ind. Eng. Chem. 53 (1961) 33-36.

[26] L.H. Slaugh, R.D. Mullineaux, J. Organomet. Chem, 13 (1968*)* 469.

[27] L.H. Slaugh, R.D. Mullineaux, US Patent by Shell Oil, 3, 239, 569, 1966, 260632000.

[28] M. Beller, B. Cornils, C. D, Frohning, C. W. Kohlpaintner, J. Mol. Catal. A 104 **(**1995) 17–85.

[29] Catalysis from A to Z: A Concise Encyclopedia, 2408 Seiten, Verlag Wiley-VCH Verlag GmbH & Co. KGaA, 2012.

[30] K. Weissermel, H. J. Arpe, Industrial Organic Chemistry, John Wiley & Sons, 2008.

[31] Union Carbide Corp. (J.E. Babin, J.M. Maher, E. Billing), US 5.364.950 (1992).

[32] R. Tudor, M. Ashley. Platinum Metals Rev., 51 (2007) 116.

[33] D. S. Breslow, R. F. Heck, Chemistry & Industry, 17 (1960) 467.

[34] W. R. Moser, Advances in Chemistry Series, ed. W.R.M.a.D.W. Slocum. Vol. 230. Washington D.C ACS. 1992.

[35] https://commons.wikimedia.org/wiki/File:Regioselectivityof_hydroformylation2.png, July 2016.

[36] D. Evans, J.A. Osborn, G. Wilkinson, J. Chem. Soc. 1968(12) 3133-3142.

[37] C. D. Frohning, C. W. Kohlpainter, In: B. Cornils, W. A. Herrmann (Eds.), Applied homogeneous catalysts with organometallic compounds, VCH, Weinheim, 1996.

[38] M. W. Balakos, S.S.C. Chuang, J. Catal. 151(1995) 253-265.

[39] L. Huang, X. Yide, G. Wengui, L. Anming, L. Darning, G. XieXian, Catal. Lett. 32 (1995) 61-81.

[40] S. S. C. Chuang, S.I. Pien, J. Catal. 135 (1992) 618-634.

[41] W. M. H. Sachtler, M. Ichikawa, J. Phys. Chem. 90 (1986) 4752-4758.

[42] S.A. Hedrick, S.S.C. Chuang, M.A. Brundage, J. Catal., 185 (1999) 73-90.

[43] T. A. Kainulainen, M. K. Niemelä, A. O. I. Krause, J. Mol. Catal. A: Chem. 122 (1997) 39-49.

[44] G. Henrici-Olive, S. Olive, The Chemistry of catalyzed hydrogenation of carbon monoxide, Speringer-Verlag, Heidelberg, 1980.

[45] J.P. Hindermann, G.J. Hutchings, A. Kiennemann, Cat. Rev. Sci. Eng. 35 (1993) 1-127.

[46] G. Lozano-Blanco, J. W. Thybaut, K. Surla, P. Galtier, G. B. Marin, Oil Gas Sci. Technol. 6I (2006) 489-496.

[47] H. Schulz, M. Claeys, Appl. Catal. A., 186 (1999) 71-90.

[48] E. Iglesia, S. C. Reyes, R. J. Madon, S. Soled, Adv. Catal. 39 (1993) 221-302.

[49] H. Pichler, H. Schulz, Chemie-Ing.-Techn., 42 (1970) 1162-1174.

[50] H. Schulz, M. Claeys, Appl. Catal. A. 186 (1999) 91-107.

[51] M.E. Dry, Appl. Catal. A. 138(1996) 319-344.

[52] M. A. Brundage, S.S.C. Chaung, J. Catal. 164 (1996) 94-108.

Chapter 2:

Procedures

Abstract: *Intrinsic hydroformylation kinetics have been measured in a high-throughput kinetics mechanistic investigation set up at temperatures varying from 448 to 498 K, with the total pressure ranging from 1 to 3MPa. A gaseous feed containing CO, C_2H_4 and H_2 was used with space times varying from 2.7 $kg_{cat}.s/mol_{C2H4,in}$ to 149 $kg_{cat}.s/mol_{C2H4,in}$. Three catalysts have been investigated, i.e., 5%Rh on Al_2O_3, 1%Co on Al_2O_3 and 0.5%Co-0.5%Rh on Al_2O_3. The conducted catalyst characterisation tests and their corresponding procedures are described. The proper correlations to verify that, at the selected operating conditions, the observations are not affected by mass or heat transfer limitations, are discussed.*

The adjustable parameters in the ethylene hydroformylation microkinetic model are determined by regression against experimental data obtained on rhodium and cobalt based catalysts. The parameter estimation method and the statistical tests applied to assess the significance of the global regression and parameter estimates are presented. A 1D pseudo-homogeneous plug-flow reactor model is applied to calculate the conversions and molar yields.

2.1 Introduction

The High-Throughput Kinetics Mechanistic Investigation (HTK-MI) set up is a powerful tool for assessing the kinetics on a well selected catalyst library [1, 2]. Hence, the possibility to study different catalysts at varying operation conditions, such as temperature, pressure and inlet composition, over a wide space time range turns the HTK-MI set up into an adequate equipment to investigate the heterogeneously catalysed, gas phase ethylene hydroformylation [3]. Although a wide range of experimental research activities have been performed on hydroformylation with various reactants, heterogeneous catalysts and operating conditions [4-11], the literature on the (fundamental) kinetic modelling of this reaction is still limited [12-14]. While a so-called Langmuir–Hinshelwood/Hougen–Watson (LHHW) kinetic model for heterogeneously catalyzed ethylene hydroformylation was constructed by Balakos and Chuang [12], see section 4.1 for a more elaborate discussion, Brundage and Chuang [13] specifically modeled the hydrogenation steps in ethylene hydroformylation, also using a LHHW model. Their work was based on a limited number of experimental results, however. Finally, Murzin et al. [14], developed a kinetic model for homogeneous propene hydroformylation in a semi batch reactor.

Catalyst characterization provides the required information about critical catalyst properties such as BET surface area, particle size and fraction of exposed metal on the catalyst surface. Such data are essential for interpreting the catalysts performance. They are also needed as input for the developed microkinetic model [15]. The procedures for catalyst characterization are discussed in section 2.2.2.2.

Potential external and internal mass and heat transport limitations in the heterogeneous catalytic reactions must be avoided on the laboratory scale investigation to allow the measurement of the intrinsic kinetics. To safely allow neglecting such limitations as well as the pressure drop over the catalyst bed, various equations and conditions are available and have been assessed [16-21].

A Single-Event MicroKinetic model (SEMK) is a model that accounts for the rate of every elementary step. Hence, detailed product profiles can be obtained making use of this model which makes it a potential tool to propose better performing catalysts. The single-event concept was first introduced by Froment et al. [22] and recently reviewed by Thybaut and Marin [23]. In this work, the adjustable parameters in the microkinetic model are determined by regression to experimental data obtained over Rh and Co based catalysts. This regression entails the minimization of an adequately defined objective function [24]. To investigate the

significance of the performed regression and the estimated parameters, some statistical tests were carried out [16].

2.2 Experimental procedures

In this work, the experimental investigation was performed in a High-Throughput Kinetics – Mechanistic Investigation (HTK-MI) set up, see Figure 2-1. This set up is introduced and discussed in detail in section 2.2.1. The selected catalysts, 5%Rh/Al_2O_3, 1%Co/Al_2O_3 and 0.5%Rh/0.5%Co/Al_2O_3, were kindly provided by Johnson Matthey. Among the provided catalysts, the above-mentioned ones have been chosen in order to compare the performance of different catalyst metals as well as assess the effect of the metal loading. In order to determine their essential properties a thorough catalyst characterization was performed.

2.2.1 High-Throughput Kinetics Mechanistic Investigation (HTK-MI) set up

The HTK-MI set up, originally constructed by Zeton B.V., essentially consists of three separate sections: a feed section, a reaction section and an analysis section. In Figure 2-2, a detailed schematic overview of the HTK-MI set up is given. A process and instrument diagram i.e., P&ID, along with a process Bill of Materials (BoM) for this set up can be found in the corresponding system manual provided by Zeton B.V. [1]. The description of the set up below is organized along the sections that have been defined.

Figure 2- 1. High-throughput kinetics mechanistic investigation (HTK-MI) set up

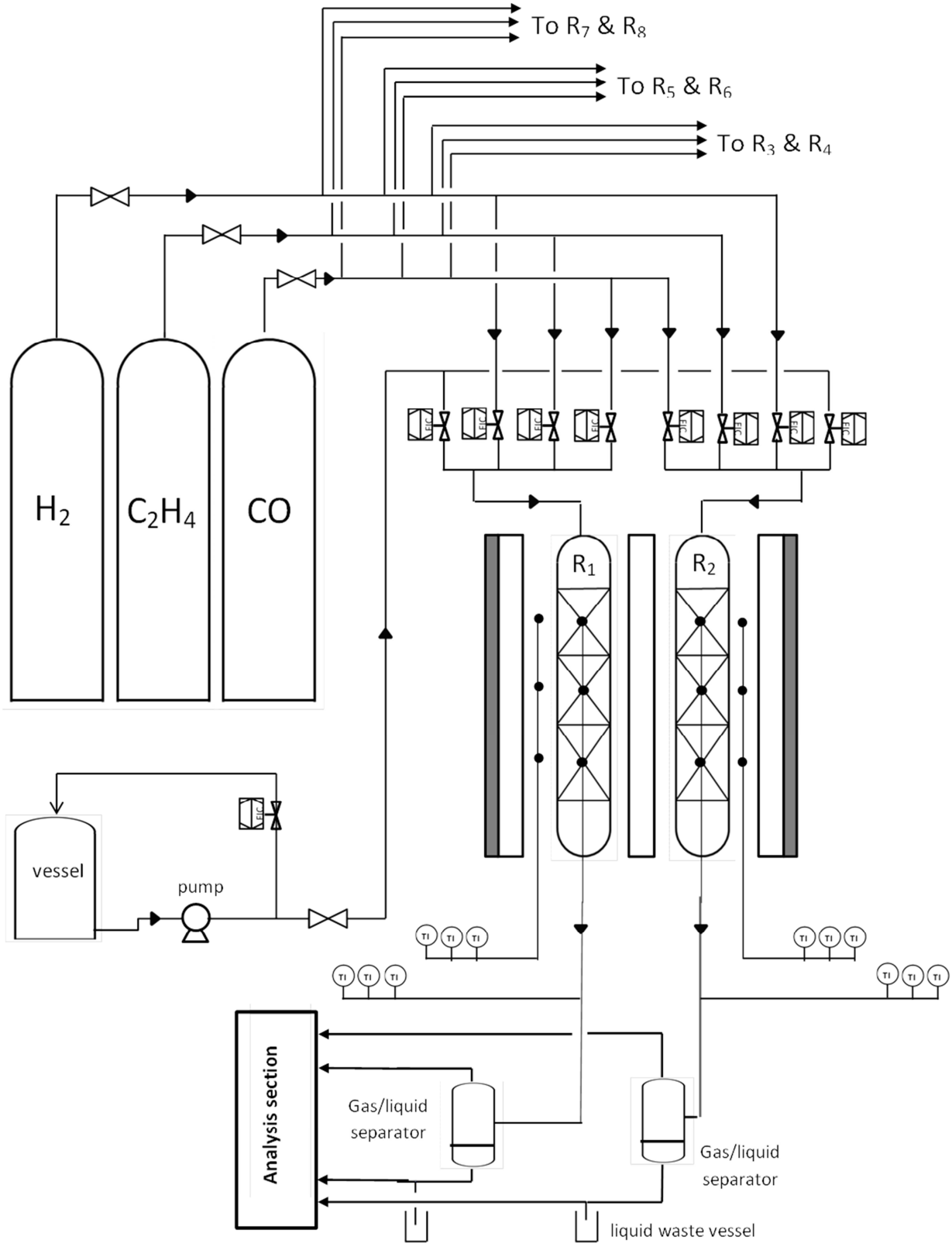

Figure 2- 2. Schematic overview of the HTK-MI set up

2.2.1.1 Feed section

The feed section contains a single liquid feed line and three gas feed lines which are used for sending complementary ranges of flow rates to each reactor individually as indicated in Figure 2-3. It allows controlling the inlet flow rates of the various reactants to each of the reactors independently.

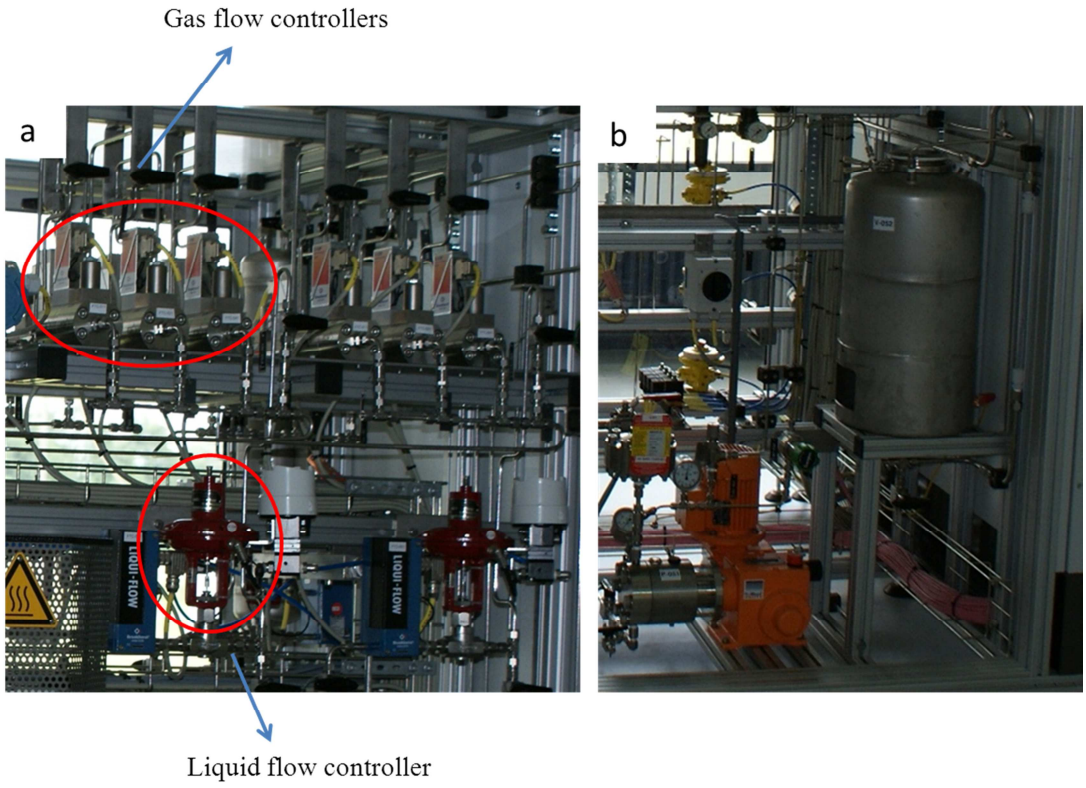

Figure 2- 3. HTK-MI set up pictures; (a) gas and liquid feed sections; (b) liquid pump section

2.2.1.1.1 Liquid feed

The liquid feed towards the reactors, as it can be seen in Figure 2-3a, comes from a stainless steel feed vessel. An auxiliary vessel equipped with a set of manually operable valves is available to refill the feed vessel without having to interrupt the continuous liquid feed to the reactor section. The vessel is equipped with the necessary lines connected to a nitrogen gas feed that, if required, can maintain the vessel under an inert nitrogen atmosphere. The nitrogen pressure in the drum can be regulated manually. The HTK-MI set up is equipped with one plunger-diaphragm dosing pump which pressurizes and feeds a liquid reactant to all liquid mass flow controllers. A pulsation damper helps to ensure a constant flow rate from the pump. This pump has a maximum capacity of 1.85 *Nl/hr* and an internal pressure safety valve

set at 225 bar. The same feed is sent to all the reactors, however, as already indicated above, the feed flow rate can be set individually per reactor. Before entering the reactor, the liquid feed is mixed with the gas feeds. This occurs after passing a check valve which prevents backflow from the reactor.

2.2.1.1.2 Gas feed

In total, five gas lines are available to the set up, i.e., two "auxiliary lines" and three "gas feed lines". The auxiliary lines are not shown in Figure 2-2 for the sake of its simplicity. These auxiliary lines are used to build up pressure in the reactors and to vent the lines, when necessary. Three Bronkhorst EI-Flow Coriolis mass flow controllers are installed per reactor. These gas mass flow controllers have complementary operating ranges, i.e., 0.2 to 10 *Nl/hr* , 2 to100 *Nl/hr* and 20 to 1000 *Nl/hr*.

The gas flow rates to each of the reactors is regulated via thermal mass flow controllers. The heart of a thermal mass flow meter/controller is a sensor, which consists of a stainless steel capillary tube with resistance thermometer elements. A part of the gas stream flows through this bypass sensor and it is warmed up by a heater. The temperature difference is directly proportional to mass flow through the sensor. These mass flow controllers are calibrated for different reference gases. The line with max 10 *Nl/hr* is calibrated for methane, the line with max 100 *Nl/hr* for hydrogen and the line with max 1000 *Nl/hr* for nitrogen. In case an alternative gas phase reagent is to be used, a corresponding conversion factor needs to be determined. This can easily be done by using a software that is available by Fluidat® [25]. Such a conversion factor is related to the heat capacity (C_p, *J/kg.K*) and the normal density (d_n, *kg/m³)* of the operation and calibration fluids as follows:

$$C_f = \frac{C_{p,1} d_{n,1}}{C_{p,2} d_{n,2}} \qquad \text{Eq. 2-1}$$

The indices refer to the operation fluid (F_{v1}) and the calibration fluid (F_{v2}), respectively. As the mass flow rate for a thermal mass flow controller is directly proportional to ($d_n \times C_p$), the equation 2-1 can be written as:

$$F_{v2} = \frac{F_{v1}}{C_f} \qquad Eq.\,2-2$$

2.2.1.2. Reaction section

Reactor tubes are made out of AISI 316 cold worked steel with dimensions of 890mm height and 11mm internal diameter. The reactors are capable of operating up to 650˚C and 15 MPa, i.e., far beyond the operating range as required for hydroformylation. A three-zone reactor temperature control was established. Heating of the reactor occurs in a furnace with heating elements spread over these three zones. The actual temperature of the catalyst bed is measured by an internal three-point thermocouple. An additional thermocouple is installed at the outer reactor wall and the temperature is controlled based on temperatures measured by this thermocouple. In order to avoid excessive temperatures in the reactor, a set of thermocouples are linked with a temperature safety switch. The latter is connected to an alarm node which will trigger a signal to stop heating when the maximum temperature is exceeded.

The reactants are mixed before entering the reactor, see Figure 2-2. A single feed line, containing the mixed feed, centrally enters the reactor from the top to ensure an equal flow distribution in the catalyst bed. The reactor pressure is ensured by means of a back pressure regulator. The operation of the set up was controlled by means of Labview software that will be discussed in section 2.2.1.4.

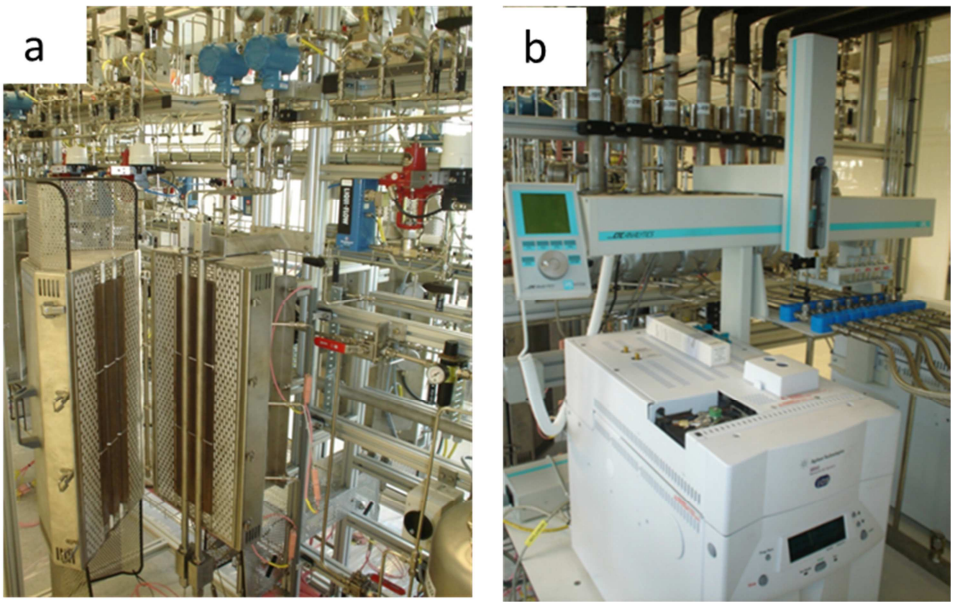

Figure 2- 4. HTK-MI set up pictures; (a) reactor block with its insulation and tracing system; (b) GC analyzer and its robotic arm for liquid streams

2.2.1.3. Analysis section

The reactor effluent is sent to a gas/liquid separator. This separator is insulated and traced, and can be heated up to 40°C. The column separates the potentially formed liquids from the gas phase effluent and, hence, ensures that no condensable components are sent to the μGC. Gas and liquid samples can be taken after the separation column. Liquid phase samples can be taken using a robotic arm system and injected into one of the two gas chromatographs, see below. Gas samples can be taken from the 8 effluent lines from the 8 reactors and 1 of the auxiliary lines by means of a 10-way valve and are sent towards the μGC. A schematic overview of the analysis section is presented in Figure 2-5.

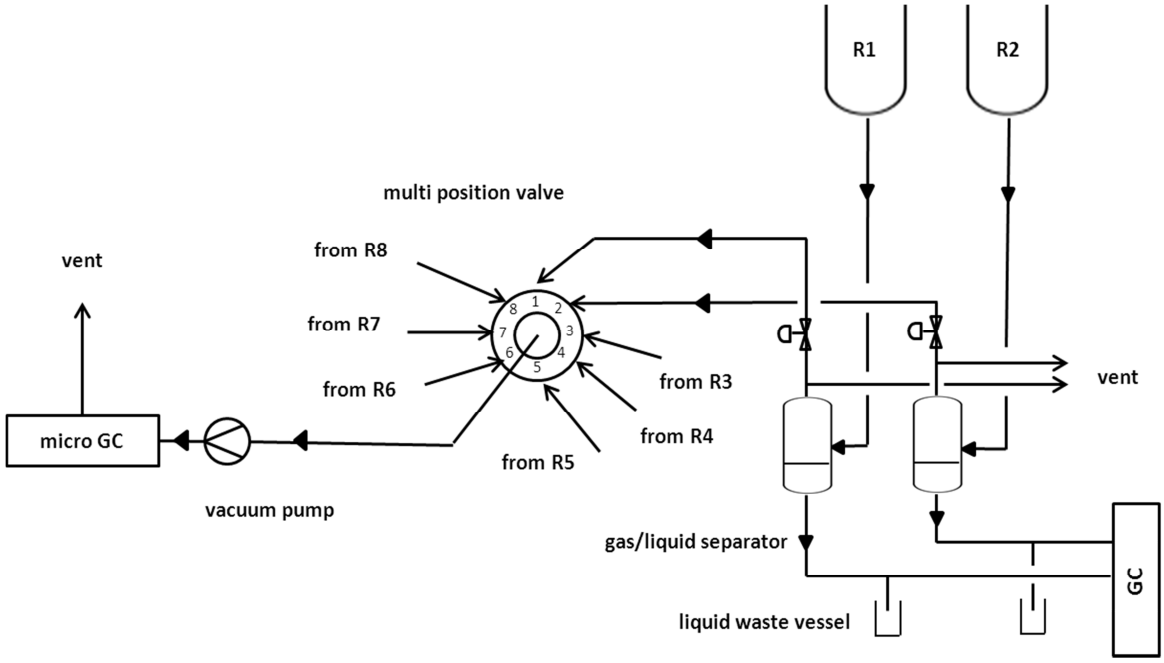

Figure 2- 5. Schematic overview of the analysis section

Two gas chromatographs i.e., Agilent Technologies 6850 series II are available in the HTK-MI for the analysis of the liquid reactor effluent. The acquired chromatograms are processed by means of the EZ Chrom software. As mentioned before and can be seen in Figure 2-4b, sampling of the reactor effluent and injection of the corresponding samples into the GCs can occur automatically by means of a GC PAL robotic arm which is operated by a separate software package. The GCs have the following specifications:

- Oven
    - Accuracy: ±1°C from the set point

    - Temperature program with heating rates up to 120°C/min
- Inlet
    - Connection of 4 gas lines (He, N_2, H_2 and air)
    - Maximum inlet temperature of 375°C
    - Split fraction possible
- Detector
    - Flame ionization detector (FID)
    - Maximum temperature of 375°C
    - Maximum sampling frequency of 200 Hz

The gas effluent from the reactor are analyzed by an Agilent 3000 micro GC (μGC). A ten way valve in the set up determines which reactor effluent is sent towards the μGC. A vacuum pump then, sucks the sample towards the instrument for analysis. The μGC is controlled by means of the same EZ Chrom software.

The μGC is a compact device which contains 4 GC columns and corresponding detectors and has run times typically below 5 minutes:

- Detectors
    - Thermal conductivity detectors (TCD)
    - Maximum temperature of 180°C
    - Detection limit < 10 ppm
    - Maximum sampling frequency of 200 Hz

- 4 Columns with TCD's
    - Channel A = molar sieve 5A PLOT column (10 m x 320 μm x 12 μm)
    - Channel B = PLOT U column (8 m x 320 μm x 30 μm)
    - Channel C = Alumina PLOT column (10 m x 320 μm x 8 μm)
    - Channel D = OV-1 column (10 m x 150 μm x 2 μm)

It is very advantageous to keep the whole products in the gas phase since it allows a fast and easy analysis of the reactor outlet effluent. The presence of a liquid phase would require additional sampling and more complex data treatment. Therefore, all downstream lines of the reactor are equipped with a tracing system. The gas effluent lines to the μGC are also traced for this reason. Temperatures up to 40^0C can be maintained by this tracing system.

In the case that the experimental products contain liquid effluent, that liquid is collected in separate storage vessels per reactor. The vessel's mass is continuously monitored with an electronic balance with an accuracy of 0.5 g. The evaporated gas from the liquid in the storage vessel can go to the central vent or mixed with the gas phase effluent of the separation column by means of a three – way valve.

2.2.1.4. Operational software and procedure

Operating the HTK-MI set up is done via a control software package developed in labview. This program, with its graphical user interface, has different screens for the feeds, reactors, products storage, safety and shutdown. Corresponding screenshots of these different sections are given in Figure 2-6, 2-7, 2-8 and 2-9. It is also possible to insert a sequence of operating instructions and to generate a history of the alarms and other events. The control software allows a continuous operation of the set up, including overnight experimentation and, in principle, even during the weekend, as far as feed vessel content and feed flow rates are adjusted to each other.

Figure 2- 6. Home page of Labview software

The feed section, see Figure 2-7, comprises three parts, regulating the gas and liquid feeds to the reactors and the analysis section.

In order to use a gas feed, the pneumatic valves must be opened via the corresponding icons. The pneumatic valve on the nitrogen line for manipulation of the back pressure regulators must be also opened to allow pressure buildup in the reactors. The reactor effluent line from which a gas sample has to be taken can be selected via this software page. The μGC vacuum pump must also be activated before taking a sample. The corresponding software screen and icons are shown in Figure 2-7.

Operating the reactor section is done with the screen shown in Figure 2-8. Inlet flow rates, temperature and pressure of the reactor block can be set via this page. The desired values for inlet flow rates for each of the reactors in the block can be separately entered in the corresponding set point boxes.

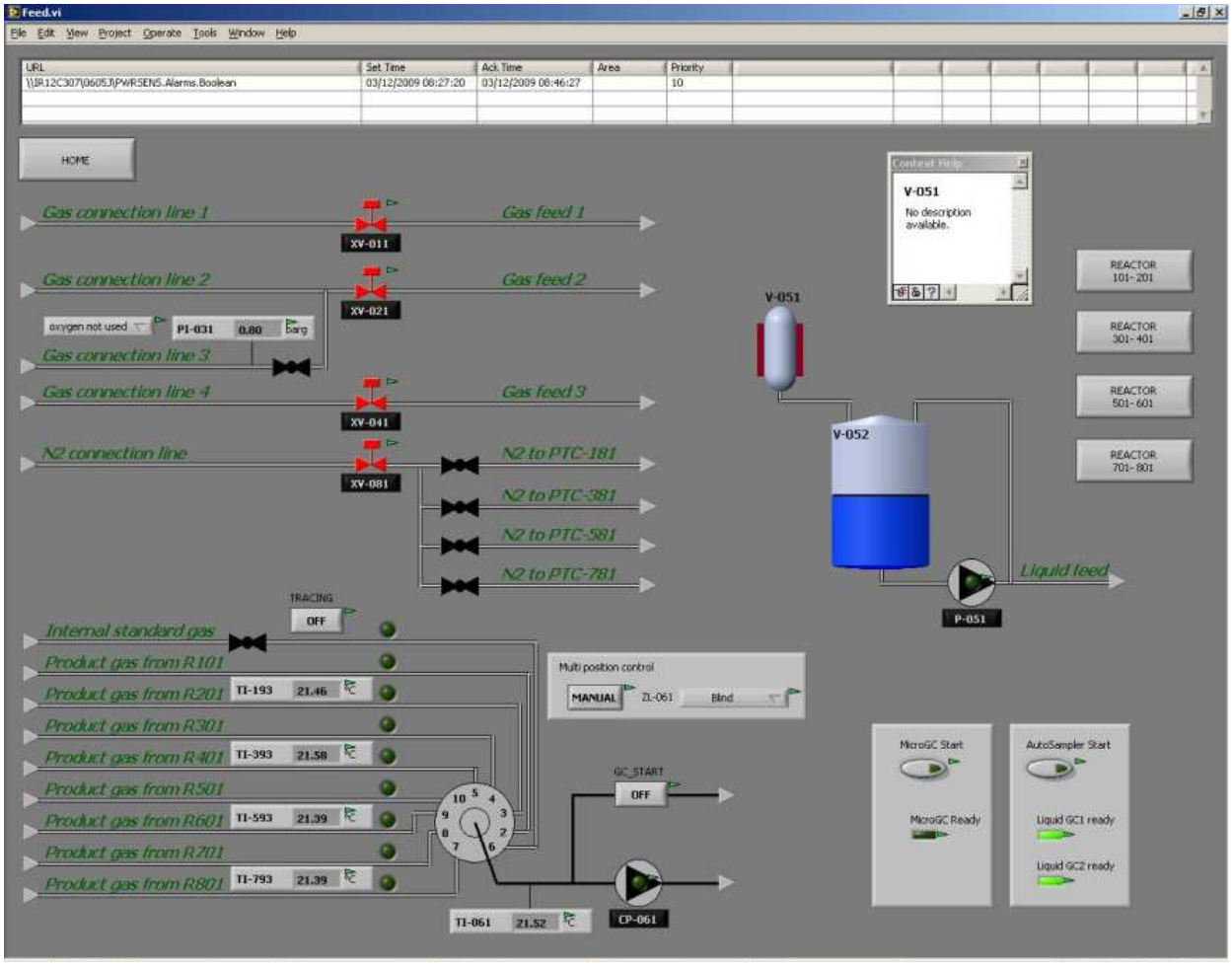

Figure 2- 7. Feed section of Labview software

To control the axial temperature profile in the reactors, the temperature is measured in three zones at different heights. The desired temperature value can be adjusted per temperature zone as it is depicted in Figure 2-8. The desired reactor pressure is simply entered in the corresponding set point box.

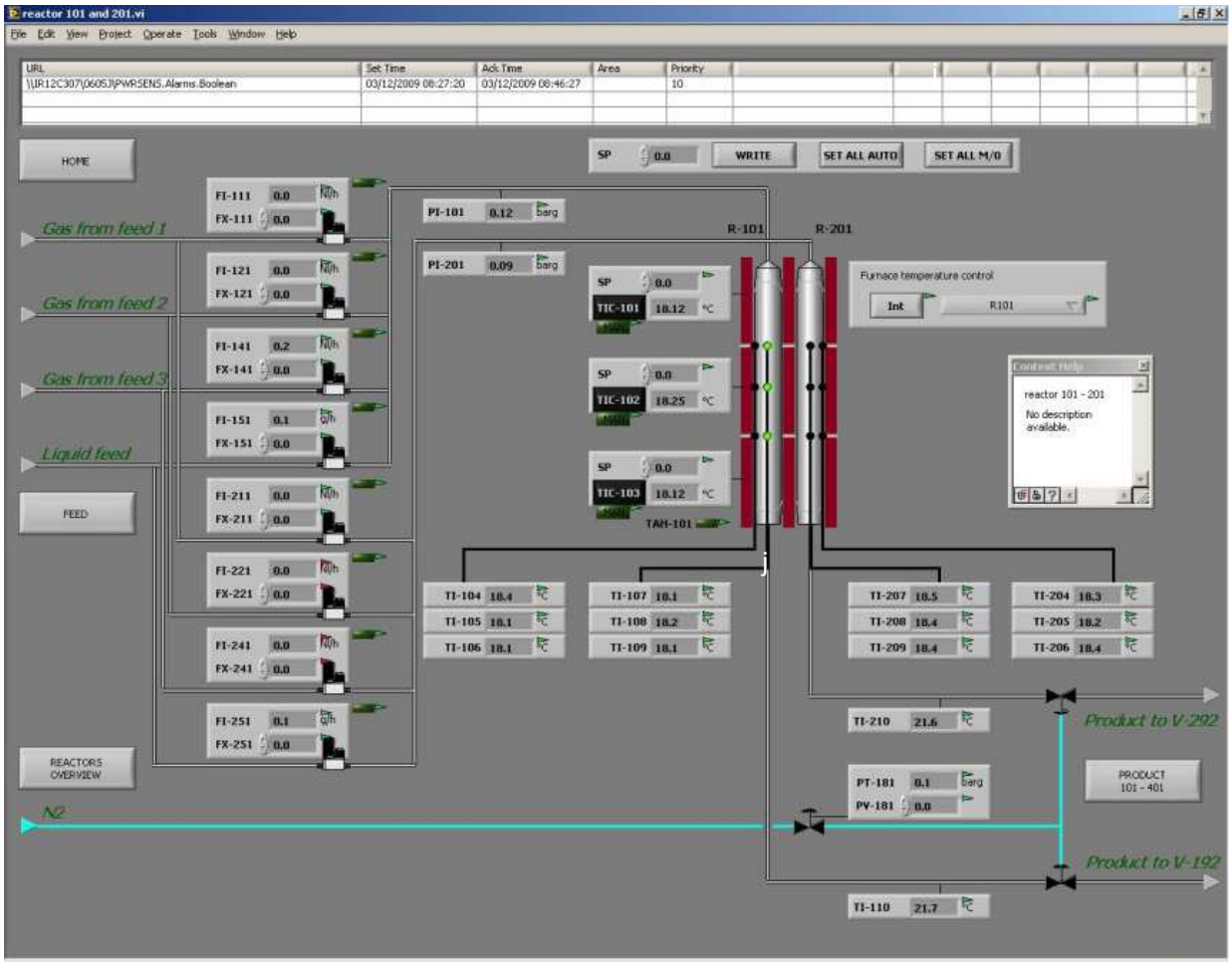

Figure 2- 8. Reactor section of Labview software

Figure 2-9 shows the corresponding control screen for the separation columns and liquid waste storage tanks. The temperature of the gas/liquid separators can be adjusted to a maximum of 40°C. The net weight of each liquid product in the vessels can be also monitored here.

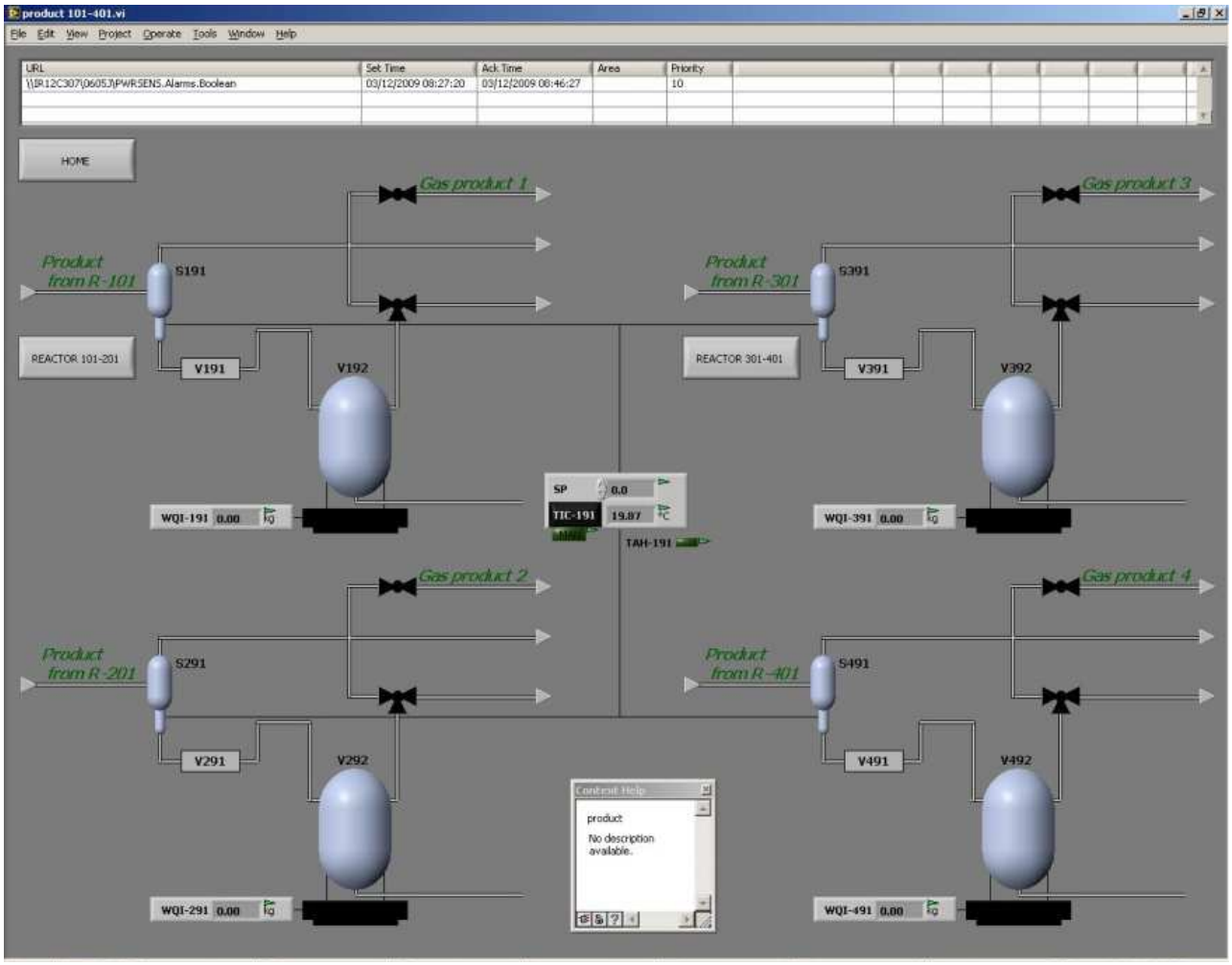

Figure 2- 9. Labview software control page for the gas/liquid separators and liquid waste storage tanks

2.2.2 Catalysts

2.2.2.1. Filling of the reactor with catalyst

To load a reactor with catalyst it must be detached from the reactor block. Before doing so, the reactor must be carefully flushed with inert nitrogen at ambient pressure. Subsequently, the reactor must be unscrewed at the two locations indicated in Figure 2-10. The corresponding thermocouples at the bottom of the reactor must also be disconnected. After decoupling the reactor from the lines, the reactor tube can be lifted from the heating block. As will be discussed later in more detail, the bottom of the reactor must be filled with inert materials. While doing so, the inner thermocouple must remain centrally located in the reactor tube. Before reinstalling the reactor, the correct position of the thermocouple in the heating

block should be verified. Leak testing with high pressure nitrogen must be carefully done before sending any chemical through the reactor.

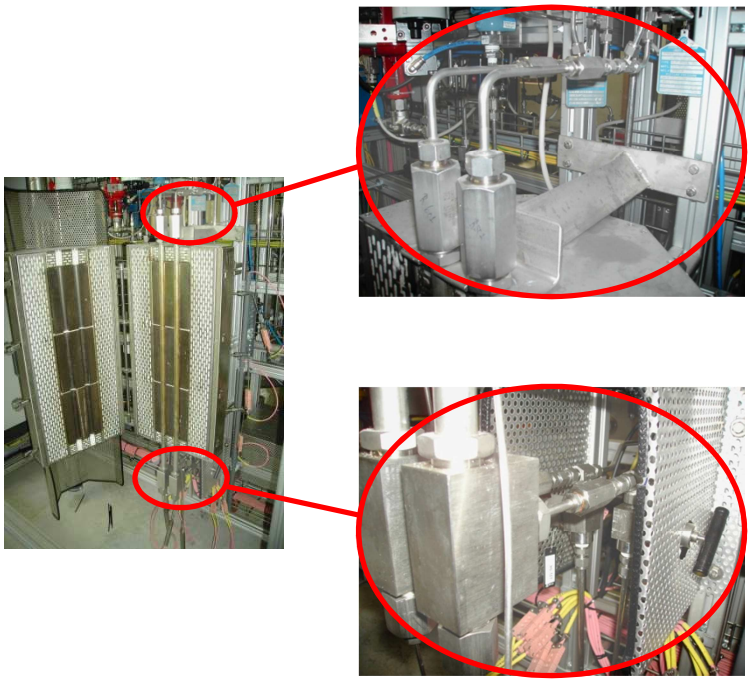

Figure 2- 10. Uncoupling the reactor tube and its thermocouples

The investigated catalysts were received as powders. Before loading the reactors with the catalysts, the latter were pelletized to avoid significant pressure drop over the catalyst bed as well as entrainment of dust towards the effluent lines. The catalyst particle diameter is directly related to the required diffusion length to reach the active sites and the pressure drop which increases with decreasing the catalyst particle size [16, 26]. It is, hence, evident that an optimal particle diameter for intrinsic kinetics measurements exists. In this work, between 10 and 20 g of 5%Rh on Al_2O_3, 1%Co on Al_2O_3 and 0.5%Rh-0.5%Co on Al_2O_3 was pelletized. The fraction with a diameter between 0.3 and 0.5mm was retained and diluted with an identical mass of inert material, α-alumina, prior to loading into the reactor tubes of the HTK-MI set up. This particle diameter was initially selected based on previous experience with other reactions and confirmed by considering the necessary correlations to ensure that the observations are not affected by mass or heat transfer limitations, see also Section 2.2.5.

In order to pelletize a catalyst to the desired size range, the catalyst powder was loaded between two Teflon plates and placed on the hydraulic press, see Figure 2-11-a. The pressure relief valve of the unit was closed and a pressure between 12 to15 bars is applied for about 5 minutes to make a catalyst disc. By using two sieves with different mesh sizes (300 μm and

500 μm) the catalyst pellets with the desired size range can obtained. The sieving procedure started by breaking the disk obtained after pelletizing and placing the fragments on the top sieve of this instrument. These sieves, on top of a fine particles collector, were placed on a vibrating plate at 60 Hz for 5 minutes, see Figure 2-11-b. The catalyst pellets caught on the top of the 300 μm sieve were collected, while the fines were pressed again to make another catalyst disc.

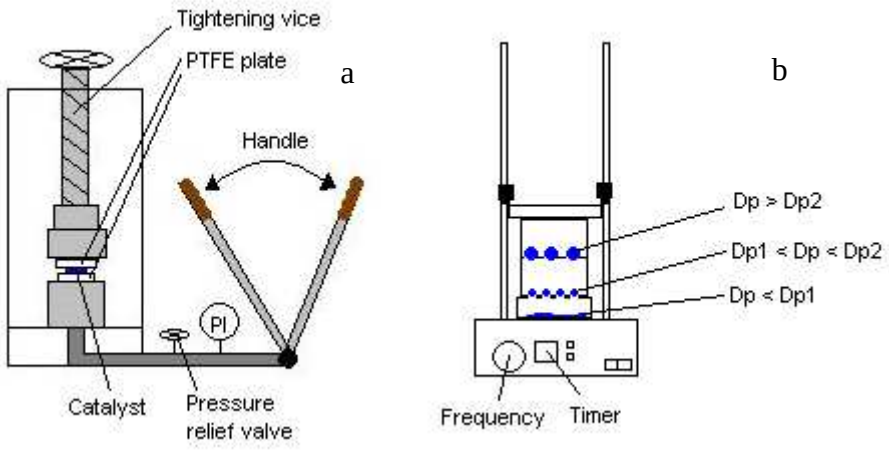

Figure 2- 11. Catalyst pelletizing instruments (a) Hydraulic press (b) Sieves on the vibrator

While loading the catalyst bed into the reactor, it was aimed at being positioned at the bottom of the second and the top of third heating zone, see Figure 2-12. The bottom of the reactor contains medium sized inert material, which serves as a support for the fine inert bed above it. These fine inert particles have the same size with the catalyst pellets in order to provide a better support for the catalyst bed. The fine and medium inert materials at the top of the reactor tube serve as entrance region to the catalyst bed in which the plug flow regime is assumed and is also used to preheat the reactants to the reaction temperature before actually reaching the catalyst. Before starting the experiments, catalysts were reduced in situ with hydrogen at 673K for at least one hour.

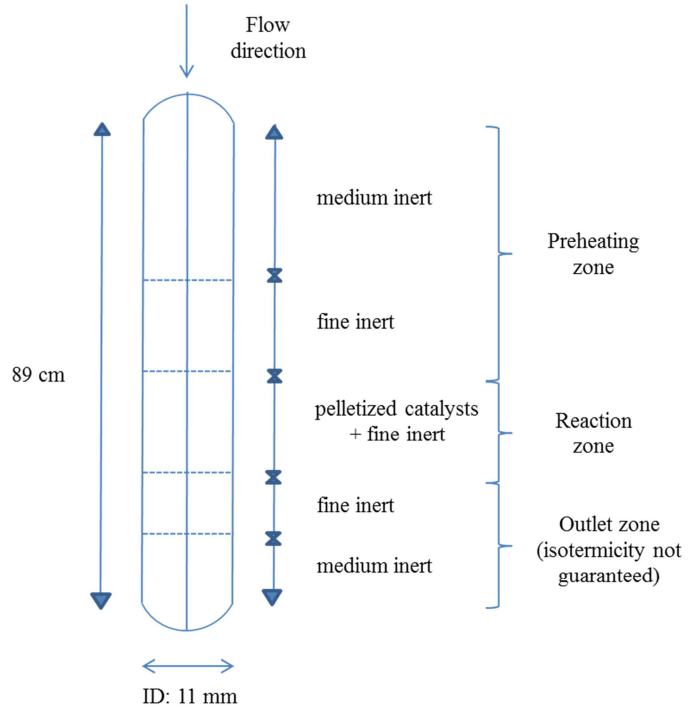

Figure 2- 12. Schematic of catalyst loading in the reactor

2.2.2.2. Catalyst characterization

Relevant catalyst properties such as total surface area (BET), average pore size, metal particle size on the catalyst surface and their corresponding fraction exposed, were determined. These values are, among others, needed to verify whether the conducted experiments at selected reaction conditions are affected by heat and/or mass transport limitations. Catalyst characterization results are also very important for understanding the hydroformylation experimental results and to assist in elucidating the corresponding reaction mechanism.

Catalysis as a commercially exploited phenomenon spans many length and corresponding time scales as indicated in Figure 2-13 for the case of the heterogeneous catalysis. At the molecular level, catalysis involves the bonding of reactant atoms or molecules on the catalyst surface to generate reactive intermediates and, subsequently, form products. The next level is that of the catalytically active phase, with dimensions typically between 1 and 10 nm, situated inside the pores of support materials with dimension in the μm range. Hence, size, shape, structure and composition of the catalyst particles, in particular of their surfaces, can be related to the activity and selectivity. The metal particles, together with their supports form the domain of catalyst preparation, characterization, laboratory scale testing and mechanistic investigation.

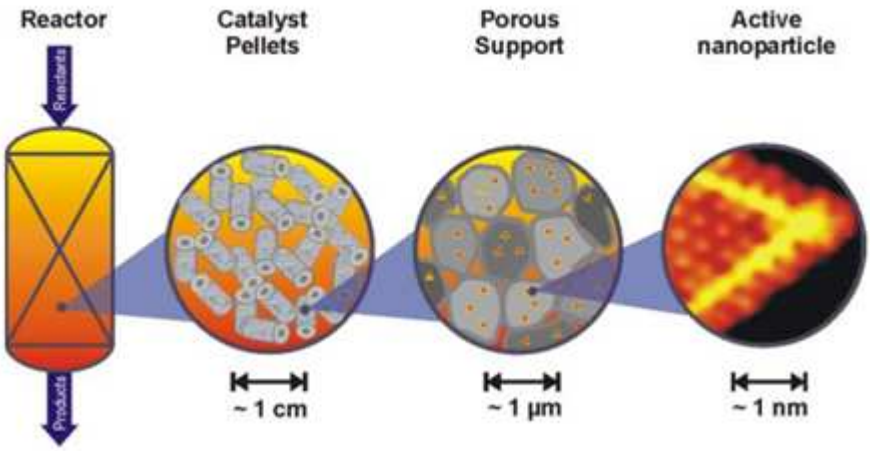

Figure 2- 13. Relevant length scales in heterogeneous catalysis [27]

2.2.2.2.1. The total surface area (BET)

The BET surface of a catalyst is an important property to compare the available area on different catalyst supports for depositing a catalytically active material. This value is obtained through non selective physical adsorption of nitrogen at a temperature of 77 K [28, 29].

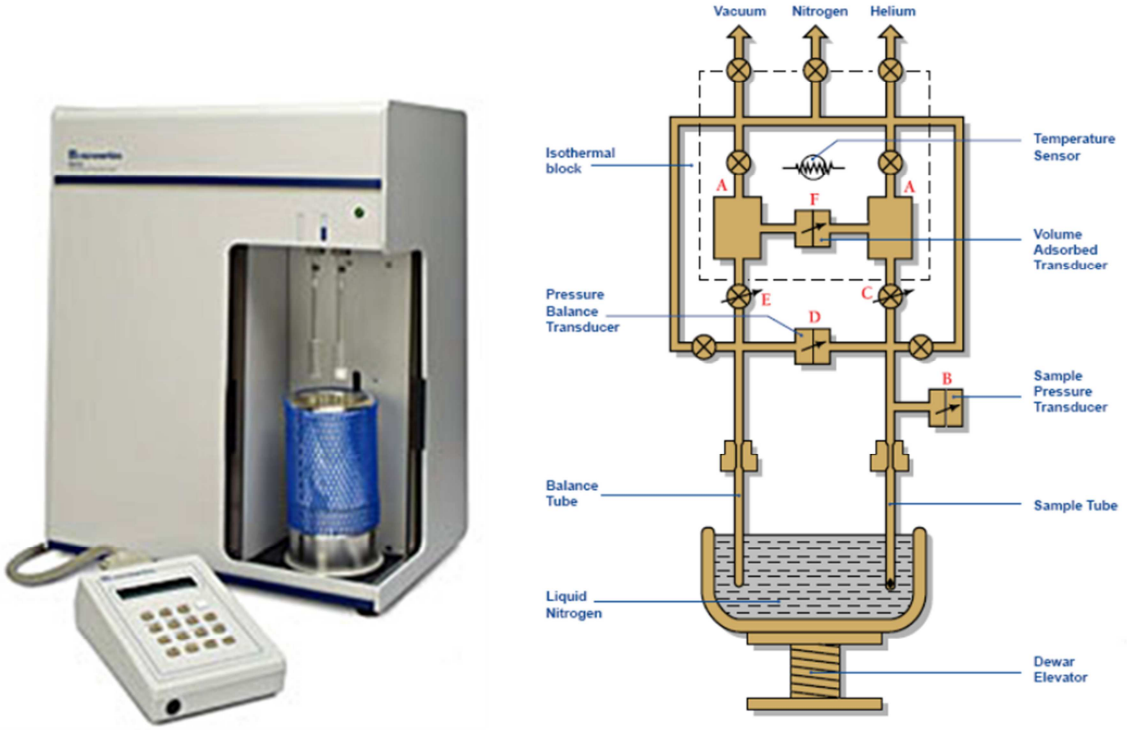

Figure 2- 14. Micromeritics Gemini module [30]

Brunauer et al, have developed a model for characterizing porous materials in general and solid catalysts in particular [29]. They proposed a model for multilayer physisorption, and derived the corresponding equation to describe it. The latter equation allows the determination of the monolayer coverage of the adsorbate from measurements of amount adsorbate vs relative pressure that was exerted.

A Micromeritics Gemini module was used to conduct this experiment. This module has an empty reference tube, a tube containing the catalyst, a vessel, a pressure indicator and a volume indicator. It is equipped with two gas feed lines for helium and nitrogen and a vacuum pump. The relative pressure was varied between 0.1 and 0.4 bar to cover the linear validity of the BET equation. This module is operated using a Stardriver software. An illustration and schematic overview of the module is shown in Figure 2-14.

2.2.2.2.2. X-ray diffraction (XRD)

The crystallinity of the samples was investigated via X-ray diffraction (XRD) measurements with a Siemens Diffractometer Kristalloflex D5000, Cu Ka radiation, in the 2 theta range from 4 to 90^0, with a step of 0.02^0.

2.2.2.2.3. Oxygen and hydrogen pulse chemisorption

Micromeritics Autochem II module, was used for pulse chemisorption experiments. This module consists of a U-shaped reactor, a thermal conductivity detector, a cold trap, 4 gas inlets for the preparation, carrier and loop gases and the appropriate valves to manipulate the various flows through the module as it is shown in Figure 2-15.

The thermal conductivity detector (TCD) in this module measures the thermal conductivity difference between two gas flows, i.e., a reference carrier gas flow and the effluent from the U-shaped reactor. Since each gas has a specific thermal conductivity, differences in thermal conductivity allow the determination of the composition of simple gas mixtures. In order to acquire an acceptable and sufficiently large signal, a combination of loop and carrier gases must be used which exhibit significant thermal conductivity differences e.g. hydrogen/argon or oxygen/helium.

Choosing the wrong combination can easily lead to indistinguishable signals from the noise on the base line. Oxygen titration experiments can be done using this module to identify the fraction of exposed metal atoms (FE) of the catalyst. FE is defined as the ratio of the number of accessible metal atoms to the total number of metal atoms. Assuming that a chemical

reaction only takes place on the catalyst surface, the total number of metal atoms needs to be corrected by the FE in the calculation of the number of available sites. This value can be obtained from oxygen titration experiments at room temperature. To do so first, the corresponding catalyst sample is reduced at 500°C with a hydrogen flow. After the reduction, helium is sent over the reduced catalyst. The reactor is left to cool to ambient temperature. Then, oxygen is sent through the pulse loop and oxygen pulses are injected in the helium stream which is going to the reactor. Oxygen pulses are sent until the peak surface of consecutive pulses does not change anymore.

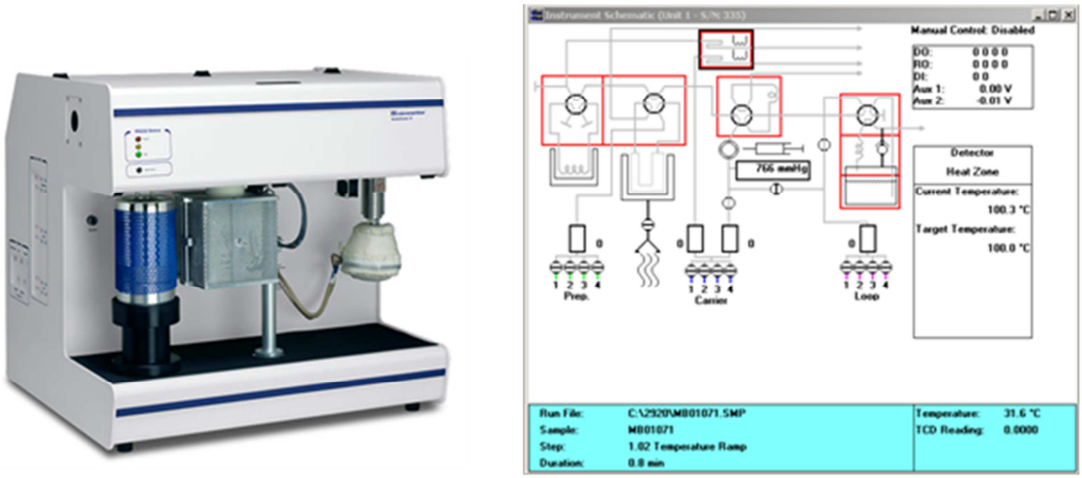

Figure 2- 15. Micromeritics Autochem II module [31]

The area difference between the first few smaller peaks and the unchanged repeated peaks allows to calculate the volume of oxygen that is chemisorbing on the catalyst at a given temperature. This volume can be calculated and related to the number of the surface metal atoms.

2.2.2.2.4. Transmission Electron Microscopy (TEM)

To have a comprehensive view on how the metal is present on the catalyst surface as well as to show that the metal was actually deposited on this surface, Scanning Transmission Electron Microscopy (STEM) measurements were performed. Transmission Electron Microscopy (TEM) tests were also conducted to measure the particle size and corresponding FE values of the metal catalysts according to the Equation 2-3 and 2-4. The fraction exposed was obtained from the relation between the particle size and dispersion as shown in these equations [32].

$$d_{rel(VS)} = \frac{d_{VS}}{d_{at}} = \frac{5.01}{FE} \qquad for\ FE < 0.2 \qquad \text{Eq. } 2-3$$

$$d_{rel(VS)} = \frac{d_{VS}}{d_{at}} = \frac{3.32}{FE^{1.23}} \qquad for\ 0.2 \leq FE \leq 0.92 \qquad \text{Eq. } 2-4$$

Where d_{VS} is the mean size of the crystallite that can be measured by performing TEM tests. d_{at} and $d_{rel(VS)}$ are the atomic diameter of the metal and the mean relative size of the metallic particles respectively.

An image of a TEM instrument and its simple schematic are illustrated in Figure 2-16. TEM samples were prepared by applying a simple immersion of a carbon-support film on a nickel grid into the catalyst powder. The excess powder was shaken off carefully afterwards. Catalyst particles that had adhered to the carbon film were investigated by different TEM modes: Conventional and high resolution (HR) TEM, electron diffraction, STEM, EDX and electron energy loss spectroscopy (EELS). A JEOL, JEM2200FS-Cs-corrected microscope was used. This microscope was operated at 200 kV and equipped with Schottky-type FEG, EDX JEOL JED-2300D and JEOL in–column omega filter. Secondary X-ray fluorescence from the analytical sample holder was eliminated by means of a beryllium retainer. However, Ni-peaks were detected in the EDX spectra due to secondary fluorescence from the Ni support grid. EEL spectra were obtained in STEM spot mode using an electron probe of 1.0 nm and objective aperture angular size of 6 mrad.

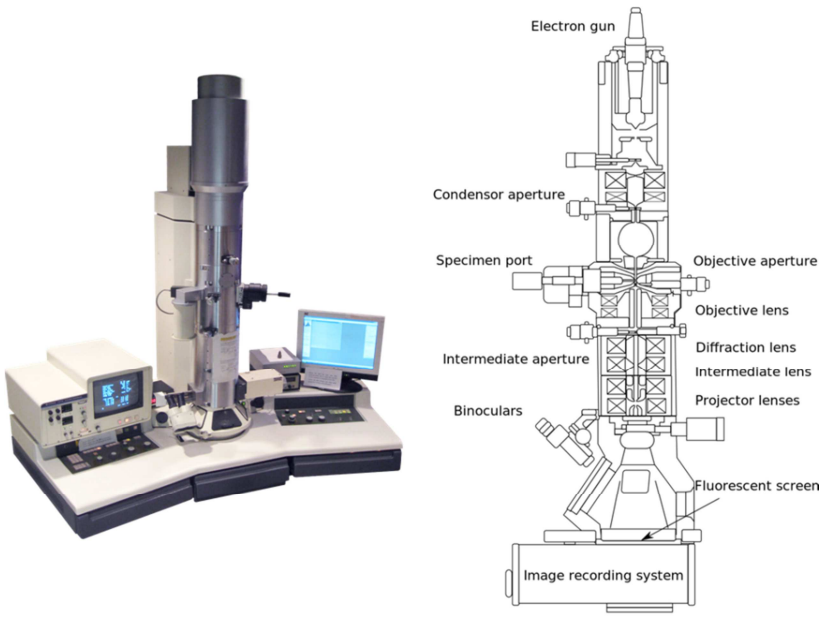

Figure 2- 16. Transmission Electron Microscopy (TEM) [33, 34]

2.2.3 Experimental operating conditions

A wide range of experimental operation conditions can be implemented using the HTK-MI set up thanks to its modern and flexible equipment and instruments. Table 2-1 presents the operating conditions applied during the experimentation as performed as part of the present work. This experimentation is aimed at comparing the performance of the three catalysts mentioned in section 2.2.2 by investigating temperature, total pressure and inlet composition effects on their hydroformylation reaction behaviour, see also Chapter 3.

Table 2- 1. Operating conditions used in the performed experimentation.

Catalyst performance				
Catalyst	Temperature (K)	Total pressure (MPa)	Space time range ($kg_{cat.}.s/mol_{C_2H_4,in}$)	$CO/C_2H_4/H_2$
$5\%Rh/Al_2O_3$ $1\%Co/Al_2O_3$ $0.5\%Rh/0.5\%Co/Al_2O_3$	473	2	5,4 to 149	1/1/1
Temperature and total pressure effect				
$5\%Rh/Al_2O_3$ $1\%Co/Al_2O_3$	448 to 498	1 to 3	2,7 to 149	1/1/1
Inlet composition effect				
$5\%Rh/Al_2O_3$	473	2	2,7 to 80	1/1/1 ; 2/1/1 1/2/1 ; 1/1/2

A typical duration of an experimental run was about two hours. When consecutive samples that were taken at 15 minutes intervals were not indicating further evolutions in the observed reaction behavior, the last measurement was taken as representative for the steady state behavior at the investigated operating conditions. Long term catalyst stability was assessed by repeating a reference experiment at regular time intervals, e.g., one every few days. Typically the catalyst activity could be maintained for 3 to 4 weeks, after which the catalyst was replaced by a fresh sample.

2.2.4 Calculation of the reactor outlet flow rates

Online effluent analysis was performed with a four channel Agilent 3000 micro gas chromatograph equipped with thermal conductivity detectors (TCDs). Hydrogen, and carbon monoxide were analysed on a molar sieve 5A PLOT column of 10m length and 0.32 inner diameter with a film thickness of 12 µm, while ethylene and ethane are detected on a PLOT U column of 8m length and 0.32 inner diameter with a film thickness of 30 µm. Heavy hydrocarbons can be detected in an Alumina PLOT column of 10m length and 0.32 mm inner diameter with a film thickness of 8 µm. Propanal, propanol and other oxygenates are only detected on the OV-1 column of 10m length and 0.15 mm inner diameter with a film thickness of 2 µm.

The effluent lines and the separation section are equipped with a tracing system that guarantees a sufficiently high temperature in that part of the set up, to avoid potential condensation of the heavier products formed, see also Section 2.2.1.3. The corresponding vessels that collect the liquid products were, nevertheless regularly verified to ensure that indeed, no liquid products were produced during the experimentation.
In this study, the internal standard method was used for the calculation of the outlet flow rates in continuous flow reactors, as it is shown in Equation 2-5, where ***A*** is the peak surface area and *CF* is the calibration factor. "*A*" and "*is*" in the dominant of this equation refers to the species *A* and internal standard, respectively. Argon was added as an internal standard to the reactor feed.

$$F_A = F_{is}\frac{CF_{is}}{CF_A}\frac{A_A}{A_{is}} \qquad \text{Eq. 2-5}$$

The corresponding calibration factors that were used in this work are those reported by Dietz [35]. The peak surface areas were determined by the control software of the µGC. The inlet flow rates, as it was discussed earlier, can be controlled and measured via the corresponding flow meters. By having the inlet and outlet reactor flow rates, the mass and element balances, e.g., for element t, can be verified using the following equations [36]:

$$\varphi_m = \frac{\dot{m}}{\dot{m}^0} = \frac{\sum_{j=1}^{ncomp} F_j M_j}{\sum_{j=1}^{ncomp} F_j^0 M_j} \qquad \text{Eq. } 2-6$$

$$\varphi_e = \frac{F_{e_t}}{F_{e_t}^0} = \frac{\sum_{j=1}^{ncomp} a_{t,j} F_j}{\sum_{j=1}^{ncomp} a_{t,j} F_j^0} \qquad \text{Eq. } 2-7$$

Where φ_m , φ_e and M_j are mass balance, element balances and molecular mass of component j, respectively, while $\dot{m}$, F_{e_t} and $a_{t,\,j}$ are mass flow rate, molar flow rate for element t and the number of t atoms in component j, respectively.
The maximum error of mass balance was less than 10% while most of the error values were below 5%. The deviations of the elemental balances were also in line with those on the total mass balance.

The conversion of component *A* (X_A) is defined as follows based on the inlet (F_A^0) and outlet (F_A) flow rates of this component:

$$X_A = \frac{F_A^0 - F_A}{F_A^0} \qquad \text{Eq. 2-8}$$

The conversion into a product *P* or molar yield of *P* (Y_P) is determined as the ratio of the outlet flow rate of this component (F_P) and carbon monoxide inlet flow rate (F_{CO}^0):

$$Y_p = \frac{F_P}{F_{CO}^0} \qquad \text{Eq. 2-9}$$

The selectivity towards a product *P*, S_P, was defined as the number of moles transformed into that product, F_P, compared to the total number of ethylene moles converted:

$$S_P = \frac{F_P}{F_{C_2H_4,0} - F_{C_2H_4}} \qquad \text{Eq. } 2-10$$

2.2.5 Calculation of site time values for the catalysts

In order to compare the catalyst performance under identical experimental conditions, the conversions will be reported versus the so-called "site time". The latter is obtained from the space time by accounting for the metal loading and the fraction of exposed metal atoms, as well as for the atomic mass.

$$Site\ time = \frac{Space\ time\ \times Metal\ loading}{M_M} \times FE \qquad \text{Eq. } 2-11$$

The value of the accessible metal atoms can be determined from the following expression:

$$Accessible\ metal\ atoms = \frac{FE \times\ Metal\ loading}{M_M} \qquad \text{Eq. } 2-12$$

2.2.6 Intrinsic kinetics measurements

Before starting the experimental work, it should be carefully verified that heat and mass transport limitations are avoided in the applied range of reaction conditions in order to allow the measurement of intrinsic kinetics. The corresponding criteria for evaluating these phenomena, as well as the assumption of the ideal plug flow, are discussed briefly in the following sections.

Observed reaction kinetics correspond to the intrinsic regime if they are not affected by heat and mass transport limitations nor by reactor hydrodynamics non-idealities. These transport phenomena are scale dependent i.e., their impact on observed kinetics is ought to be different at the laboratory compared to at the industrial scale. A reactor that is implemented to measure intrinsic kinetics is usually a continuous reactor that operates at steady state conditions and at a constant pressure and temperature. In the current work, a packed bed plug flow reactor was used to investigate the heterogeneous ethylene hydroformylation. This reactor type easily allows conversion versus space time measurements by varying the flow rates or the catalyst amount in the reactor.

The potential occurrence of concentration and temperature gradients over the external layer around the catalyst pellet must be carefully considered since they are equivalent with the establishment of a mass and heat transport limited regime in which the observed kinetics deviate from the intrinsic ones. A series of the proper correlations by Berger et al [37] was used to investigate the intrinsic kinetics character of the experiments performed in this work.

2.2.6.1 Mass transport limitations

2.2.6.1.1 External mass transport limitations

External mass transport limitations entail that the rate of reactant transport towards and of product transport away from the catalyst surface is one of the limiting factors that affects the overall observed reaction rate. The following criterion has been suggested by Mears for being able to neglect this phenomenon [18]:

$$Ca = \frac{R_{v,A}}{k_f\ a_v C_{A,b}} = \frac{C_{A,b} - C_{A,s}}{C_{A,b}} < \frac{0.05}{n} \quad (n > 0) \qquad \text{Eq. } 2-13$$

Where *Ca* is the Carberry number and *n*, $C_{A,b}$ and $C_{A,s}$ are the reaction order, the concentration of component *A* in the bulk and at the external catalyst surface respectively.

$R_{v,A}$ is the observed volumetric reaction rate per unit of catalyst pellet volume, k_f is the mass transfer coefficient between the pellet and the fluid bulk and a_v is the specific external surface area of one catalyst pellet.

2.2.6.1.2 Internal mass transport limitations

Apart from external mass transport limitations, the diffusion of species in the internal channels of the catalyst pellet can also become an important factor determining the observed reaction rate. In order to be able to neglect such internal diffusion limitations, the Weisz-Prater criterion, Equation 2-14, must be met [16]:

$$\Phi = \left[\frac{n+1}{2}\right]\frac{R_{v,A}\left(d_p/6\right)^2}{D_{A,eff}\ C_{A,s}} \ < \ 0.33\ if\ n = 0\ ;\ 0.08\ if\ n \geq 0.5 \qquad \text{Eq. } 2-14$$

Where Φ and $D_{A,eff}$ are Weisz modulus and effective diffusivity of component *A* in the pellet respectively, d_p represents the catalyst pellet diameter.

The effect of the internal mass transfer can be also investigated by conducting some experiments with different particle sizes of the same amount of catalyst. Internal mass transport limitations can be neglected as long as the reaction rate remains constant with the catalyst particle size.

2.2.6.2 Heat transport limitations

2.2.6.2.1 External heat transport limitations

For significantly endothermic or exothermic reactions, insufficient heat transfer towards or away from the catalyst pellets can result in hot or cold spots in the catalyst bed. This phenomenon will impact on the (observed) reaction rate. The following criterion has been suggested by Mears in which the temperature difference over the film surrounding the catalyst pellet must remain below a threshold value to allow safely neglecting external heat transport limitations in the reaction [20]:

$$\Delta T\ (film) = \frac{R_{v,A}|\Delta_r H| d_p}{6\ \alpha_p} \ < \frac{0.05 R T_f^2}{E_a} \qquad \text{Eq. } 2-15$$

With $\Delta_r H$ and α_p the reaction enthalpy and heat transfer coefficient between pellet and bulk respectively. T_f refers to the temperature of the fluid within the bed and E_a is the apparent activation energy.

2.2.6.2.2 Internal heat transport limitation

The last concern when dealing with the heat transfer phenomena is the heat transfer inside the catalyst particle. Mears has suggested the following criterion to neglect the effect of internal heat transport limitations [20]:

$$\Delta T = \frac{R_{v,A}|\Delta_r H| d_p^2}{60\lambda_p} < \frac{0.05 R T_f^2}{E_a} \qquad \text{Eq. } 2-16$$

ΔT is the difference between the temperature at the catalyst surface and the average temperature in the pellet. λ_p refers to the catalyst pellet heat conductivity.

2.2.6.3 Ideal plug flow

In the plug flow regime, it is assumed that the fluid velocity is constant along any cross-section of a tubular reactor. The hydrodynamics in a Plug Flow Reactor (PFR) can be regarded as a series of infinitely thin plugs, each of them having a radially uniform composition and moving along the axial direction of the reactor without any exchange of heat and or mass between consecutive plugs. As a result, while it is assumed in the PFR that the fluid is perfectly mixed in the radial direction this is not a case in the axial direction. Criteria have been developed in order to validate the assumption of the plug flow regime [38]. These criteria will be briefly described in the following parts. A schematic representation of an ideal plug flow pattern in a tubular reactor is given in Figure 2-17.

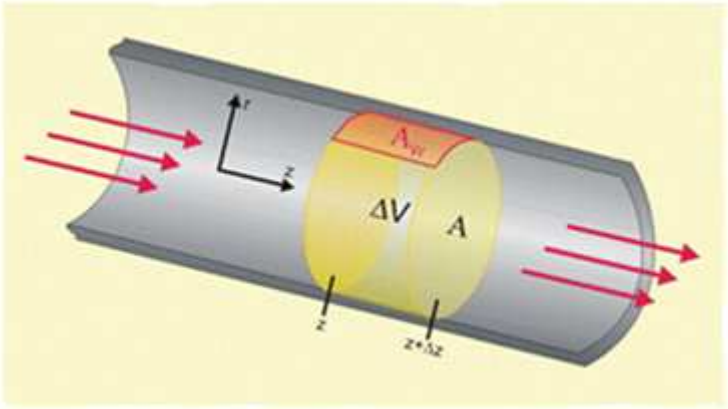

Figure 2- 17. Ideal plug flow in a tubular reactor [39]

2.2.6.3.1 Axial dispersion

The first criterion that must be satisfied to be able to assume ideal plug flow behavior is related to the back mixing phenomenon in a tubular reactor. Back mixing is defined as the axial diffusion-like movement of reactants and/or product molecules in the reactor superimposed on the convective flow. This phenomenon leads to a broadening of the residence time distribution for the species along the reactor, in contrast with the ideal plug flow regime in which a unique residence time occurs. Hence, in the case of a positive reaction order, a reactor with axial diffusion must be longer than a reactor with ideal plug flow to obtain the same conversion.

Mears and Gierman suggested a criterion, i.e., Equation 2-17, for assessing the assumption of the plug flow regime [38]:

$$\frac{L}{d_p} > \frac{8}{B_o}\, n\, ln\left\{\frac{1}{1-x_A}\right\} \qquad \text{Eq. } 2-17$$

With L, d_p and X_A the catalyst bed height, catalyst pellet diameter and component conversion respectively. B_o is Bodenstein or the Péclet number i.e., Pe_p, for the axial mass transport that is defined as:

$$B_0 = Pe_p = \frac{d_p u_0}{D_{A,ax}} \qquad \text{Eq. } 2-18$$

With u_0 and $D_{A,ax}$ the superficial fluid velocity and axial dispersion coefficient respectively.

A commonly used rule of thumb for considering this regime is based on the assumption that effective axial diffusion can be neglected when:

$$\frac{L - L_{ideal\ plug\ flow}}{L} < 0.05 \qquad \text{Eq. } 2-19$$

Which ultimately translates into the practical guideline [16]:

$$\frac{L}{d_p} > 50 \qquad \text{Eq. } 2-20$$

2.2.6.3.2 Radial dispersion

Another reason which can cause deviations from the plug flow regime is a lower concentration of the catalyst particles near the reactor wall that results in a radial velocity profile inside the reactor. The velocity near the wall is then significantly higher than in the center of the catalyst bed, which consequently affects the reactor performance. The ratio between the catalyst bed diameter, d_t, and the catalyst pellet diameter, d_P, determines if such effects can be neglected or not [38]:

$$\frac{d_t}{d_p} > 8 \qquad \text{Eq. } 2-21$$

The threshold value of 8 is a matter of debate, since alternative sources have suggested a minimum of 10 to 20 for neglecting radial dispersion effects [16]. If the above criterion is not fulfilled, considerable bypassing of the fluid through the void spaces close to the reactor wall compared to the centre can be expected.

2.2.6.3.3 Radial heat transport limitations

The reactor wall of a non-adiabatic reactor is in contact with a heating and/or cooling medium. A radial temperature profile may develop during reaction depending on factors such as the reaction enthalpy and the conductivity of the catalyst bed. Since the reaction rate highly depends on the temperature, such a radial temperature profile, if developed, will have a considerable effect on the observed kinetics. In order to be able to neglect such an effect, Mears proposed the following criterion, Eq. 22 [20]:

$$\Delta T = \frac{R_{v,A}|\Delta_r H|(1-\varepsilon_b)(1-b)d_t^2}{32\ \lambda_{er}} < \frac{0.05RT_w^2}{E_a} \qquad \text{Eq. } 2-22$$

ΔT being the difference between the wall temperature, T_w, and the average temperature in the bed. In the above equation, d_t, b, ε_b and λ_{er} are the bed diameter, volume of inert material as

fraction of total solids, bed porosity and effective radial bed thermal conductivity respectively. Many empirical correlations are available in literature to find the λ_{er}. [21, 40].

Also an experimental verification can be used to assess the extent of radial heat transfer limitations in the reactor. To experimentally investigate the presence of such temperature gradients in the reactor, the amount of the inert material can be increased in the catalyst bed. If temperature gradients are present, lower conversions for the exothermic and higher conversions for the endothermic reactions should be obtained.

2.2.6.4 Pressure drop in the catalyst bed

In the case that the pressure drop in the catalyst bed becomes too high, the assumption of plug flow regime, which considers a constant density through the reactor tube, is no longer valid. In this case the number of moles significantly varies between consecutive 'plugs' and, hence, the integration over the entire reactor is not straightforward.

To determine the pressure drop, Δp, over the axial direction in the catalyst bed of a PFR, the following relation can be used:

$$\frac{\Delta P}{L} = \frac{f_m \rho u^2}{d_p} \qquad \text{Eq. } 2-23$$

With ρ and u the density of the gas stream and the gas flow velocity respectively. In the above equation, f_m, is defined as modified friction factor.

The equation developed by Ergun [26] can be used to calculate the modified friction factor:

$$f_m = \frac{(1-\varepsilon_b)}{\varepsilon_b^3}\left(1.75 + 150\frac{(1-\varepsilon_b)}{Re}\right) \qquad \text{Eq. } 2-24$$

In which, ε_b is the bed porosity and Re is the Reynolds number that is defined as:

$$Re = \frac{d_p u}{\mu} \qquad \text{Eq. } 2-25$$

With μ refering to the dynamic viscosity of the corresponding flow in the reactor.

To assume no pressure drop in the reactor, next condition must be fulfilled [37].

$$\Delta P < \frac{0.2 P_{tot}}{n} \qquad \text{Eq. } 2-26$$

2.3 Modeling procedures

The determination of the adjustable parameters in the Single Event MicroKinetic (SEMK) model for ethylene hydroformylation is performed by regression to the experimental data obtained on rhodium and cobalt based catalysts. The regression analysis, the reactor model and a short description about the information flow in microkinetic modelling will be described in what follows.

2.3.1 Regression analysis

2.3.1.1 Parameter estimation method

The adjustable model parameters are estimated by minimizing the following objective function ***SSQ(β)*** with respect to the model parameter vector β:

$$SSQ(\beta) = \sum_{j=1}^{n_{resp}} \sum_{k=1}^{n_{resp}} \sigma^{jk} \sum_{i=1}^{n_{ob}} (Y_{ij} - \hat{Y}_{ij})(Y_{ik} - \hat{Y}_{ik}) \xrightarrow{\beta} min \qquad \text{Eq. 2-27}$$

With Y_{ij} and Y_{ik} the j^{th} and k^{th} experimental response values in the i^{th} observation, respectively, $\hat{Y}_{ij}$ and $\hat{Y}_{ik}$ the calculated j^{th} and k^{th} response values for observation i, and σ^{jk} is the element for the j^{th} and the k^{th} responses of Σ^{-1}, the inverse of the error covariance matrix Σ on the experimental observations.

$$\Sigma = \{\sigma_{jk}\} = \begin{bmatrix} \sigma_{11} & \sigma_{12} & . & . & \sigma_{1nresp} \\ \sigma_{21} & \sigma_{22} & . & . & \sigma_{2nresp} \\ . & . & . & . & . \\ . & . & . & . & . \\ \sigma_{nresp1} & . & . & . & \sigma_{nrespnresp} \end{bmatrix} \qquad \text{Eq. 2-28}$$

where, the elements σ_{jk} are calculated as follows:

$$\sigma_{jk} = (Y_j - \hat{Y}_j)(Y_k - \hat{Y}_k)/(nob \times nresp - npar) \qquad \text{Eq. 2-29}$$

Multi-response Rosenbrock and Levenberg-Marquardt algorithms [41, 42] were successively used in the minimization of the above-mentioned objective function. In order to do so, first an in-house implementation of the more robust Rosenbrock methodology was employed to find an adequate direction leading to the potential, global optimum and afterwards the more efficient Levenberg-Marquardt algorithm was applied when the intermediate estimates are believed to have sufficiently approached the optimal parameter values. The latter algorithm

was used as implemented in the ODRPACK package [43] that is available in the NETLIB software library [44]. The applications of these algorithms were modified and reviewed in a LCT internal memo by P. Reyniers [45].

The model performance can be evaluated using parity diagrams in which the simulated values are plotted on the y-axis against the experimental values on the x-axis. In order to have a good model, the model results must be as close as possible to the experimental data, so that the experimental responses are described accurately by the simulated values. Moreover the deviation of the model simulations from the experimental observations should exhibit a normally distributed behaviour.

2.3.1.2 Statistical testing

Some statistical tests are carried out to investigate the significance of the performed regression and the estimated parameters [16]. The global significance of the regression can be verified by implementing the corresponding F test, which compares the ratio of the mean regression sum of squares and the mean residual sum of squares:

$$F_c = \frac{\sum_{j=1}^{nresp}\sum_{k=1}^{nresp}\sigma^{jk}\sum_{i=1}^{nob}\hat{Y}_{ij}\hat{Y}_{ik} \Big/ npar}{\sum_{j=1}^{nresp}\sum_{k=1}^{nresp}\sigma^{jk}\sum_{i=1}^{nob}\left(Y_{ij} - \hat{Y}_{ij}\right)\left(Y_{ik} - \hat{Y}_{ik}\right) \Big/ \left(nob \times nresp - npar\right)} \qquad \text{Eq. 2-30}$$

The regression is considered significant if the corresponding ratio exceeds the tabulated α-percentage point of the F distribution with *npar* and (*nob*×*nresp*-*npar*) degrees of freedom. 0.05 is selected for α that means a 95% probability level.

The *t* value is applied to verify the significance of the individual parameter estimates with respect to a reference value. The reference value typically equals zero, while the remaining parameters can, in principle, vary over their entire domain.

$$t_c = \frac{\left|b_j - \beta_j\right|}{\sqrt{[V(b)]_{jj}}} \qquad \text{Eq. 2-31}$$

In the above equation, b_j is the estimate, β_j is the reference parameter value and *V(b)jj* is the j^{th} diagonal element of the variance-covariance matrix of the parameter estimates that is defined by equation 2-32:

$$V(b)=\left(\sum_{j=1}^{nresp}\sum_{k=1}^{nresp}\sigma^{jk}J_j^T J_k\right)^{-1} \quad \text{Eq. 2-32}$$

Where J_i is the Jacobian matrix of the response Y_j with respect to the parameter as it is shown in the following equation:

$$J_j=\left[\frac{\partial y_j(b)}{\partial b}\right] \quad \text{Eq. 2-33}$$

Here, the confidence interval is defined by the limits at the probability level of 1-α within which the estimates do not significantly vary from the optimal value of b_j:

$$b_j - t\left(nob\ nresp - npar, 1-\frac{\alpha}{2}\right)\sqrt{[V(b)]_{jj}} \le \beta_j \le b_j + t\left(nob\ nresp - npar, 1-\frac{\alpha}{2}\right)\sqrt{[V(b)]} \quad \text{Eq. 2-34}$$

Again α is taken as 0.05, indicating a 95% confidence interval.
Finally binary correlation coefficients are used to investigate possible correlations between the parameter values:

$$\rho_{jk}=\frac{V(b)_{jk}}{\sqrt{V(b)_{jj}V(b)_{kk}}} \quad \text{Eq. 2-35}$$

Correlation coefficients, i.e., ρ_{jk} that are close to unity (in absolute value) imply a strong linear relationship between the estimated corresponding parameter.

2.3.2 Reactor model

As discussed before, the experimental data in this work have been acquired using a HTK-MI set up comprising fixed bed reactors. An isothermal plug-flow reactor model is, hence, used to calculate the product outlet flow rates:

$$\frac{dF_i}{dW}=R_i \quad \text{Eq. 2-36}$$

Where F_i represents the molar flow rate of component *i*, *W* the catalyst mass and R_i the net rate of formation of component *i*.

For the surface species the pseudo-steady state approximation was applied, expressing that their net production rate equals zero:

$$R_i = 0 \qquad \text{Eq. 2-37}$$

R_i, i.e., the net rate of formation of component *i*, is a function of the temperature, the total pressure, the partial pressure of every component, and concentration of the intermediate species on the surface. These equations are solved using the numerical subroutines DASPK [46, 47] and DNSQE [48] available in the NETLIB [44] software library, according to the code described in more detail by Lozano et al. [15]. The structure of the overall program is discussed in more detail in Section 2.3.3.

The partial pressure of a component *j* in the gas phase in the observation *i* is calculated as follows:

$$P_{ij} = \frac{F_{ij}}{\sum_{j=1}^{nresp} F_{ij}} P_{tot,i} \qquad \text{Eq. 2-38}$$

Where F_{ij} is the molar flow rate of response *j* in observation *i*.

2.3.3 Summary of the information flow during simulation and regression

The structure of the parameter estimation program and the relation between the different parts of this code are schematically presented in Figure 2-18.

The model input comprises the variables that must be defined by the user, i.e., initial guesses for the atomic chemisorption enthalpies and the activation energies, and the number of degrees of freedom lost or gained between reactant and transition state species. Via the appropriate statistical thermodynamics relationships, the latter are translated into entropy differences which, together with the symmetry numbers calculated for the corresponding elementary steps that are generated by Reaction Network Generation Program (ReNGeP) allow determining the pre-exponential factors, see chapter 4 for a more elaborate discussion of this methodology. The formation of all considered species is accounted for via the elementary steps implemented in the reaction network. Reaction and adsorption enthalpies have been calculated according to the UBI-QEP method. This method is a practical theoretical approach for determining the reaction energetics on transition metal surfaces [15, 49].

The *atomic* chemisorption enthalpies are used to determine the *molecular* chemisorption enthalpies. These values, together with reaction enthalpies of analogous molecules in the gas phase, are implemented via Born-Haber cycles to calculate the standard enthalpies of surface reactions that can be used to find the reverse activation energies of elementary steps from the corresponding forward activation energies; see Lozano Blanco et al. for more details [15].

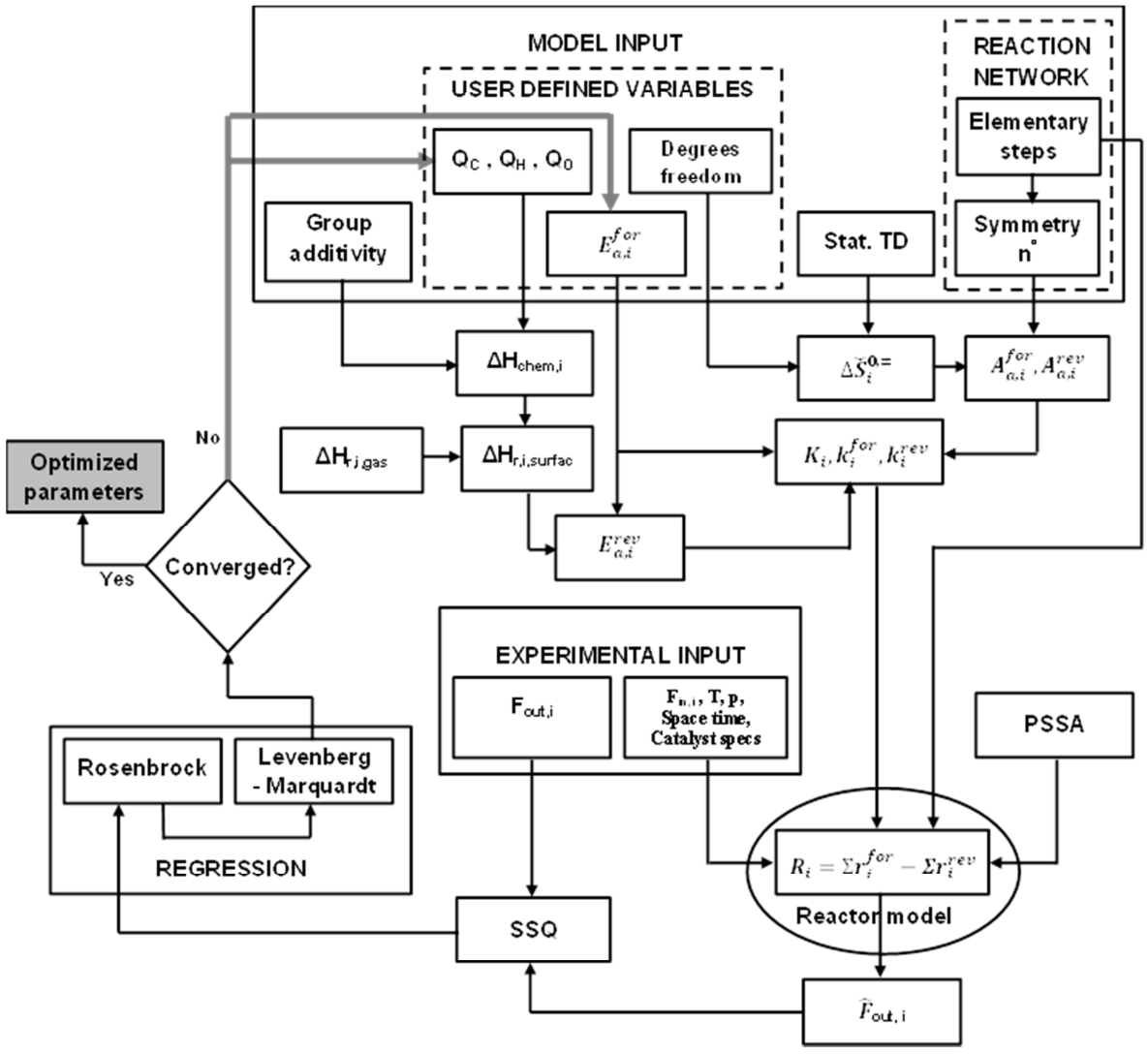

Figure 2- 18. Overview of the thermodynamic calculations and the parameter estimation strategy

Forward and reverse activation energies, in addition to the pre-exponential factors are used to determine the rate coefficients. These coefficients, together with the experimental operating conditions, are then used in a set of rate expressions corresponding to the different elementary steps accounted for in the net production rates as required within the above mentioned reactor model to calculate the product outlet flow rates and those of the unconverted reactants. These

simulated values are then compared to the experimentally observed outlet flow rates through the minimization of the residual sum of squares. This procedure ultimately leads to the optimized activation energies and atomic chemisorption enthalpies.

2.4 Conclusions

Gas phase heterogeneous ethylene hydroformylation experiments have been conducted on 5%Rh on Al_2O_3, 1%Co on Al_2O_3 and 0.5%Co-0.5%Rh on Al_2O_3 catalysts using a HTK-MI set up. Using this high tech pilot plant, different catalysts can be investigated in a wide range of operation conditions. The different parts of the HTK-MI set up and the procedures and steps for conducting the experiments were adequately described.

The implemented operating conditions in the current study were introduced and discussed. These ranges were selected in order to compare the performance of the corresponding catalysts as well as to investigate the effect of the temperature, pressure and inlet composition on the conversions and yields. Reported correlations as well as some practical guidelines concerning heat and mass transport limitations in an experimental plug flow reactor have been summarized and discussed. Additionally, expressions to verify the assumption of ideal plug flow and the pressure drop in the reactor were also presented. These conditions should be met to guarantee the measurement of intrinsic kinetics.

Catalyst characterization by BET, XRD, pulse chemisorption,… allow determining the number of active sites as well as other relevant properties that may determine the catalyst performance. Independently measured catalyst properties are also of key importance for mickrokinetic model construction.

The corresponding relations and equations for calculating the reactor outlet flow rates and site time values for the catalysts were introduced. In order to compare the performance of the investigated catalysts on an identical basis, observed conversions will be reported versus the so-called “site time”. The latter is obtained from the space time by accounting for the metal loading and the fraction of exposed metal atoms.

The determination of the adjustable parameters in the single-event microkinetic model is performed by regression to experimental data. This procedure is based on the minimization of the sum of squared residuals between the experimentally observed and model simulated outlet flow rates through successive use of the Rosenbrock and Levenberg – Marquardt algorithms.

The F test and t test for the individual significance of the parameter estimates were carried out in order to evaluate the regression. A plug-flow reactor model is applied to numerically calculate the conversions and molar yields.

2.5 References

[1] Zeton, B.V., Multiphase high throughput kinetics test unit - system manual, Enschede. 2007.

[2] K. Van der Borght, K. Toch, V. V. Galvita, Y.W. Thybaut, G. B. Marin, Catalysts 5 (2015) 1948-1968.

[3] N. Navidi, J. W. Thybaut, G. B. Marin, Appl. Catal. A. 469 (2014) 357–366.

[4] T. A. Zeelie, Rhodium and cobalt catalysts in the heterogeneous hydroformylation of ethane, propene and 1-hexene. PhD thesis, Helsinki, 2007.

[5] U. J. Jauregui-Haza, O. Diaz-Abin, A. M. Wilhelm, H. Delmas, Ind. Eng. Chem. Res. 44 (2005) 9636-9641.

[6] K. Tomishige, I. Furikado, T. Yamagishi, S. Ito, K. Kunimori, Catal. Lett. 103 (2005) 15-21.

[7] V. I. Zapirtan, B. L. Mojet, J.G.V. Ommen. J. Spitzer, L. Lefferts, Catal. Lett. 101 (2005) 43-47.

[8] T. Hanaoka, H. Arakawa, T. Matsuzaki, Y. Sugi, K. Kanno, Y. Abe, Catal. Today. 58 (2000) 271-280.

[9] F.S. Xiao, M. Ichikawa, J. Catal. 147 (1994) 578-593.

[10] C. U. Pittman Jr, G. M. Wilemon, J. Org. Chem. 46 (1981) 1901–1905.

[11] W. Junfan, S. Juntan, L. Hong, H. Binglin, React. Polym. 12 (1990) 177–186.

[12] M.W. Balakos, S.S.C. Chuang, J. Catal. 151 (1994) 266-278.

[13] M. A. Brundage, S.S.C. Chuang, J. Catal. 164 (1996) 94-108.

[14] D. Y. Murzin, A. Bernas, T. Salmi, AIChE Journal. 58 (2012) 2192-2201.

[15] G. Lozano-Blanco, J.W. Thybaut, K. Surla, P. Galtier, G.B. Marin, Ind. Eng. Chem. Res. 47 (2008) 5879-5891.

[16] G.F. Froment K.B. Bischoff, Chemical Reactor Analysis and Design. 2 ed. New York: Wiley, 1990.

[17] R. J. Berger, J. Perez-Ramirez, F. Kapteijn, J. A. Moulijn, Chem. Eng. Sci. 57 (2002) 4921-4932.

[18] D.E. Mears, Ind. Eng. Chem. Process Des. Dev. 10 (1971) 541-547.

[19] N. Wakao, S. Kaguei, T. Funazkri, Chem. Eng. Sci. 34 (1979) 325-336.

[20] D. E. Mears, J. Catal. 20 (1971) 127-131.

[21] A. P. Dewasch, G. F. Froment, Chem. Eng. Sci. 27 (1972) 567-576.

[22] G.F. Froment, Catal. Today. 52 (1999) 153-163.

[23] J.W. Thybaut, G.B. Marin, J. Catal. 308 (2013) 352-362.

[24] J. A. Dumesic, R. D. F., L. M. Aparicio, J. E. Rekoske, A. A. Trevifio, The microkinetic of heterogeneous catalysis. American Chemical Society. Washington, 1993.

[25] www.fluidat.com; July 2016.

[26] S. Ergun, Chem. Eng. Prog. 48 (1952) 9-94.

[27] F. Besenbacher, INANO, Aarhus university; http://inano.au.dk/research/research-areas/nano-materials-materials-science/nanocatalysis/; July 2016.

[28] M.A. Vannice, Kinetics of Catalytic Reactions. Springer, New York, 2005.

[29] S. Brunauer, P. H. Emmett, E. Teller, J. Am. Chem. Soc. 60 (1938) 309-319.

[30] http://www.micromeritics.com/pdf/products/Gemini_Series_Brochure.pdf; July 2016.

[31] http://www.micromeritics.com/product-showcase/Product-Selector-Tool/ChemiSorption.aspx; July 2016.

[32] A. Borodzinski, M. Bonarowska, Langmuir. 13 (1997) 5613-5620.

[33] http://www.nuance.northwestern.edu/epic/instruments-epic/tem/index.html; July 2016.

[34] https://commons.wikimedia.org/wiki/File:Scheme_TEM_en.png; July 2016.

[35] W.A. Dietz, J. Gas. Chromatogr. 5 (1967) 68-71.

[36] K. Toch, G. B. Marin, "Calculation of outlet composition, flow rates, conversions and selectivities in continuous flow (multiphase) reactors", Laboratory for Chemical Technology internal memo, August 2011.

[37] R.J. Berger, E. H. Stitt, G. B. Marin, F. Kapteijn, J. Moulijn, CATTECH. Vol. 5 (2001) 30-60.

[38] D. E. Mears, Chem. Eng. Sci. 26 (1971) 1361-1366.

[39] http://www3.konetic.or.kr/main/report/REPORTVIEW.asp?PARENT_NUM=1171&MENU1=5926; July 2016.

[40] S. Yagi, D. Kunii, AIChE Journal, 3 (1957) 373-381.

[41] H.H. Rosenbrock, Comput. J. 3 (1960) 175-184.

[42] D. W. Marquardt, J. Soc. Ind. Appl. Math. 11 (1963) 431-441.

[43] T. P. Boggs, J. W. Tolle, SIAM J. Numer. Anal. 26 (1989) 600-623.

[44] Netlib, http://netlib.org; June 2012.

[45] P. Reyniers, " Software library", Laboratory for Chemical Technology internal memo, June 2016.

[46] U. M. Ascher, R. J. Spiteri, SIAM J. Sci. Comput. 15 (1994) 938-952.

[47] P. N. Brown, A. C. Hindmarsh, L. R. Petzold, SIAM J. Sci. Comput. 19 (1998) 1495-1512.

[48] M. J. D. Powell, A hybrid method for nonlinear equations. Gordon and Breach, London, 1970.

[49] E. Schustorovich, H. Sellers, Surf. Sci. Rep. 31 (1998) 5-119.

Chapter 3:

Catalyst characterization and experimental kinetic measurements

Experimental ethylene hydroformylation results as observed over 5%Rh on Al_2O_3, 1%Co on Al_2O_3 and 0.5%Co-0.5%Rh on Al_2O_3 at well-selected operating conditions are discussed in this chapter. BET, EDX and TEM measurements allowed to independently determine some key characteristics of the investigated catalysts and, hence, a more fundamental understanding of the observed kinetics. The main products observed were ethane, propanal and propanol. The Rh catalyst exhibited the highest hydroformylation and hydrogenation site time conversions in the investigated range of operating conditions. Moreover it was found on all investigated catalysts that the hydrogenation activation energy was about 15 to 20 kJ mol^{-1} higher than that for hydroformylation. On the Rh catalyst, higher ethylene feed concentrations have a more pronounced effect on CO conversion and production of propanal and propanol compared with an increase in the inlet concentration of the other reactants.

3.1 Introduction

The present chapter concentrates on heterogeneous ethylene hydroformylation on a series of Rh and Co based catalysts. Gas phase experimentation was performed in a high-throughput kinetics - mechanistic investigation set up to compare the Rh and Co catalysts and to investigate the effect of the operation conditions on the main and by-product formation rates. A fundamental analysis is aimed at, both in terms of operating conditions as well as in terms of catalyst properties and how they could, potentially, be enhanced. Even if the investigated catalysts give only moderate oxygenate yields, the mechanistic investigation provides key insight into the corresponding reaction mechanism that may be exploited in further catalyst design.

3.2 Heterogeneous ethylene hydroformylation reaction network

Reaction mechanism elucidation is an important subject in the heterogeneous hydroformylation literature. The most referenced hydroformylation reaction mechanism was that proposed by Wilkinson and co-authors [1]. It is accepted today that Wilkinson's mechanism is, indeed, the most likely one for hydroformylation [2, 3, 4]. In this mechanism, it is assumed that carbon monoxide does not dissociate on the catalyst surface, but rather inserts in a metal alkyl bond, see also Chapter 1. Considering the discussion in the introductory chapter, a more pronouncedly heterogenized version of the mechanism presented in section 1.5.2 is proposed in what follows, see Figure 3.1. It is specifically developed for ethylene heterogeneous hydroformylation aiming at its subsequent single-event microkinetic modelling, see also Chapter 4. In general the steps in this figure, are the same as the ones proposed by Wilkinson, see Figure 1-9, except for steps 1, 2, 9 and 10. In the proposed mechanism, it is assumed that CO does not specifically has to liberate on active site prior to other adsorption or surface reaction steps to occur. Hence, step 1 from Figure 1-9 is no longer considered. Apart from that, hydrogen is not specifically required to be present on the catalyst surface prior to CO or alkene adsorption. It suffices when it is adsorbed as one of the steps in the reaction network. Between the adsorbed species, the first surface reaction will be that between the alkene species and hydrogen, reaction 3, to form a metal alkyl species in which adsorbed CO can insert, reaction 6. Steps 9 and 10 in Figure 3.1 represent the further hydrogenation of the metal propanal into metal propanol and desorption of the produced propanol molecule which are not part of the Wilkinson's mechanism.

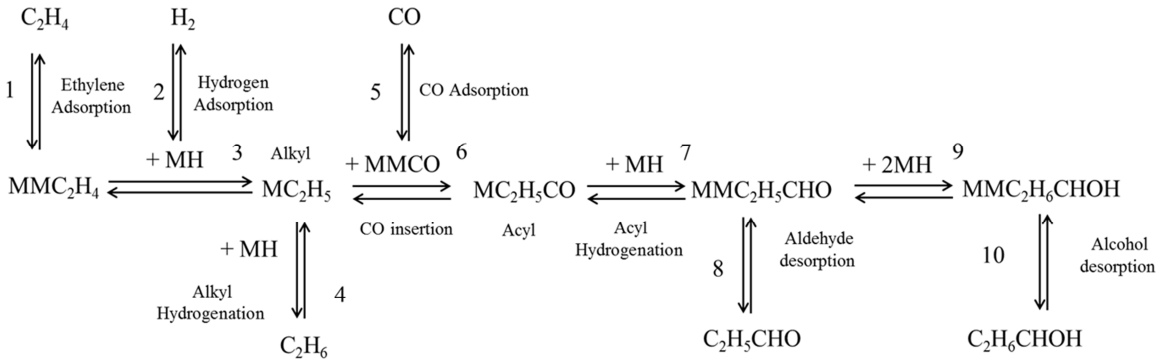

Figure 3- 1. Proposed reaction mechanism for ethylene hydroformylation, after [3]

This mechanism includes two parallel, i.e., competitive points, the first one starting from the metal bound alkyl species obtained after ethylene chemisorption on the metal surface and subsequent hydrogen addition. The desired pathway in hydroformylation from this metal alkyl species, involves CO insertion and leads to aldehyde or alcohol formation. The alternative of the parallel pathway is ethylene hydrogenation into ethane. In this mechanism, the same hydrogen and ethylene surface species are involved in the formation of both ethane and propanal. A similar competition occurs for the adsorbed aldehyde species which can either desorb and yield the desired end product or be further hydrogenated into the corresponding alcohol.

The most generally reported products for ethylene hydroformylation, in descending order of importance, are ethane, propanal, propanol and small amounts of C3+ hydrocarbon products [3, 5, 6, 7, 8, 9]. The potential presence of propene and higher carbon number alkenes, alkanes, aldehydes and alcohols can be explained by CO bond dissociation in the produced aldehydes or by CO bond dissociation and subsequent C hydrogenation to methylene prior to insertion in a metal alkyl species, as it may occur in Fischer-Tropsch synthesis which is discussed in detail in part 1.6.3 in chapter 1 [10, 11, 12]. As will be evident from the description of the experimental results later in this chapter, such reactions only occurred to a minimal extent.

It is anticipated that the proposed mechanism will be able to, at least qualitatively, if not quantitatively, see chapter 4, in line with the experimental observations. Because this comprehensive mechanism allows describing the formation of all hydroformylation products observed in this work, i.e., aldehydes and alcohols, as well as ethane, it is further used in the assessment of the kinetic data.

3.3 Catalyst characterization

3.3.1 BET Surface area

The BET surface areas of the investigated catalysts are reported in Table 3-1. The corresponding experiments were performed on fresh catalyst samples. Only minor differences are observed between the considered catalysts, indicating that the BET surface area of Al_2O_3 support is governing the observations. The slightly lower BET value for the catalyst with highest metal loading can be explained by the increased weight. If the increase in catalyst surface by metal deposition is smaller than that in catalyst weight, the overall effect will be a decrease in BET surface area. Moreover, metal deposition may also lead to pore blocking, resulting in an even more pronounced decrease in the surface area.

Table 3- 1. BET surface area for the three catalysts

Catalyst	BET surface area (m^2/g)
5%Rh/Al_2O_3	120
0.5%Rh-0.5%Co/Al_2O_3	147
1%Co/Al_2O_3	143

3.3.2 TEM analysis

Given the small size of the deposited metal particles and relatively limited metal loading the metal particle sizes of the employed catalysts could not be determined via XRD or chemisorption tests, see also Appendix A. Hence, Scanning *Transmission Electron Microscopy* (STEM) coupled with Energy Dispersive X-ray (EDX) and *Transmission Electron Microscopy* (TEM) measurements, as a more sensitive and accurate method, were recurred to for this purpose.

The presence of Rh and Co was confirmed first by STEM EDX measurements. It was confirmed by STEM EDX that, on 0.5%Rh/0.5%Co on Al_2O_3, Rh and Co did not form an alloy. The TEM measurement subsequently allowed determining the metal particle on the catalyst surface. The corresponding pictures are given in Figures 3.2-a and 3-2-b for 5%Rh on Al_2O_3, Figures 3-2-c and 3-2-d for 1%Co on Al_2O_3 and in Figures 3-2-e and 3-2-f for 0.5%Rh/0.5%Co on Al_2O_3. 5%Rh on Al_2O_3, see Figure 3-2-a and 3-2-b, has well dispersed particles with a small size, i.e., 2nm, resulting in 51.1% fraction of exposed metal.

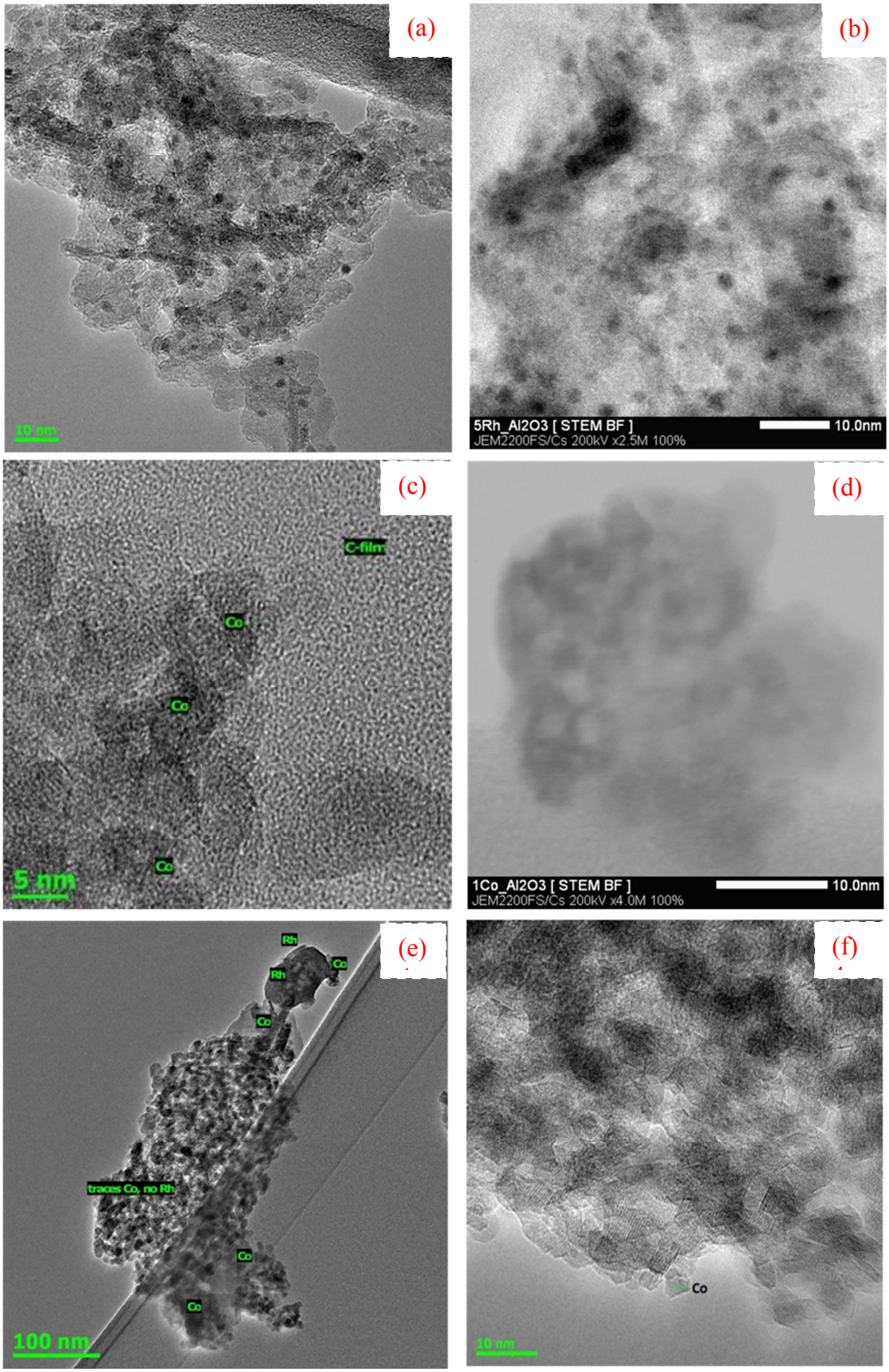

Figure 3- 2. TEM images for: (a, b) 5%Rh on Al_2O_3 catalyst, (c, d) 1% Co on Al_2O_3 catalyst, (e, f) 0.05%Rh/0.05%Co on Al_2O_3 catalyst

The images indicate a, still small, yet significantly larger particle size, i.e., 11nm, for the 1%Co catalyst while the 0.5%Rh/0.5%Co contained large Rh clusters, i.e., 20 to 50nm, but small Co particles, i.e., 4.3 nm. In other words, while Rh was finely dispersed on the 5%Rh catalyst and Co was somewhat more poorly dispersed on the 1%Co catalyst, the Rh dispersion on the 0.5%Rh/0.5%Co catalyst was extremely poor, while the Co dispersion was again better on this latter catalyst. The measured particle sizes and corresponding fractions exposed and accessible metal atoms are reported in Table 3-2. The fraction of exposed metal was determined using the measured particle size according to equations 2-3 and 2-4, see section 2.2.2.2.4. Considering the high precision of the measurements, any remaining errors on the calculated values for accessible metal atoms will not impact on the ranking in terms of particle size between these catalysts.

Table 3- 2. Particle size, fraction of exposed metal and accessible metal atoms for the Rh and Co based catalysts used in this work.

Catalyst	Particle size (nm) TEM	Fraction of exposed metal (%)	Accessible metal atoms (mol/$g_{cat.}$)
5%Rh/Al_2O_3	2	51.1	$2.48\ 10^{-4}$
1%Co/Al_2O_3	11	12.4	$0.21\ 10^{-4}$
0.5%Rh-0.5%Co/Al_2O_3	4.3 for Co 35 for Rh	28.1 for Co 3.8 for Rh	$0.26\ 10^{-4}$

3.4 Intrinsic Kinetics Character of the Experimental Measurements

The selected range of experimental conditions allowed the acquisition of intrinsic kinetics, see also Section 2.2.6 in Chapter 2 for a more elaborate discussion of the corresponding criteria [13]. The calculated values are reported in Table 3-3 for the experimental conditions at which the transport limitations, if any, would be expected to become most pronounced, i.e., the highest temperature and pressure.

Table 3- 3. Calculated versus limit values in the criteria for intrinsic kinetics evaluation at the most severe operating conditions used for ethanol conversion to hydrocarbons (T = 498 K, P = 3 MPa, W/F= 40 $kg_{cat}.s.mol^{-1}$).

Phenomenon	Criterion		Experiment
Mass transfer	external	Ca	$8.1\ 10^{-5} < 0.05$
	internal	Φ	$4.2\ 10^{-3} < 0.08$
Heat transfer	external	ΔT_{ext}	$8.3\ 10^{-1} < 1.45$ K
	internal	ΔT_{int}	$1.2\ 10^{-2} < 1.45$ K
Flow pattern ideally Plug flow	radial dispersion	d_t/d_p	$20 > 8$
	axial dispersion	L_B/d_p	$601 > 14$
	pressure drop	$\Delta P/P$	$1.6\ 10^{-3} < 0.2$

3.5 Catalytic performance

Figure 3-3 shows the observed CO and C_2H_4 conversion as a function of the site time at 473 K and 2MPa. The corresponding CO and C_2H_4 site time conversions are reported in Table 3-4.

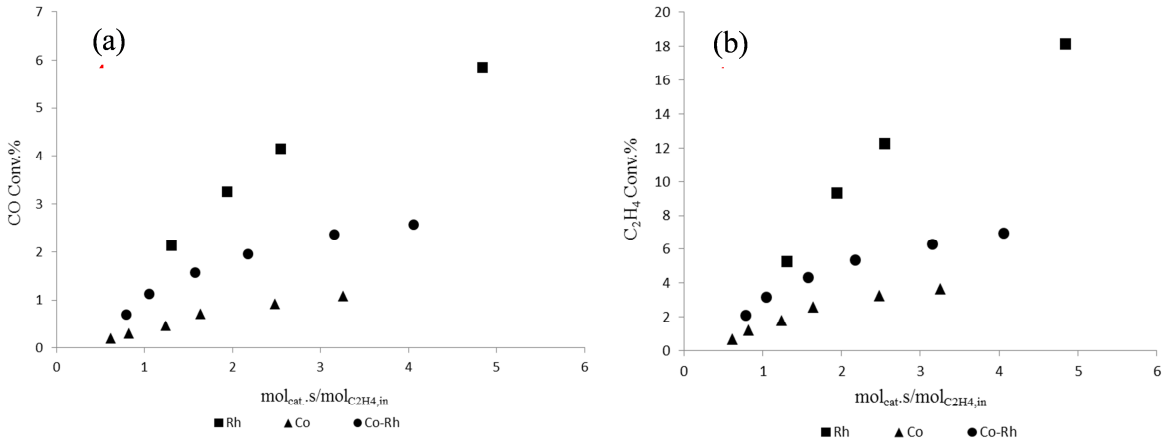

Figure 3- 3. (a) CO conversion versus molar site time, (b) C_2H_4 conversion versus molar site time Reaction conditions: Temperature 473K; pressure 2.0 MPa; gas inlet composition, C_2H_4:CO:H_2:Ar=30:30:30:10

Table 3- 4. CO and C_2H_4 site time conversions per catalyst at 473 K, 2.0 MPa and equimolar C_2H_4/CO/H_2 gas inlet composition

Catalyst	CO site time conversion ($mol_{CO,\ converted}$ /$mol_{cat.\ atoms}$ /s)*	C_2H_4 site time conversion ($mol_{C2H4,converted}$ /$mol_{cat.\ atoms}$ /s)*
5%Rh/Al_2O_3	0.01356	0.04071
1%Co/Al_2O_3	0.00359	0.01486
0.5%Rh-0.5%Co/Al_2O_3	0.00746	0.02626

5%Rh on Al_2O_3 exhibited the highest site time conversions in the entire range of operating conditions, while the lowest site time conversions were obtained on 1%Co on Al_2O_3.

Based on the site time conversions obtained with the monometallic catalysts and the knowledge of the fractions exposed on the bimetallic catalyst, see Table 3-2, an expected site time conversion on this bimetallic catalyst amounting to 0.00429 $mol_{CO,\ converted}$ /$mol_{cat.\ atoms}$ /s was calculated, which is lower than the experimentally observed site time conversion. Given the large Rh particle size on the 0.5%Rh/0.5%Co on Al_2O_3 catalyst, the higher than expected site time conversions observed on the latter catalyst are attributed to the finely dispersed Co. Indeed, particle size effects, also denoted as structure sensitivity, have already been reported in hydroformylation [14, 15] as well as in Fischer-Tropsch synthesis [16] on Co catalysts.

The product distributions obtained on these catalysts are reported in Table 3-5. The 5%Rh on Al_2O_3 catalyst exhibited the highest selectivity for oxygenates. The 0.5%Rh/0.5%Co on Al_2O_3 catalyst exhibited a higher selectivity for oxygenated compounds compared to the Co catalyst. Given the large size of the Rh particles on this catalyst, this selectivity effect on the 0.5%Rh/0.5%Co on Al_2O_3 catalyst compared to the 1%Co on Al_2O_3 is rather attributed to differences in Co particle size. The previously reported particle size effects [14, 15] particularly concern the CO insertion activity rather than the hydrogenation activity and, hence, result in an increase of the oxo-selectivity.

Table 3- 5. Product distribution obtained on Rh and Co based catalysts used in the present work at 473K, 2.0 MPa and C_2H_4:CO:H_2:Ar=30:30:30:10 gas inlet composition

Catalyst	Product selectivities (mol%)					
	CH_4	C_2H_6	C_3H_6	C_4H_8+C_4H_{10}	C_3H_5OH	C_3H_7OH
5% Rh/Al_2O_3	0.4	62.4	0.6	1.6	28	7
1% Co/Al_2O_3	1.1	71.7	1.3	1.9	18	6
0.5% Rh-0.5%Co/Al_2O_3	0.7	66.8	1	2.2	19.6	9.7

Overall 95% of the product selectivity goes into propanal, ethane and propanol. Ethane is an undesired by-product and its selectivity must be reduced for rendering the industrial application of heterogeneous hydroformylation economically viable. A minor presence of methane in the product stream can be the result of CO chemisorption, dissociation and hydrogenation. The selectivity of methane never exceeded 2%, however. Upon insertion of an intermediate methylene species into a metal alkyl species, the latter will grow as it occurs in the Fischer-Tropsch synthesis reaction mechanism. Of course, CO bond dissociation after a prior insertion in a metal alkyl species may also explain the formation of heavier hydrocarbons [17]. The amounts of methane and C_{3+} hydrocarbon products on the tested catalysts barely exceeded 5%, which is sufficiently low to assume that practically all of the converted CO ended up in hydroformylation products, i.e., propanal or propanol, or in ethane. Hence, the selected mechanism for ethylene hydroformylation, see Figure 3-1, can appropriately describe the reaction.

The maximum deviation from mass and elemental balances was below 10% and generally even below 5%, see also section 2.2.4. The possible error on the calculated site time conversions and product selectivities was, hence, considered to be in the same relative range.
Long term catalyst stability was assessed by repeating a reference experiment at regular time intervals. Upon the observation of any changes in catalyst activity, the catalyst was replaced by a fresh sample, see section 2.2.3. Therefore, catalyst aging and deactivation will be of relatively lower importance and its further investigation is considered beyond the scope of the present work. No evidence of product condensation, both physically and chemically was found during the experimentation.

3.5.1 Temperature effect

The temperature and pressure effect on the hydroformylation rate were investigated on the 5%Rh on Al_2O_3 and 1%Co on Al_2O_3 catalysts. The temperature effect on CO and C_2H_4 conversion and, hence, the ethylene hydroformylation and hydrogenation rates on the Rh and Co catalyst at a fixed pressure of 2MPa is presented in Figure 3-4.

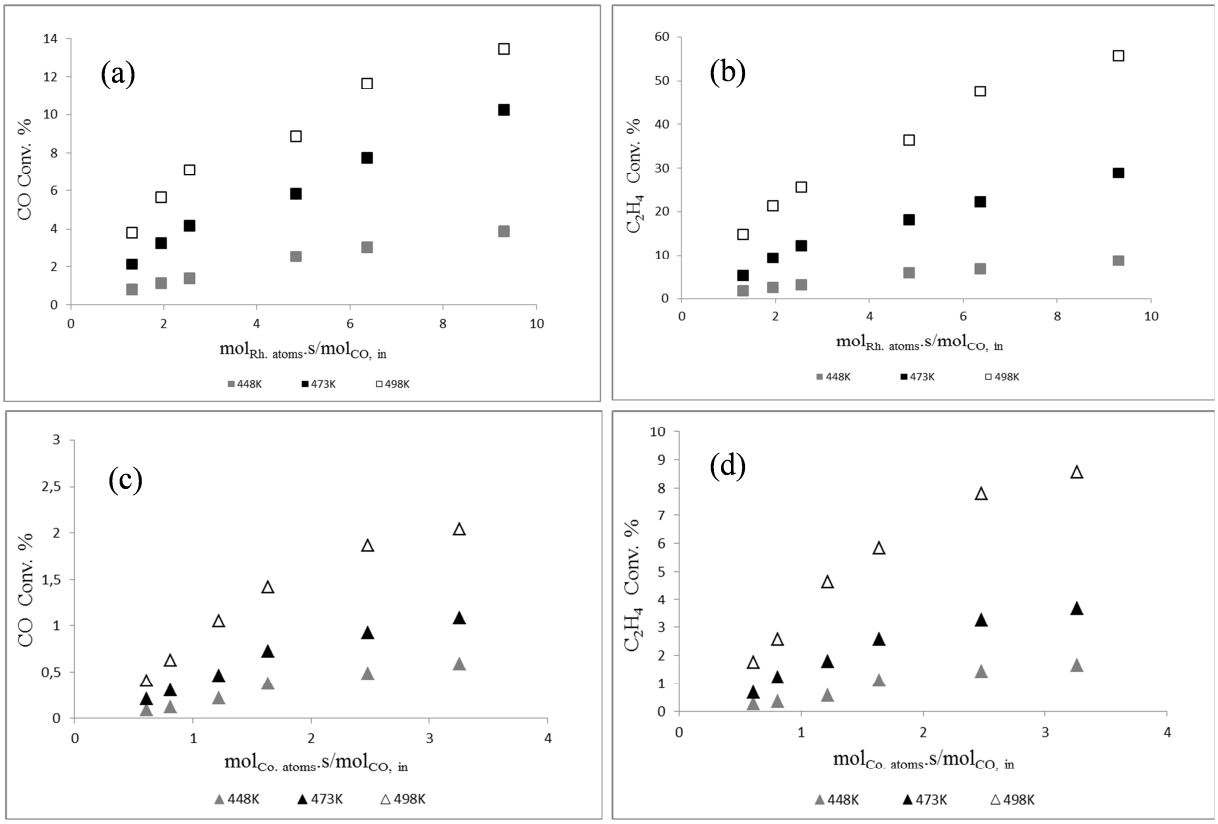

Figure 3- 4. (a) CO conversion versus site time on 5%Rh on Al_2O_3, (b) C_2H_4 conversion versus site time on 5%Rh on Al_2O_3, (c) CO conversion versus site time on 1%Co on Al_2O_3, (d) C_2H_4 conversion versus site time on 1%Co on Al_2O_3. Reaction conditions: temperature, 448, 473 and 498K; pressure 2.0 MPa, gas inlet composition, C_2H_4:CO:H_2:Ar=30:30:30:10.

The correspondingly calculated site time conversions are represented in Figure 3-5 as a function of the inverse of the temperature. A temperature increase leads to a more pronounced increase of the C_2H_4 site time conversion than of the CO site time conversion on both tested catalysts. Correspondingly, the apparent activation energy for ethane formation as determined from the Arrhenius diagram presented in Figure 3-5 exceeds that for propanal formation on both tested catalysts by 15 to 20 kJ mol^{-1}. Hence, as it can be seen in Figure 3-6, a temperature increase has a negative effect on the selectivity towards oxygenated compounds on both catalysts. For example by increasing the temperature from 448 K to 498 K on 5%Rh on Al_2O_3 at 2 MPa, the oxygenates selectivity decreased from 0.45 to 0.26. Similar observations are encountered in the literature [7, 18], where increased ethane selectivities with the temperature were reported. It was observed by Balakos and Chuang [18] that in heterogeneous ethylene hydroformylation on 4%Rh/SiO_2 with increasing the temperature from 483 K to 573 K the hydroformylation selectivity, defined as $\mathrm{TOF}_{\mathrm{Propanal}}/\mathrm{TOF}_{\mathrm{C_2H_6},in}$

decreased from 0.136 to 0.039. Hence, a good hydroformylation catalyst should exhibit a high activity at lower operating temperatures to avoid a too significant loss in product selectivity.

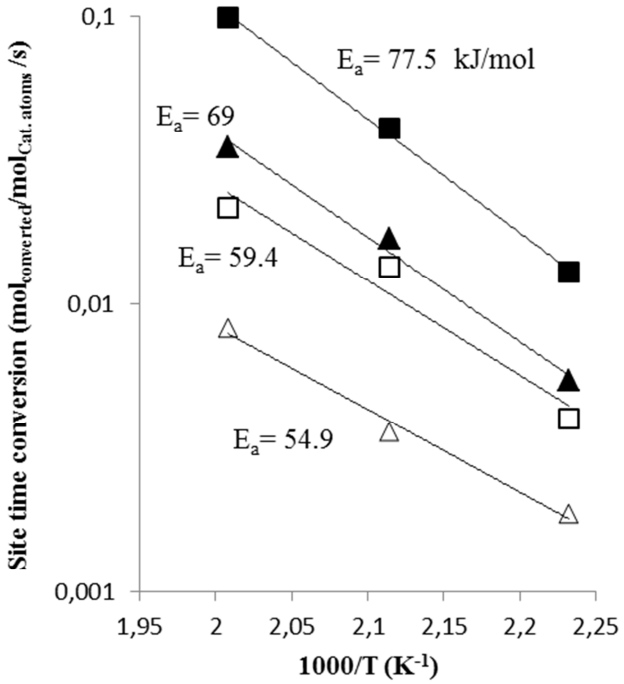

Figure 3- 5. Relation between space-time yield and temperature for ethane formation rate on Rh (■) and Co (▲) and propanal and propanol formation rate on Rh(□) and Co (Δ)

The more pronounced temperature effect on hydrogenation than on hydroformylation can be assessed using the previously discussed heterogeneous ethylene hydroformylation mechanism, see Figure 3-1: with increasing temperature, adsorbed C_2H_4 molecules apparently exhibit a higher affinity towards reductive elimination into ethane, step 4, than reacting with adsorbed CO molecule, step 6, on the catalyst surface. This can be related to the expected evolution in the hydrogen and CO surface concentrations. Because the chemisorption heat of CO is typically about the double of that of hydrogen [19], the CO concentration will decrease much faster with increasing temperature than the hydrogen concentration. As a result, the relative importance of hydrogenation in the overall ethylene conversion will increase at the expense of hydroformylation.

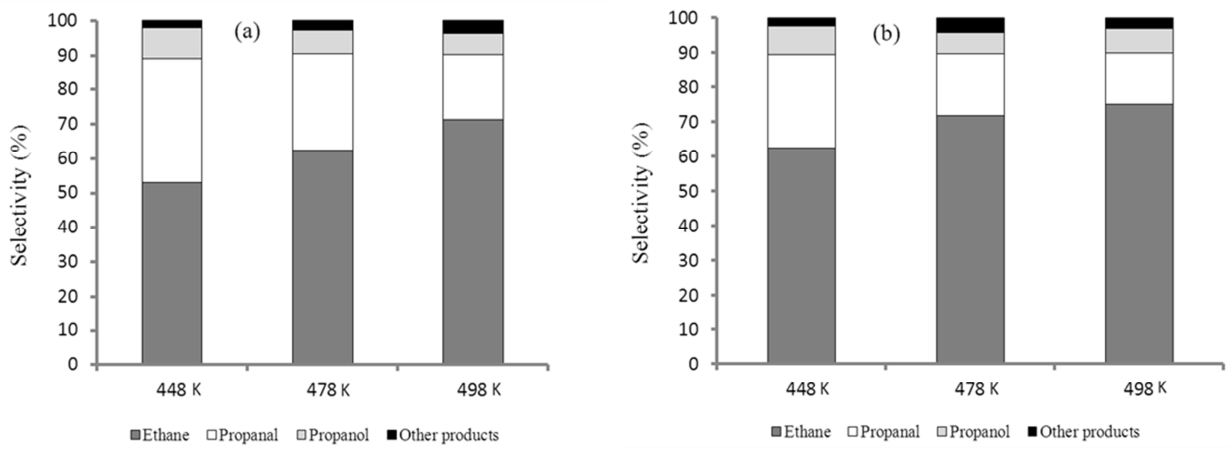

Figure 3- 6. Product selectivities (mol%) at 2.0 MPa and equimolar $C_2H_4/CO/H_2$ gas inlet composition (a) on the 5% Rh/Al_2O_3 catalyst and (b) the 1% Co/Al_2O_3 catalyst.

3.5.2 Pressure effect

The pressure effect on the CO and ethylene conversion as a function of the site time at 473 K on the Rh and Co catalyst is shown in Figure 3-7. All conversions and consequently hydroformylation and hydrogenation rates increase with the total pressure to a similar extent. A slightly more pronounced enhancement of the hydroformylation rate compared to the hydrogenation rate may be discerned, in agreement with the literature [8]. At a higher total pressure also the surface concentrations on the metal particles are correspondingly higher. The slightly increased oxygenates selectivity indicates that in particular the CO surface concentration has increased.

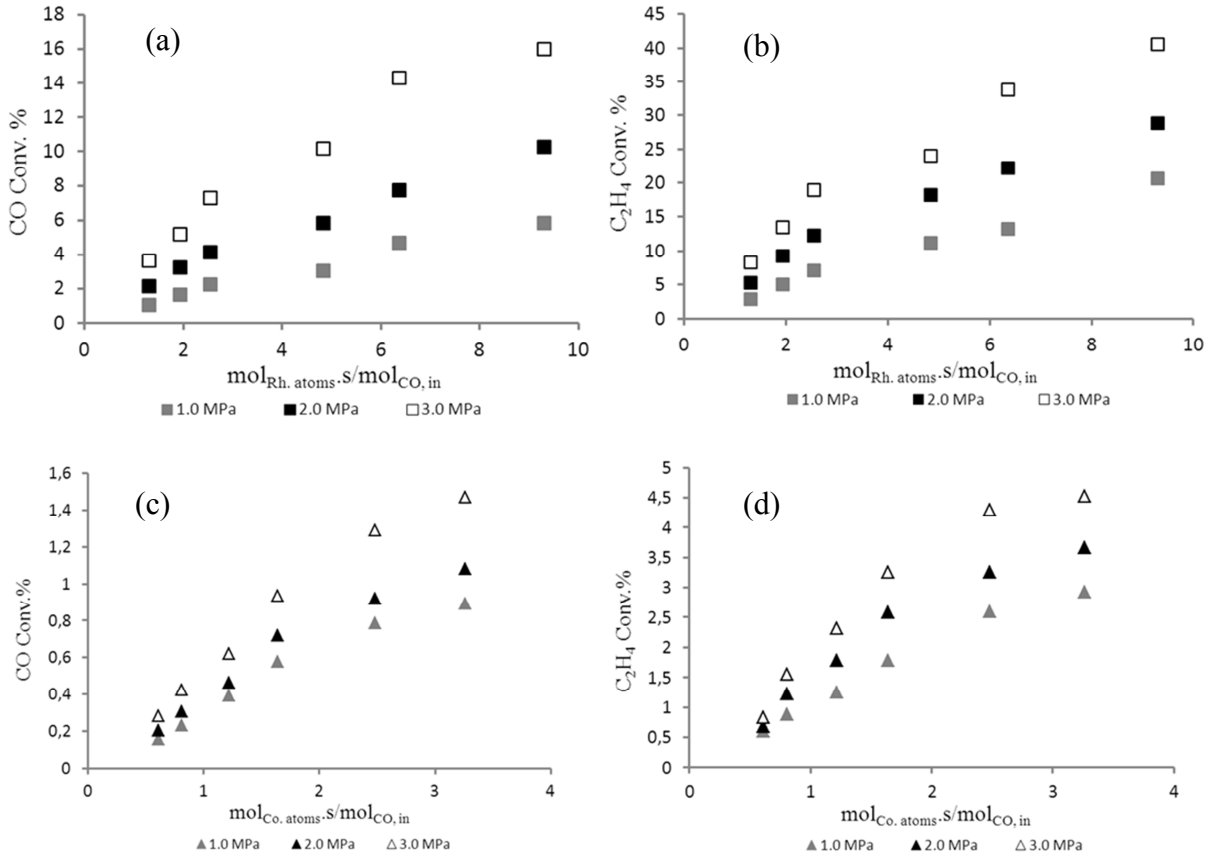

Figure 3- 7. (a) CO conversion versus site time on 5%Rh on Al_2O_3, (b) C_2H_4 conversion versus site time on 5%Rh on Al_2O_3, (c) CO conversion versus site time on 1%Co on Al_2O_3 and (d) C_2H_4 conversion versus site time on 1%Co on Al_2O_3 at different total pressures. Reaction conditions: temperature, 473 K; gas inlet composition, C_2H_4:CO:H_2:Ar=30:30:30:10.

3.5.3 Inlet composition effect

The effect of variations in C_2H_4, CO and H_2 inlet composition on the CO and C_2H_4 conversion, was investigated on 5%Rh on Al_2O_3 and is reported in Figure 3-8. As it can be observed from Figure 3-8-a, the CO conversion and, hence, the hydroformylation rate, increases with the ethylene inlet concentration. Also the C_2H_4 conversion by hydrogenation is enhanced by increasing its inlet concentration, see Figure 3-8-b. This can be understood when C_2H_4 concentrations on the catalyst surface are rather low and, hence, when an increasing C_2H_4 surface concentration has a negligible impact on the other surface concentrations. Increasing the inlet H_2 concentration leads to a significantly higher ethylene conversion but only to a slightly higher CO conversion.

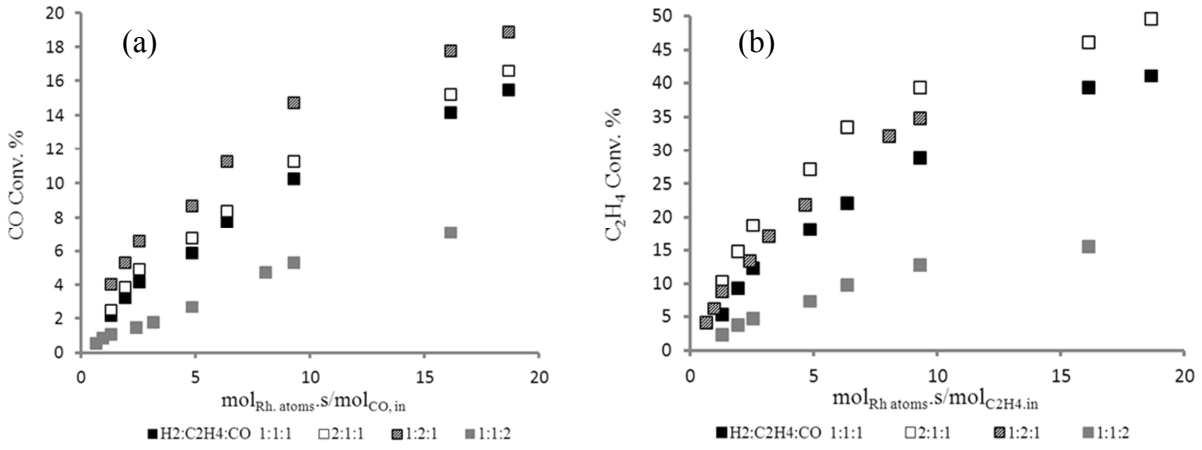

Figure 3- 8. CO and C_2H_4 conversions versus site time. Reaction conditions: catalyst 5%Rh on Al_2O_3, temperature, 473K; pressure 2.0 MPa

Increasing the inlet CO concentration as it is depicted in Figures 3-8-a and 3-8-b, has a considerable, negative effect on both the CO as well as the ethylene conversion. The overall effect of increasing inlet concentration on CO and C_2H_4 conversion is also summarized in Table 3-6. This can be understood if CO is the most abundant surface species and, hence, if the higher CO surface concentration results in a more pronounced decrease of the H_2 and C_2H_4 concentrations on the catalyst surface, such that both hydroformylation and hydrogenation rates decrease.

Table 3- 6. The effect of increasing inlet concentration on CO and C_2H_4 conversions

Increasing inlet concentration	CO conversion	C_2H_4 conversion
C_2H_4	++	+
CO	-	-
H_2	+	++

These results were in line with what Balakos et al. reported for dependence of the reaction rates on the partial pressures of reactants [18]. They observed both ethane and propanal formation rates are negative order in CO while positive order in both hydrogen and ethylene in heterogeneous hydroformylation on Rh/SiO_2 at 0.1 MPa and 513 K.

3.6 Conclusions

Gas phase hydroformylation on 5%Rh on Al_2O_3, 1%Co on Al_2O_3 and 0.5%Co-0.5%Rh on Al_2O_3 practically exclusively resulted in propanal, ethane and propanol formation. Finely dispersed Rh particles were the most active and selective (up to 45%) in ethylene hydroformylation to propanal and propanol. Structure sensitivity in ethylene hydroformylation has been explicitly observed for Co based catalysts. Finer Co particles appear to be more active and selective than larger ones.

Irrespective of the investigated catalyst, the temperature effect is more pronounced on ethylene hydrogenation than on hydroformylation. The 15 to 20 kJ mol^{-1} higher apparent activation energy for ethane than for propanal formation is a result of the higher heat of chemisorption for CO than for hydrogen. CO was found to be the most abundant surface intermediate, resulting in an inhibiting effect on both hydroformylation and hydrogenation. Surface concentrations of hydrogen and ethylene were lower and did not result in inhibition effects within the investigated range of operating conditions. An ideal catalyst for ethylene hydroformylation must consist of a finely dispersed metal such as Rh with a maximum activity at temperatures below 483 K.

3.7 References

[1] D. Evans, J.A. Osborn, G. Wilkinson, J. Chem. Soc. 1968(12) 3133-3142.

[2] B. Breit, W. Seiche, Synth. (2001) 1–36.

[3] M. A. Brundage, S.S.C. Chaung, J. Catal. 164 (1996) 94-108.

[4] C. D. Frohning, C. W. Kohlpainter, In: B. Cornils, W. A. Herrmann (Eds.), Applied homogeneous catalysts with organometallic compounds, VCH, Weinheim, 1996.

[5] Ullmann's Encyclopedia of Industrial Chemistry, sixth ed., John Wiley & Sons, 2002.

[6] U. J. Jauregui-Haza, O. Diaz-Abin, A. M. Wilhelm, H. Delmas, Ind. Eng. Chem. Res. 44 (2005) 9636-9641.

[7] M. A. Brundage, M. W. Balakos, S.S.C. Chaung, J. Catal. 173 (1998) 122-133.

[8] V. I. Zapirtan, B. L. Mojet, J.G.V. Ommen. J. Spitzer, L. Lefferts, Catal. Lett. 101 (1-2) (2005) 43-47.

[9] C. U. Pittman Jr, G. M. Wilemon, J. Org. Chem. 46 (1981) 1901–1905.

[10] J. P. Hindermann, G.J. Hutchings, A. Kiennemann, Catal. Rev. 35 (1993) 1-127.

[11] P. Biloen, W.M.H. Sachtler, Adv. Catal. 30 (1981) 165-216.

[12] G. Lozano-Blanco, J. W. Thybaut, K. Surla, P. Galtier, G. B. Marin, G.B., Oil Gas Sci. Technol. – Rev. IFP. 61 (2006) 489-496.

[13] R.J. Berger, E. H. Stitt, G. B. Marin, F. Kapteijn, J. Moulijn, CATTECH. Vol. 5 (2001) 30-60.

[14] T. A. Zeelie, Rhodium and cobalt catalysts in the heterogeneous hydroformylation of ethane, propene and 1-hexene. PhD thesis, Helsinki, 2007.

[15] T. Hanaoka, H. Arakawa, T. Matsuzaki, Y. Sugi, K. Kanno, Y. Abe, Catal. Today. 58 (2000) 271-280.

[16] G. L. Bezemer, J. H. Bitter, H.P.C.E. Kuipers, H. Oosterbeek, J. E. Holewijn, X. Xu, F. Kapteijn, A. J. van Dillen, K. P. de Jong, J. Am. Chem. Soc. 128 (2006) 3956-3964.

[17] H. Pichler, H. Schulz, Chemie-Ing.-Techn., 42 (1970) 1162-1174.

[18] M.W. Balakos, S.S.C. Chuang, J. Catal. 1994. 151 (1994) 266-278.

[19] G. Lozano-Blanco, J. W. Thybaut, K. Surla, P. Galtier, G. B. Marin, Ind. Eng. Chem. Res. 47 (2008) 5879-5891.

Chapter 4:

A Single-Event MicroKinetics for ethylene hydroformylation on Rh and Co based catalysts

Abstract: In this chapter, a Single-Event MicroKinetic (SEMK) model, originally developed for Fischer-Tropsch (FT) synthesis, has been extended towards ethylene hydroformylation into propanal. This model was applied to experimental data obtained on 5%Rh/Al_2O_3 and 1%Co/Al_2O_3 catalysts in a temperature range from 443 to 498 K, at total pressures between 1.0 to 3.0 MPa and in a space time range from 5.4 to 149 kg_{cat} s/$mol_{C2H4,\ in}$. The activation energies of the considered elementary steps and the atomic chemisorption enthalpies of carbon, hydrogen and oxygen, i.e., the so-called kinetic and catalyst descriptors, were determined via model regression to the experimental data. The single-event pre-exponential factors were calculated based on statistical thermodynamics considerations. In total 95 forward and reverse elementary steps were accounted for in the corresponding reaction network. The SEMK model well describes the product distribution over a wide range of operating conditions on both investigated catalysts. It also quantitatively describes the experimentally observed temperature and pressure variations. The finally obtained parameter values are statistically significant and physically meaningful, i.e., in the range of literature reported observations. CO insertion into a metal alkyl species was identified as the kinetically relevant surface elementary step in hydroformylation product formation. Metal carbide and metal oxide surface concentrations were found to be negligible. The SEMK model developed in this work provides a sound basis for extrapolation to innovative hydroformylation catalysts. Based on the results a catalyst with Q_C=597, Q_O=494 and Q_H=250 kJ/mol for carbon, oxygen and hydrogen atomic chemisorption, respectively, is expected to exhibit ideal ethylene hydroformylation behavior into propanal.

4.1 Introduction

Hydroformylation, or oxo synthesis is an important process for production of aldehydes from alkenes. Hydroformylation exhibits significant similarities with Fischer-Tropsch (FT) synthesis. The research into heterogeneously catalysed hydroformylation is still in an early stage. Although a wide range of research activities has been performed on experimental heterogeneous hydroformylation with various reactants, catalysts and operation conditions [1-9], the literature on its (fundamental) kinetic modelling is limited [10-12]. Balakos and Chuang [10] constructed a so-called Langmuir–Hinshelwood/Hougen–Watson (LHHW) kinetic model for heterogeneously catalyzed ethylene hydroformylation, that allowed them to accurately describe their experimental data. The reaction mechanism assumed in their work is similar with the one proposed in the present work, the major difference being situated in the specification of the catalytically active sites, i.e., one or more metal atoms, see also section 2.1. Another difference is the lack of elementary steps leading to hydroformylation byproducts, considered in this LHHW model by Balakos and Chuang [10].

A Single-Event MicroKinetic model (SEMK) is a model that accounts for the rate of every elementary step. Hence, detailed product profiles can be simulated making use of this model which turns it into a potent tool for designing more highly-performing catalysts. The single-event concept was first introduced by Froment et al. [13] and recently reviewed by Thybaut and Marin [14]. SEMK has already been successfully applied in many reactions such as hydroconversion [15, 16], alkylation [17], catalytic reforming [18], FT synthesis [19] and hydrogenation [20]. The SEMK methodology consists of classifying elementary steps into reaction families and, within such a reaction family, of filtering out the symmetry factors from the entropic factor in the kinetic coefficient. As a result a single rate coefficient suffices to describe the rates of all elementary steps belonging to this same reaction family, e.g., the hydrogenation of alkenes to alkanes. This means that the number of adjustable kinetic parameters is reduced to the number of reaction families, a feature which can be well exploited in the simulation of hydroformylation reactions. Besides, by the incorporation of so-called catalyst descriptors in addition to the kinetic descriptors, the SEMK model applicability can be enhanced such that it becomes a useful tool in the assessment of experimental results on a (wide) range of catalysts rather than being limited to a single one.

In the present chapter a SEMK model is discussed for hydroformylation. Starting from the model available for FTS [19] a mechanism based upon elementary steps is implemented and

used in the simulation of data acquired on a Rh and a Co catalyst. This will allow gaining deeper insight in the determining factors for the catalyst activity and selectivity.

4.2 Heterogeneous ethylene hydroformylation reaction network

4.2.1 Elementary steps in heterogeneous ethylene hydroformylation

As discussed before in Section 1.6.3, heterogeneously catalysed hydroformylation is very closely related to FT synthesis. As a result, a mechanistic investigation of the hydroformylation reaction will benefit from what is already known for FT synthesis. The applied model in this work is constructed by extension of the existing reaction network for FT synthesis [19]. The corresponding network used in this chapter has been more elaborately described in Section 3.2, where it has been derived, among others, from the interpretation of the experimental data. This mechanism is proposed because it explains the formation of major ethylene hydroformylation products observed, i.e., ethane and propanal. In order to focus on the effect of the metal used as catalyst and avoid a high number of adjustable parameters, no explicit changes have been considered in the reaction mechanism on Rh and Co. The majority of the elementary steps in this network were already included in the FT synthesis SEMK model [19, 21]. The forward and reverse elementary steps for the reaction family of aldehyde reductive elimination were added to adapt the available model for FTS towards hydroformylation. The probable presence of propene and higher carbon number alkenes and alkanes can also be explained by CO bond dissociation and subsequent carbon hydrogenation to methylene prior to insertion in a metal alkyl species, as it may occur in FT synthesis which is discussed earlier in detail in Section 1.6.3. As will be demonstrated further in this chapter, this mechanism can quantitatively explain the kinetics, reaction pathways and rate-determining steps in the formation of ethane and propanal, as was already qualitatively demonstrated in the previous chapter [1].

The elementary steps of the selected mechanism for ethylene hydroformylation, see Section 3.2, and the corresponding ones for FT synthesis, were all accounted for in the model. All implemented reaction families in this work are summarized in Table 4-1 and 4-2. Because in the experimental data used [1], n-alkanes, 1-alkenes, aldehydes and alcohols up to carbon number 4 were observed, a maximum carbon number considered in the present work was 4. This resulted in an overall reaction network comprising 95 elementary steps, as they are illustrated in Table 4-1.

Table 4- 1. Forward and reverse elementary steps (maximum carbon number = 4)

1	CO molecular chemisorption	$CO + 2M \rightleftarrows MMCO$
2	CO dissociation	$MMCO + 3M \rightleftarrows MMMC + MMO$
3	H_2 dissociative chemisorption	$H_2 + 2M \rightleftarrows 2MH$
4	Hydrogenation of metal bound C	$MMMC + MH \rightleftarrows MMMCH + M$
5	Hydrogenation of metal bound CH	$MMMCH + MH \rightleftarrows MMCH_2 + 2M$
6	Hydrogenation of metal bound CH_2	$MMCH2 + MH \rightleftarrows MCH_3 + 2M$
7	Hydrogenation of metal bound O	$MMO + MH \rightleftarrows MOH + 2M$
8	Reductive elimination of H_2O	$MOH + MH \rightarrow H_2O + 2M$
9	Methylene insertion	$MCH_3 + MMCH_2 \rightleftarrows MCH_2CH_3 + 2M$ $MC_2H_5 + MMCH_2 \rightleftarrows MCH_2CH_2CH_3 + 2M$ $MC_3H_7 + MMCH_2 \rightleftarrows MCH_2CH_2CH_2CH_3 + 2M$ $MC_3H_7 + MMCH_2 \rightleftarrows MCH(CH_3)(CH_2CH_3) + 2M$ $MC_3H_7 + MMCH_2 \rightleftarrows MCH_2CH(CH_3)_2 + 2M$ $MC_3H_7 + MMCH_2 \rightleftarrows MC(CH_3)_3 + 2M$
10	Reductive elimination of alkane	$MCH_3 + MH \rightleftarrows CH_4 + 2M$ $MC_2H_5 + MH \rightleftarrows C_2H_6 + 2M$ $MC_3H_7 + MH \rightleftarrows C_3H_8 + 2M$ $MC_4H_9 + MH \rightleftarrows CH_3CH_2CH_2CH_3 + 2M$ $MC_4H_9 + MH \rightleftarrows CH(CH_3)_3 + 2M$
11	β – hydride elimination	$MC_2H_5 + M \rightleftarrows MC_2H_4 + MH$ $MC_3H_7 + M \rightleftarrows MC_3H_6 + MH$ $MC_4H_9 + M \rightleftarrows MCH_2CHCH_2CH_3 + MH$ $MC_4H_9 + M \rightleftarrows MCH_2C(CH_3)_2 + MH$
12	Desorption of alkenes	$MC_2H_4 \rightleftarrows C_2H_4 + M$ $MC_3H_6 \rightleftarrows C_3H_6 + M$ $MC_4H_8 \rightleftarrows CH_2CHCH_2CH_3 + M$ $MC_4H_8 \rightleftarrows C(CH_2)(CH_3)_2 + M$
13	CO insertion	$MH + MMCO \rightleftarrows MCHO + 2M$ $MCH_3 + MMCO \rightleftarrows MCH_3CO + 2M$ $MC_2H_5 + MMCO \rightleftarrows MC_2H_5CO + 2M$ $MC_3H_7 + MMCO \rightleftarrows M(CH_2CH_2CH_3)CO + 2M$ $MC_3H_7 + MMCO \rightleftarrows MC(CH(CH_3)_2)O + 2M$

Table 4-1. Forward and reverse elementary steps (maximum carbon number = 4), continued.

14	H addition to metal carbonyl	$MCHO + MH \rightleftarrows MMCH_2O$ $MCH_3CO + MH \rightleftarrows MMCHCH_3O$ $MC_2H_5CO + MH \rightleftarrows MMCH(CH_2CH_3)O$ $MC_3H_7CO + MH \rightleftarrows MMCH(CH_2CH_2CH_3)O$ $MC_3H_7CO + MH \rightleftarrows MMCH(CH(CH_3)_2)O$
15	Reductive elimination of alcohols	$MMCH_2O + 2MH \rightleftarrows CH_3OH + 4M$ $MMCHCH_3O + 2MH \rightleftarrows CH_3CH_2OH + 4M$ $MMCH(CH_2CH_3)O + 2MH \rightleftarrows CH_3CH_2CH_2OH + 4M$ $MMCH(CH_2CH_2CH_3)O + 2MH \rightleftarrows CH_3CH_2CH_2CH_2OH + 4M$ $MMCH(CH(CH_3)_2)O + 2MH \rightleftarrows CH(CH_3)_2CH_2OH + 4M$
16	Reductive elimination of aldehydes	$MMCH_2O \rightleftarrows CH_2O + 2M$ $MMCHCH_3O \rightleftarrows CH_3CHO + 2M$ $MMCH(CH_2CH_3)O \rightleftarrows CH_3CH_2CHO + 2M$ $MMCH(CH_2CH_2CH_3)O \rightleftarrows CH_3CH_2CH_2CHO + 2M$ $MMCH(CH(CH_3)_2)O \rightleftarrows CH(CH_3)_2CHO + 2M$

The number of free sites to which adsorbates are bond potentially differ from adsorbate to adsorbate and are, at present, still a matter of debate. Nevertheless, a discrimination between models with different assumptions about the number of sites required for different adsorbates, will typically be inconclusive, such that it can be reasonably expected that a qualitative comparison of different catalysts will not depend on the exact assumptions made.

4.2.2 Automated reaction network generation

Using the above-discussed reaction network, the formation of all observed main and by-products in experimental data for ethylene hydroformylation can be explained. The forward and reverse elementary steps in the proposed reaction network were generated using the Reaction Network Generation Program (ReNGeP) as it was originally implemented for FT synthesis [21]. In this program, the molecules are represented numerically using standardized labels and Boolean matrices for storage and elementary step generation purposes respectively. The Boolean matrices express the connectivity between the atoms in a molecule in such a way that, if there is a bond between the atoms, the corresponding element in the matrix is set to 1 while it is set to 0 otherwise, i.e., if there is no bond, as it is depicted in Figure 4-1.

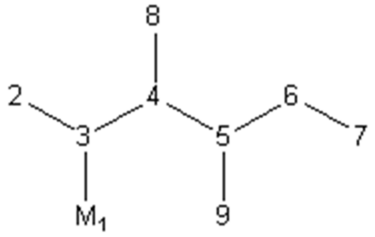

		1	2	3	4	5	6	7	8	9
1	M	0	0	1	0	0	0	0	0	0
2	C	0	0	1	0	0	0	0	0	0
3	C	1	1	0	1	0	0	0	0	0
4	C	0	0	1	0	1	0	0	1	0
5	C	0	0	0	1	0	1	0	0	1
6	C	0	0	0	0	1	0	1	0	0
7	C	0	0	0	0	0	1	0	0	0
8	C	0	0	0	1	0	0	0	0	0
9	C	0	0	0	0	1	0	0	0	0

Figure 4- 1. The Boolean matrix for a reference molecule [21]

The aldehyde is formed through metal alkyl oxide desorption, step 8 in Figure 3-1 in chapter 3, leaving two vacant adsorption sites. This reaction, together with aldehyde chemisorption, were the two reactions that had to be added into ReNGeP for FT synthesis. The corresponding operations on the Boolean matrix are represented in Figure 4-2.

The rows and columns corresponding to the metal sites are eliminated from the matrix and the vector indicating the double bond between the carbonyl carbon and oxygen reappears. In the current work the total number of generated species with ReNGeP amounted to 44 for reaction networks including hydrocarbons up to 4 carbon atoms. These species comprise 5 alkanes, 4 alkenes, 5 aldehydes, 5 alcohols and 25 metal alkyls. In total 95 forward and reverse elementary steps were accounted for in the network for interconverting these species.

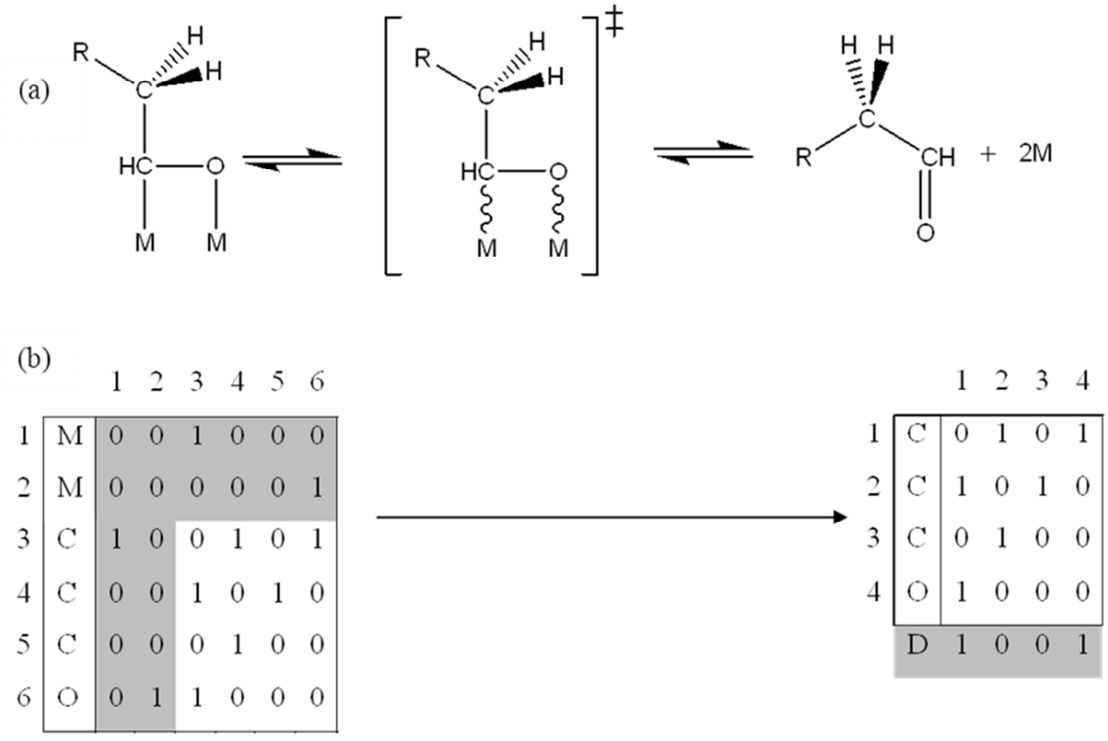

Figure 4- 2. (a) Aldehyde desorption reaction, (b) Corresponding matrixes for metal alkyl oxide and aldehyde.

4.3 The single-event microkinetic model for heterogeneous ethylene hydroformylation

The Single-Event MicroKinetic (SEMK) methodology has been developed based on transition state theory and exploits molecular structure similarities via the reaction family concept to reduce the number of adjustable kinetic parameters, while preserving the fundamental character of the microkinetic model [14].

The rate coefficient of an elementary step *k (1/s* or *1/MPa.s)* can be written as follows:

$$k = \frac{\sigma_{gl,r}}{\sigma_{gj,\neq}} \frac{k_B T}{h} \exp\left(\frac{\Delta \tilde{S}^{0,\neq}}{R}\right) \exp\left(\frac{-\Delta H^{0,\neq}}{RT}\right) \qquad \text{Eq. 4-1}$$

$$k = \frac{\sigma_{gl,r}}{\sigma_{gl,\neq}} \tilde{k} = n_e \tilde{k} \qquad \text{Eq. 4-2}$$

$$\tilde{k} = \tilde{A} \exp\left(-E_a / RT\right) \qquad \text{Eq. 4-3}$$

Where k_B is the Boltzmann constant (m^2 *kg/s K); h is* the Planck constant (m^2 *kg/s) and R* is the universal gas constant (*J/mol K). T* is the temperature in Kelvin and $\sigma_{gl,r}$ and $\sigma_{gl,\neq}$ are the global symmetry number of reactant(s) and of the transition state, respectively. ΔS is entropy change (*J/mol K*), ΔH enthalpy change (*J/mol K*). The sub- and superscript ~, *0* and $\neq$ in theses equations refer to the *single-event*, *standard state* and *activated complex*, respectively.

In Eq. 4-2, $\tilde{k}$ is the so-called single-event rate coefficient and n_e is the number of single events. The latter determines in how many structurally indistinguishable ways a reactant can be converted into a transition state/product via the same elementary step. The salient feature of the SEMK methodology is that the symmetry contribution can be filtered out from the entropic part of the rate coefficient. The remaining term is denoted as the *single-event kinetic coefficient*, which is unique for a given reaction family. This means that instead of having one kinetic coefficient per elementary step, which would lead to an overwhelming number of parameters, the number of adjustable kinetic parameters is reduced to the number of reaction families. This is described in more detail in literature [14, 22, 23]. The corresponding symmetry numbers are calculated using ReNGeP, see section 4.2.2 and the work by Lozano Blanco et al [21].

In Eq. 4-3, $\tilde{k}$ is also written in the Arrhenius form to account for the temperature dependence. In this equation, two different parameters appear, i.e., the pre-exponential factor, $\tilde{A}$(*1/s* or *1/MPa s*) and the activation energy, E_a *(kJ/mol)*. Pre-exponential factors have been determined a priori from an assessment based on statistical thermodynamics, see section 4.4.2.1. Activation energies are then typically determined by model regression to experimental data.

In a mickrokinetic model the rate of every elementary step is accounted for. The reaction rate, as can be seen in Eq. 4-1 and Table 4-2, is a function of temperature, partial pressure of every component involved in the reaction, as well as the intermediate species concentration on the catalyst surface. The law of mass action is applied for calculating the rates of the elementary steps in the reaction networks. Rate equations are written in terms of surface concentrations *C* (*mol/*kg_{cat}) and kinetic coefficients of an elementary step *k* (*1/s or 1/MPa.s*).
The surface coverage of a component *A*, θ_A *(mol* mol^{-1}*)* is defined as a fraction of sites covered by *A* atoms on the catalyst surface:

$$\theta_A = \frac{C_{MA}}{C_{tot}} \qquad \text{Eq. 4-4}$$

As it can be seen in Table 4-2, some of the surface species such as MMCO or MMMCH are bound to two or more metal atoms. The probability of finding adjacent occupied or unoccupied atoms is included in the rate expression [24]. The number of nearest neighbor metal atoms *z* depends on the catalyst structure. This number is divided by two to prevent double counting of the neighbor metal atoms. It is supposed that a rhodium crystal mainly has a so-called face centered cubic (fcc) structure, resulting in 100 surface facets. For such a structure, *z* equals 4. Cobalt typically exhibits a simple hexagonal crystal structure for which z equals 6 [25].

The rate equations corresponding to the different elementary steps are given in Table 4-2. Note that the rate expressions are written in terms of one surface concentration and surface fractions for the other components involved. In particular the free metal site concentration is included as $C_{M,tot}\ \theta_M$ rather than as C_M. To clarify these equations better, the way how the concentration of the two adjacent free metal atoms i.e., C_{MM} , evolved in the rate equation for the dissociative chemisorption of H_2, number 3 in Table 4-2, is elaborated in more detail in equations 4-5 and 4-6. As it is depicted in equation 4-6, the forward reaction rate is function of the concentration of two adjacent free metal atoms, while the reverse reaction rate is a function of the concentration of two hydrogen atoms bonded to two adjacent metal atoms. These concentrations are then expressed in terms of individual metal atoms and considering the aspect of probability to find an appropriate adjacent atom on the surface.

$$C_{MM} = C_M \cdot \frac{C_M}{C_{M,tot}}\left(\frac{z}{2}\right) = C_M \cdot \frac{C_M}{C_{M,tot}}\left(\frac{z}{2}\right)\frac{C_{M,tot}}{C_{M,tot}} = C_{M,tot}\left(\frac{C_M}{C_{M,tot}}\right)^2\left(\frac{z}{2}\right) = C_{M,tot}\,\theta_M^2\left(\frac{z}{2}\right) \qquad Eq.4-5$$

$$r_3 = k_{\rightarrow}.C_{M,tot}.P_{H_2}.\theta_M^2.\left(\frac{z}{2}\right) - k_{\leftarrow}.C_{M,tot}.\theta_{MH}^2.\left(\frac{z}{2}\right) \qquad Eq.4-6$$

Table 4- 2. Rate equations for all the elementary reactions or reaction families

N°	Elementary step	Rate expression ($mol/kg_{cat.}/s$)
1	CO molecular chemisorption CO + 2M ↔ MMCO	$r_1 = k_{\rightarrow}.C_{M,tot}.P_{CO}.\theta_M^2.\left(\frac{Z}{2}\right) - k_{\leftarrow}.C_{MMCO}$
2	CO dissociation MMCO + 3M ↔ MMMC + MMO	$r_2 = k_{\rightarrow}.C_{MMCO}.\theta_M^3.\left(\frac{Z}{2}\right)^3 - k_{\leftarrow}.C_{MMMC}.\theta_{MMO}.\left(\frac{Z}{2}\right)$
3	H_2 dissociative chemisorption H_2 + 2M ↔ 2 MH	$r_3 = k_{\rightarrow}.C_{M,tot}.P_{H_2}.\theta_M^2.\left(\frac{Z}{2}\right) - k_{\leftarrow}.C_{M,tot}.\theta_{MH}^2.\left(\frac{Z}{2}\right)$
4	Hydrogenation of metal bound C MMMC + MH ↔ MMMCH + M	$r_4 = k_{\rightarrow}.C_{MMMC}.\theta_{MH}\left(\frac{Z}{2}\right) - k_{\leftarrow}.C_{MMMCH}.\theta_M\left(\frac{Z}{2}\right)$
5	Hydrogenation of metal bound CH MMMCH + MH ↔ $MMCH_2$ + 2M	$r_5 = k_{\rightarrow}.C_{MMMCH}.\theta_{MH}.\left(\frac{Z}{2}\right) - k_{\leftarrow}.C_{MMCH_2}.\theta_M^2.\left(\frac{Z}{2}\right)^2$
6	Hydrogenation of metal bound CH_2 MMCH2 + MH ↔ MCH_3 + 2M	$r_6 = k_{\rightarrow}.C_{MMCH_2}.\theta_{MH}.\left(\frac{Z}{2}\right) - k_{\leftarrow}.C_{MCH_3}.\theta_M^2.\left(\frac{Z}{2}\right)^2$
7	Hydrogenation of metal bound O MMO + MH ↔ MOH + 2M	$r_7 = k_{\rightarrow}.C_{MMO}.\theta_{MH}.\left(\frac{Z}{2}\right) - k_{\leftarrow}.C_{MOH}.\theta_M^2.\left(\frac{Z}{2}\right)^2$
8	Reductive elimination of H_2O MOH + MH → H_2O + 2M	$r_8 = k_{\rightarrow}.C_{MOH}.\theta_{MH}.\left(\frac{Z}{2}\right) - k_{\leftarrow}.P_{H_2O}.C_{M.tot}.\theta_M^2.\left(\frac{Z}{2}\right)$
9	Methylene insertion MAlkyl(n) + $MMCH_2$ ↔ MAlkyl(n+1) + 2M	$r_9 = k_{\rightarrow}.C_{MAlkyl(n)}.\theta_{MCH_2}.\left(\frac{Z}{2}\right) - k_{\leftarrow}.C_{MAlkyl(n+1)}.\theta_M^2.\left(\frac{Z}{2}\right)^2$
10	Reductive elimination of alkanes MAlkyl(n) + MH ↔ Alkane(n) + 2M	$r_{10} = k_{\rightarrow}.C_{MAlkyl(n)}.\theta_{MH}.\left(\frac{Z}{2}\right) - k_{\leftarrow}.C_{M.tot}.P_{Alkane(n)}.\theta_M^2.\left(\frac{Z}{2}\right)$
11	β – hydride elimination MAlkyl(n) + M ↔ MAlkene(n) + MH	$r_{11} = k_{\rightarrow}.C_{MAlkyl(n)}.\theta_M.\left(\frac{Z}{2}\right) - k_{\leftarrow}.C_{MAlkene(n)}.\theta_{MH}\left(\frac{Z}{2}\right)$
12	Desorption of alkenes MAlkene(n) ↔ Alkene(n) + M	$r_{12} = k_{\rightarrow}.C_{MAlkene(n)} - k_{\leftarrow}.P_{Alkene(n)}.C_{M.tot}.\theta_M$
13	CO insertion MAlkyl(n) + MMCO ↔ MCarbonyl(n+1) + 2M	$r_{13} = k_{\rightarrow}.C_{MAlkyl(n)}.\theta_{MMCO}.\left(\frac{Z}{2}\right) - k_{\leftarrow}.C_{MCarbonyl(n)}.\theta_M^2.\left(\frac{Z}{2}\right)^2$
14	H addition to metal carbonyl MCarbonyl(n) + MH ↔ MMAlkoxide(n)	$r_{14} = k_{\rightarrow}.C_{MCarbonyl(n)}\theta_{MH}.\left(\frac{Z}{2}\right) - k_{\leftarrow}.C_{M.tot}.\theta_{MAlkoxide(n)}$
15	Reductive elimination of alcohols MMAlkoxide(n) + 2MH ↔ Alcohol(n) + 4M	$r_{15} = k_{\rightarrow}.C_{MMAlkoxide(n)}.\theta_{MH}^2.\left(\frac{Z}{2}\right)^2 - k_{\leftarrow}.C_{M.tot}.P_{Alcohol(n)}.\theta_M^4.\left(\frac{Z}{2}\right)^3$
16	Reductive elimination of aldehydes MMAlkoxide(n) ↔ Aldehyde(n) + 2M	$r_{16} = k_{\rightarrow}.C_{MMAlkoxide(n)} - k_{\leftarrow}.C_{M.tot}.P_{Aldehyde(n)}.\theta_M^2.\left(\frac{Z}{2}\right)$

The net production rates of all different species are obtained as the sum of the rates of all the elementary steps in which the species are produced or consumed.

4.4 Kinetic modelling of ethylene hydroformylation

4.4.1 Overall regression results and assessment

Five representative responses have been considered in the regression. The first four are the carbon monoxide and hydrogen conversion as well as the ethane and propanal yields, as the main products observed during the experimentation. Ethane and propanal represent more than 90% of the observed products [1]. The fifth response comprises the yield of all observed alkanes other than ethane, i.e., methane, propane and butane. Although only small amounts of methane and C_{3+} products were observed in the experimental work, this response is still presented to demonstrate the ability of the model to simulate these little amounts of FT products. Because of the lower amounts of these products formed, the agreement between model simulations and experimental observations may, visually seem of lower quality compared to the other responses, however, accounting for the inherent experimental error which is relatively larger for the smaller responses and the lack of systematic deviations, all parity diagrams given in Figure 4-3 and 4-4 for the 5%Rh/Al_2O_3 and 1%Co/Al_2O_3 catalysts respectively, can be considered of good quality. This conclusion also stems from the obtained F values for the global significance of the regression which amount to 13000 for 5%Rh/Al_2O_3 and 12000 for 1%Co/Al_2O_3 catalyst and largely exceed the tabulated value of 2.79.

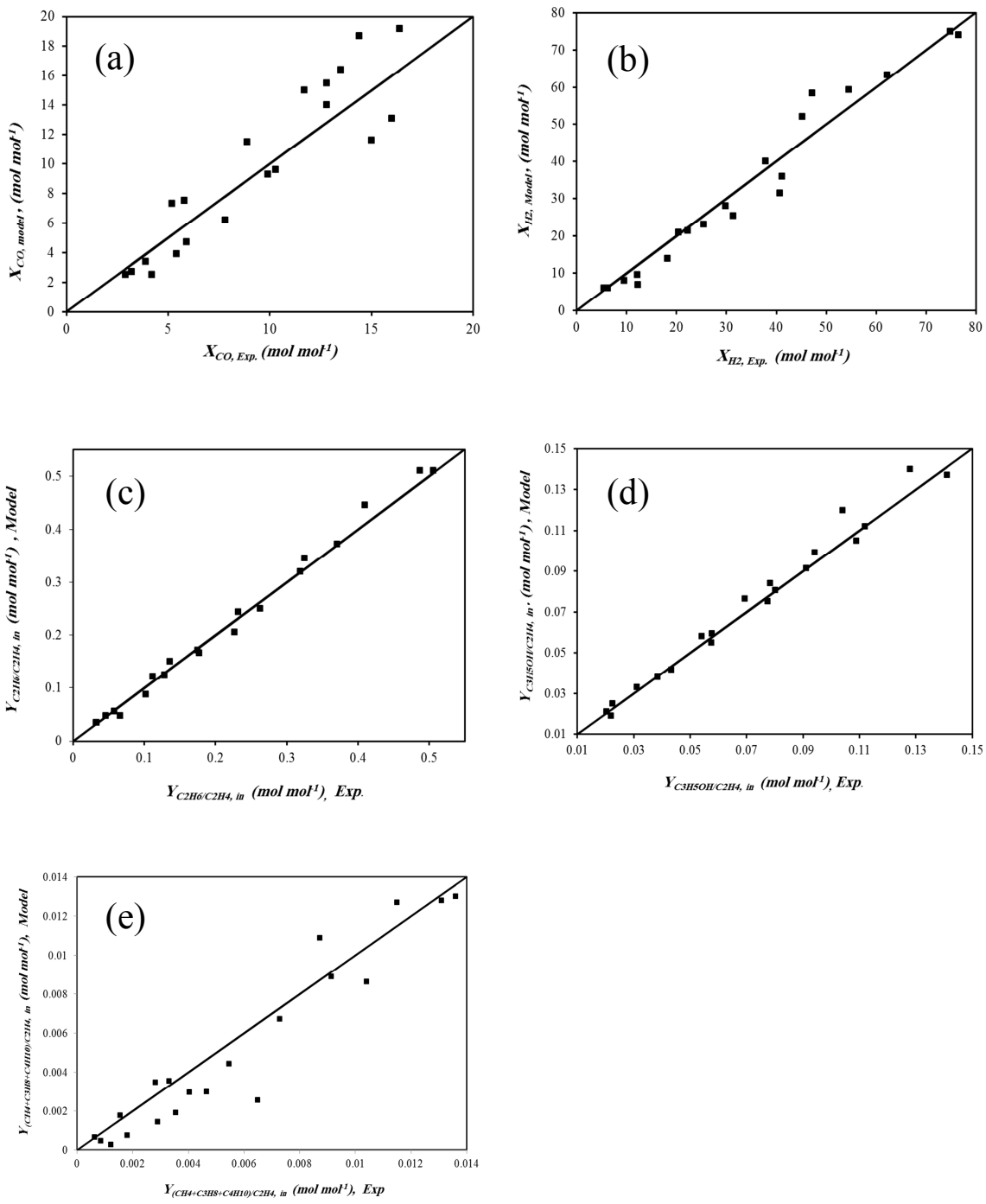

Figure 4- 3. Parity diagrams for the responses of the kinetic model for ethylene hydroformylation on a 5%Rh/Al_2O_3 catalyst: (a) carbon monoxide conversion, (b) hydrogen conversion, (c) ethane yield, (d) propanal yield, (e) methane, propane and butane yields; Full lines, calculated by solving the set of rate equations for all the elementary steps mentioned in Table 4-2 and using the estimated parameters in Table 4-3 and 4-4.

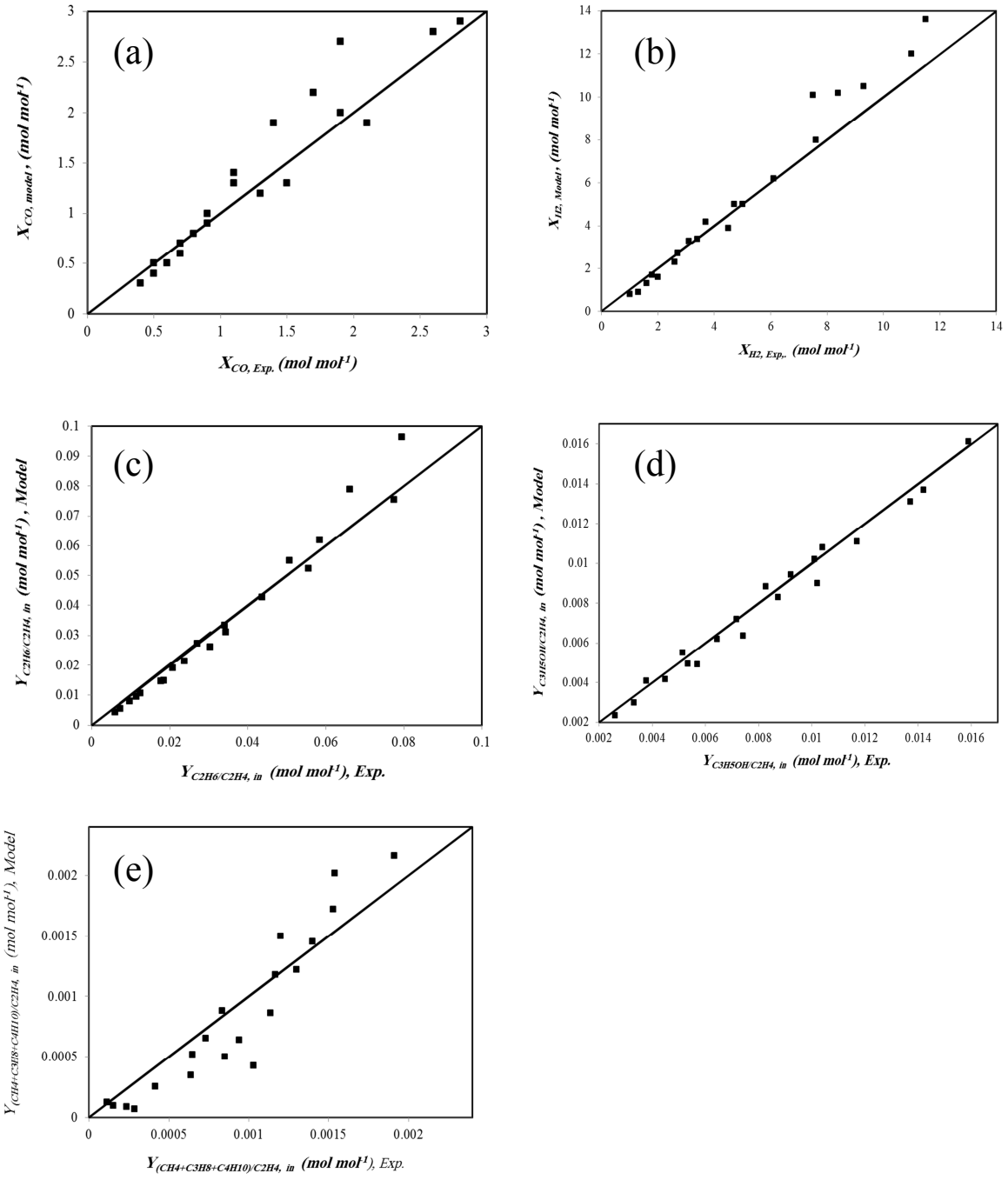

Figure 4- 4. Parity diagrams for the responses of the kinetic model for ethylene hydroformylation on a 1%Co/Al_2O_3 catalyst: (a) carbon monoxide conversion, (b) hydrogen conversion, (c) ethane yield, (d) propanal yield, (e) methane, propane and butane yields; Full lines, calculated by solving the set of rate equations for all the elementary steps mentioned in Table 4-2 and using the estimated parameters in Table 4-3 and 4-4.

As a more firm validation of the model performance, the simulation results have also been included as the lines in Figures 4-5 and 4-6 representing the temperature and pressure effect on the ethane and propanal yield. The experimental results on these figures came from chapter 3, see Figure 3-4 and 3-7. It is observed that the model can reproduce the experimental results quite well under the applied operating conditions on both catalysts particularly at higher temperatures. Slight deviations can be observed between the experimental results and the model simulations at the highest pressure used. However, for the type of fundamental kinetic modelling based on a limited number of adjustable parameters such deviations are not indicative of any (major) inconsistency.

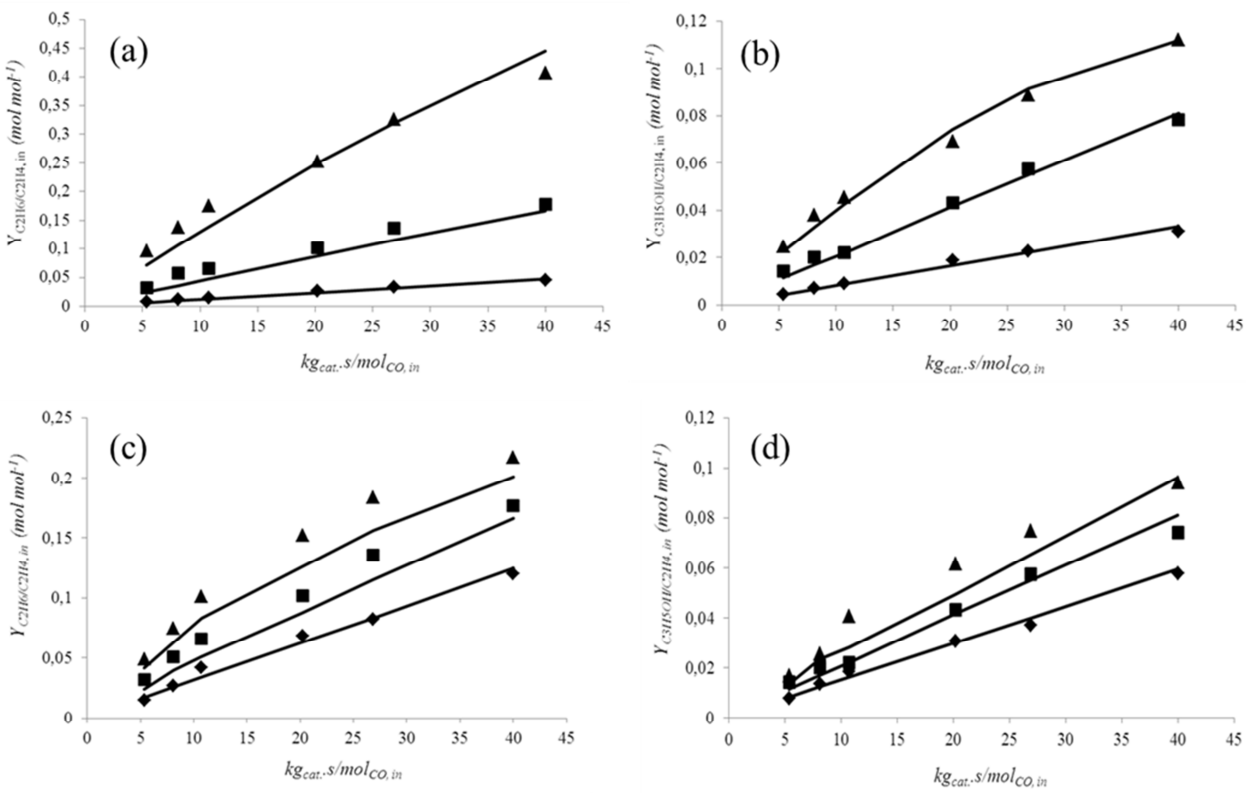

Figure 4- 5. Experimentally observed and model simulated yields of ethane (a, c) and propanal (b, d) versus space time on 5%Rh/Al_2O_3 catalyst, (a, b) at 2MPa pressure (C_2H_4:CO:H_2:Ar=30:30:30:10) and at 448 (♦), 473 (■) and 498K (▲); (c, d) at 473K and at (C_2H_4:CO:H_2:Ar=30:30:30:10) 1 (♦), 2 (■) and 3MPa (▲). Full lines, calculated by solving the set of rate equations for all the elementary steps mentioned in Table 4-2 and using the estimated parameters in Table 4-3 and 4-4.

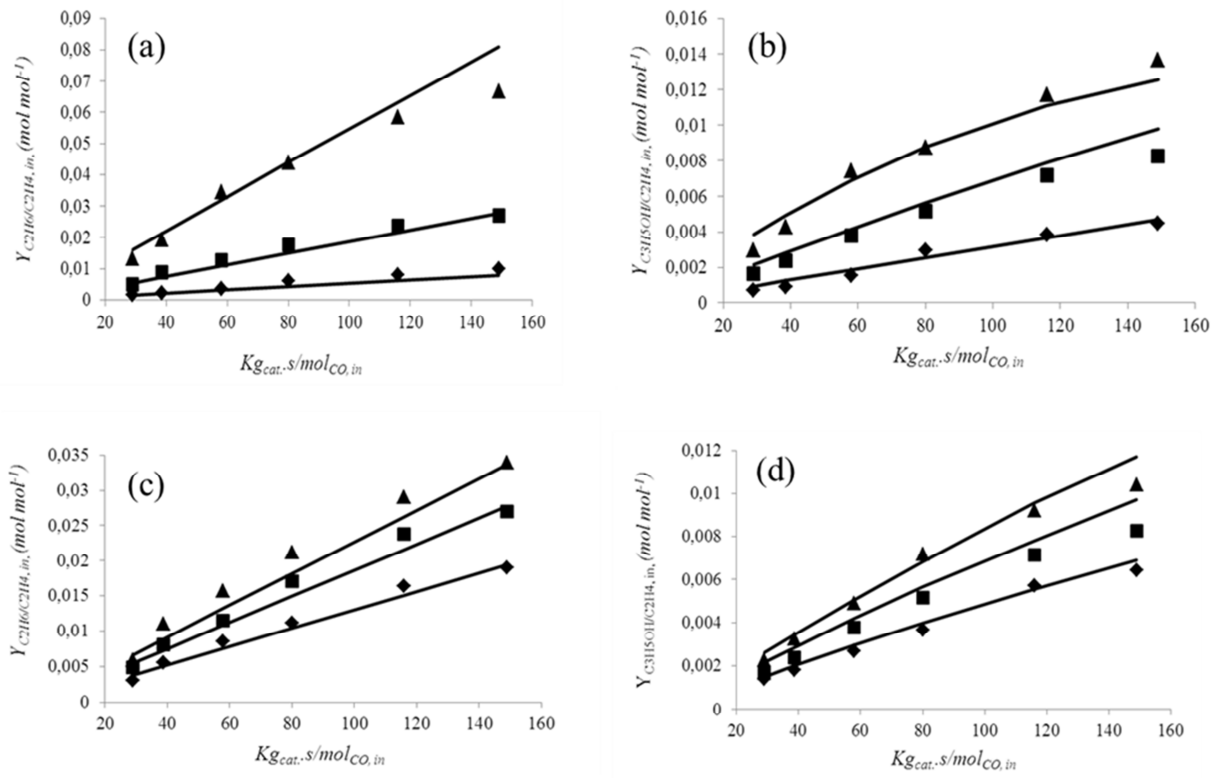

Figure 4- 6. Experimentally observed and model simulated yields of ethane (a, c) and propanal (b, d) versus space time on 1%Co/Al_2O_3 catalyst, (a, b) at 2MPa pressure (C_2H_4:CO:H_2:Ar=30:30:30:10) and at 448 (♦), 473 (■) and 498K (▲); (c, d) at 473K and at (C_2H_4:CO:H_2:Ar=30:30:30:10) 1 (♦), 2 (■) and 3MP (▲)**.** Full lines, calculated by solving the set of rate equations for all the elementary steps mentioned in Table 4-2 and using the estimated parameters in Table 4-3 and 4-4.

A random selection of 20 out of the 54 available experimental data points per catalyst was used to perform the regression, apart from the constraint that at least 2 measurements per investigated temperature and pressure should be included. It means that in figures 4-5 and 4-6, 10 out of 30 points have been used in the regression, while the others purely served for validation. Within the boundaries of statistical significance, the regression results did not depend on the 20 points that were selected.

4.4.2 Model parameters values

4.4.2.1 Calculated single-event pre-exponential factors

The pre-exponential factor in the *single-event kinetic coefficient* for an elementary step *j* is obtained from:

$$\tilde{A}_j^{for} = \frac{k_B T}{h} \exp\left(\frac{\Delta \tilde{S}_j^{0,\neq}}{R}\right) \quad \text{Eq. 4-7}$$

By calculating the entropy change between the reacting species and transition state, the single-event standard activation entropy for an elementary step j, $\Delta \tilde{S}_j^{0,\neq}$, is obtained.

Single-event pre-exponential factors for the reverse elementary steps are calculated according to the principle of microscopic reversibility:

$$\tilde{A}_j^{rev} = \frac{\tilde{A}_j^{for}}{\exp\left(\frac{\Delta \tilde{S}_{r,j}^{0}}{R}\right)} \quad \text{Eq. 4-8}$$

The procedure employed to calculate these values has been more elaborately discussed by Lozano Blanco et al. [19]. A loss of all three degrees of translational freedom from the gas phase molecule is assumed for the transition state species involved in carbon monoxide dissociation, hydrogenation of metal bound oxygen atom and β-hydride elimination. For the other transition states, a loss amounting to two degrees of translational freedom has been adopted. Even if entropy changes occur related to rotational and vibrational degrees of freedom, all entropy changes are expressed in equivalents of translational degrees of freedom. The total translational entropy of a gas-phase molecule is calculated with the Sackur-Tetrode equation [35]:

$$S_{trans}^{0} = R\, ln\left[\frac{RT}{P^0 N_A}\left[\frac{2\pi(M_W/N_A)k_B T}{h^2}\right]^{3/2}\right] + \frac{5}{2}R \quad \text{Eq. 4-9}$$

Where P^0 is the standard pressure, N_A the Avogadro constant and M_W the molecular mass.

The pre-exponential factors for the forward and reverse elementary reactions at 473 K are shown in Table 4-3. The obtained values for forward and reverse pre-exponential factors are within the range of reported values in the literature for the same type of elementary steps [26].

Because of the increasing mobility and corresponding entropy gain during carbon monoxide desorption, its pre-exponential factor is comparatively larger than the other pre-exponential factors. For the same reason, the pre-exponential factors for reductive elimination of alkanes

and alcohols and desorption of alkenes and aldehydes exceed the corresponding reverse pre-exponential factors by several orders of magnitude.

Table 4- 3. Forward and reverse single-event pre-exponential factors at 473K and estimated forward activation energies for the different elementary steps or reaction families (maximum carbon number= 4)

Elementary step	$\tilde{A}^{for}$ (s^{-1})	$\tilde{A}^{rev}$ (s^{-1})	E_A (kJ/mol)	*t value*
CO + 2M ↔ MMCO	2.74×10^{7}	5.45×10^{15}	0	-
MMCO + 3M ↔ MMMC + MMO	9.34×10^{12}	5.31×10^{13}	70.94 ± 2.79	49.9
H_2 + 2M ↔ 2MH	3.80×10^{8}	4.31×10^{11}	0	-
MMMC + MH ↔ MMMCH + M	4.49×10^{14}	9.33×10^{12}	80.12 ± 2.93	53.74
MMMCH + MH ↔ $MMCH_2$ + 2M	3.97×10^{11}	9.33×10^{12}	6.47 ± 0.29	43.37
MMCH2 + MH ↔ MCH_3 + 2M	1.58×10^{11}	9.33×10^{12}	74.98 ± 0.08	199.5
MMO + MH ↔ MOH + 2M	8.74×10^{11}	2.05×10^{10}	89.55 ± 1.51	116.9
MOH + MH → H_2O + 2M	1.82×10^{11}	4.26×10^{7}	76.93 ± 2.31	65.38
MAlkyl(n) + $MMCH_2$ ↔ MAlkyl(n+1) + 2M	2.79×10^{9}	7.96×10^{12}	44.12 ± 0.68	127.2
MAlkyl(n) + MH ↔ Alkane(n) + 2M	1.67×10^{12}	5.59×10^{8}	116.67 ± 0.54	417.4
MAlkyl(n) + M ↔ MAlkene(n) + MH	1.23×10^{10}	6.02×10^{8}	83.64 ± 1.67	198.5
MAlkene(n) ↔ Alkene(n) + M	9.33×10^{12}	1.75×10^{7}	53.84	-
MAlkyl(n) + MMCO ↔ MCarbonyl(n+1) + 2M	9.39×10^{13}	2.28×10^{12}	125.36 ± 0.51	476.8
MCarbonyl(n) + MH ↔ MMAlkoxide(n)	4.13×10^{10}	9.46×10^{12}	17.35 ± 0.23	151.4
MMAlkoxide(n) + 2MH ↔ Alcohol(n) + 4M	5.57×10^{9}	1.74×10^{7}	77.11 ± 1.15	133.2
MMAlkoxide(n) ↔ Aldehyde(n) + 2M	5.75×10^{12}	9.00×10^{7}	126.78	-

The pre-exponential factor for carbon monoxide dissociation on a transition metal is usually smaller than the one for carbon monoxide desorption, their ratios lying within 10^{-1}-10^{-4} [27, 28]. The ratio obtained in the present work amounts to 1.71×10^{-3} and is, hence, in agreement with the reported range.

In general, the reported pre-exponential factors for the hydrogenation of chemisorbed species are about 10^{11} s^{-1} [28], which is close to the values obtained in the current work for the hydrogenation of methylidyne and methylene, see Table 4-3. The higher pre-exponential factor for the hydrogenation of metal carbide in this work (~10^{14}) can be explained by the lower mobility assumed for the metal carbide compared to the other carbonaceous species, i.e., methylidyne and methylene. As a result, entropy has to be gained during metal carbide hydrogenation into the methylidyne species.

4.4.2.2 Activation energy and atomic chemisorption enthalpy estimates

Thanks to the SEMK methodology the number of parameters that need to be determined is reduced to two per reaction family, i.e., the (single-event) pre-exponential factor and the activation energy. While the first one was obtained from statistical thermodynamics, see Section 4.4.2.1, the second one is determined via regression. By applying the principle of microscopic reversibility, this number of adjustable parameters can be further reduced if the reaction enthalpy of every elementary reaction is calculated from thermodynamics considerations. As a result, the activation energy for the reverse step can be calculated as follows from the one in the forward direction and this reaction enthalpy:

$$E_a^{rev} = E_a^{for} - \Delta H_r^0 \qquad \text{Eq. 4-10}$$

Surface reaction enthalpies are expressed as linear combinations of standard formation enthalpies of surface species and standard reaction enthalpies of the analogous gas-phase reactions making use of a Born – Haber cycle. Chemisorption enthalpies are calculated as a function of gas-phase bond energies and atomic chemisorption enthalpies by means of the so-called unity bond index-quadratic exponential potential (UBI/QEP) method [19, 29].

Considering the proposed elementary steps in the kinetic model in this work, 19 independent kinetic parameters have to be estimated via regression. 16 correspond to the activation energies of the various elementary steps, that were considered in the reaction network. These are the kinetic descriptors that are catalyst independent and have a precise physical meaning. Apart from these activation energies three atomic chemisorption enthalpies, i.e., Q_C, Q_H and Q_O, are the catalyst descriptors that are also determined as adjustable parameters. When assessing kinetic data acquired on alternative catalysts, only the latter parameters need to be redetermined to simulate the observed behaviour.

For the data modeled in the present chapter, it was not necessary to account for a potential impact on the activation energies or changes in the reaction network when going from one catalyst to another. In case such effects would become more pronounced [30], a more extended reaction network could be used. The catalyst descriptors, e.g., the atomic chemisorption enthalpies, should then ensure that only the part of the network relevant for the behavior observed on the corresponding catalyst contributes to the simulations for that catalyst. Alternatively, via Polanyi relationships catalyst thermochemistry effects could be extrapolated to the kinetics [24].

The number of parameters is further reduced to 12 by assuming that CO molecular chemisorption, hydrogen dissociative chemisorption and chemisorption of alkenes and aldehydes are non-activated steps [19]. The estimated kinetic and catalyst descriptors as well as the corresponding confidence intervals and t values are given in Tables 4-3 and 4-4. For the two latter non-activated reactions, values reported are the enthalpy differences between the gas phase species and the metal bound species of the forward reaction.

Table 4- 4. Estimated and reported catalyst descriptors for 5%Rh/Al_2O_3 and 1%Co/Al_2O_3 catalysts

Catalyst descriptor	Rh		Co	
	Estimated value (*kJ/mol*)	Reported value (*kJ/mol*)	Estimated value (*kJ/mol*)	Reported value (*kJ/mol*)
Q_C	591.11 ± 0.72	736 [31]	576.18 ± 0.82	678 [34] 611 [35] 621 [36]
Q_O	544.39 ± 0.61	427[a] [32] 464[b] [32]	558.39 ± 2.64	507 [37] 554 [35] 514 [36]
Q_H	250.34 ± 0.18	226[a] [33] 225[b] [33]	251.20 ± 0.26	234 to 267 [33] 264 [36] 243 [35]

[a] from calculation, [b] from experiment

The number of observations used in the present regression amounted to 20 for each catalyst. The result of the t test indicates that all parameters are significant with respect to a reference value of zero. The tabulated t value is 1.965, which is exceeded by all of the t values of the estimated parameters.

The activation energies of the β-hydride elimination, reductive elimination of alkanes and alcohols and CO insertion together with the three atomic chemisorption enthalpies had the narrowest confidence intervals and, hence, are the most influential on the model simulations. Considering the atomic chemisorption enthalpies reported in Table 4-4, the trends obtained in the present work agree with literature reported values but are less pronounced. It can be seen in Table 4-4 that, indeed, the atomic carbon chemisorption enthalpy on Rh exceeds the corresponding value on Co, while the oxygen chemisorption enthalpy is higher on Co compared to Rh. It is reported in the literature that the binding energy of the carbon adatom increases upon moving down along a particular column of the periodic table while the trend is opposite for oxygen [38]. Besides, the metal-hydrogen binding energies are rather uniform with an average value of 251 *kJ/mol* [39]. It should be kept in mind in this respect that these bonding energies can be affected by many factors such as support, catalyst dopants, etc. and

that high surface coverage will typically lead to lower chemisorption enthalpies, see also Section 4.3 [40, 41]. The estimated values in this work for chemisorption enthalpies are considered coverage independent.

The activation energy estimated for the reductive elimination towards alkanes is higher than those for the CH_x hydrogenation steps, which is in agreement with the literature [42]. The activation energy for metal alkyl hydrogenation to alkane amounts to 117 *kJ/mol* and exceeds those of methylene insertion and β-hydride elimination. This explains the increased amounts of ethane produced with increasing temperature. Even though the estimated activation energy for carbon monoxide insertion is relatively high, the overall temperature dependence of the pathway to aldehydes is not solely determined by this step. The evolution of CO and H atoms on the catalyst surface upon increasing the temperature has also a strong effect on the product selectivities as will be discussed in 4.4.3.

4.4.2.3 Optimal catalyst properties

Catalyst descriptor values, i.e., the atomic chemisorption enthalpies, have been systematically varied to identify an optimal catalyst for ethylene hydroformylation in terms of activity or product selectivity. Within the allowable operating conditions, a maximum propanal to ethane yield ratio was observed at Q_C=597, Q_O=494 and Q_H=250 kJ/mol, see Figure 4-7. The average propanal yield and selectivity increased by 80% and 35% respectively compared with the results for Rh presented in Figure 4-5.

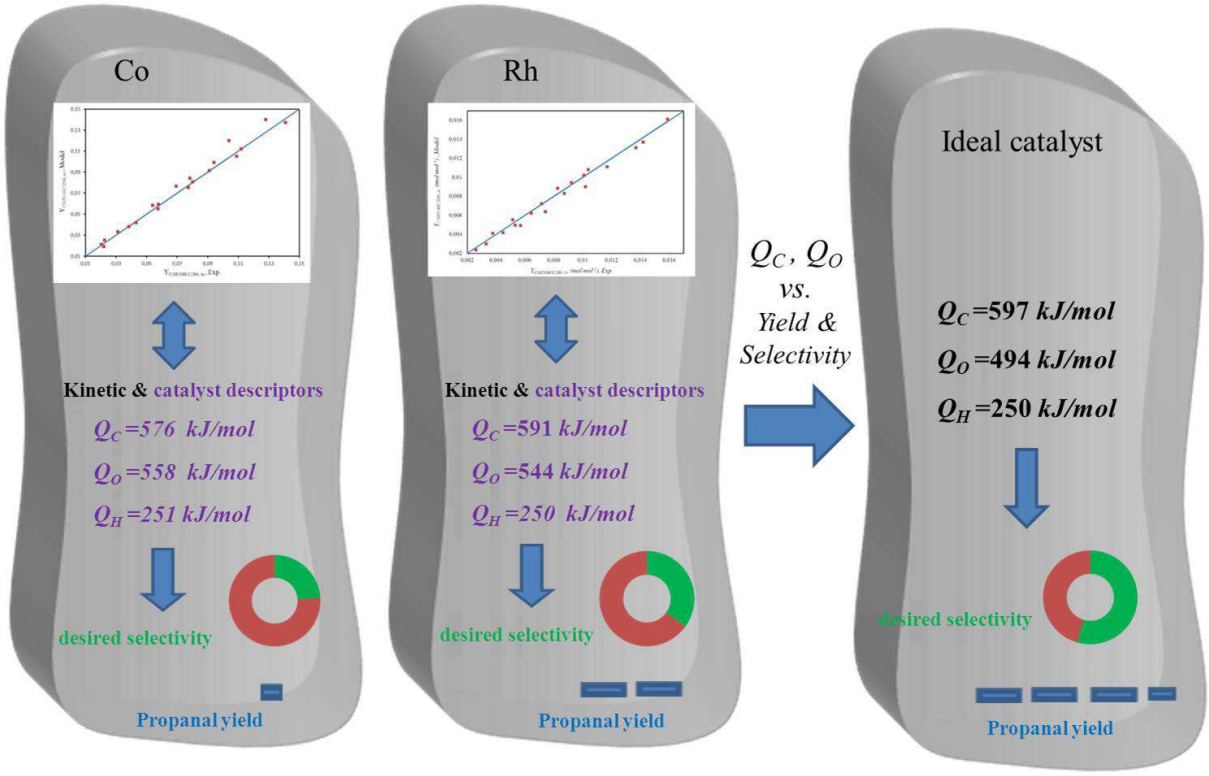

Figure 4- 7. Schematic overview of a procedure to find the ideal catalyst for heterogeneous ethylene hydroformylation

As observed experimentally, the overall hydrogenation rate more strongly depends on the temperature than the overall hydroformylation rate and, correspondingly, oxygenated product selectivities decrease with the temperature. When the maximum operating temperature would be limited to 473K, an even higher Q_C, Q_C=615 *kJ/mol* would be less problematic, because hydrogenation is less pronounced at such conditions.

Considering all these results, a highly dispersed catalyst with above-mentioned characteristics, e.g., an alloy of Rh with higher atomic number metals such as Ir, might be considered as an ideal catalyst in the ethylene heterogeneous hydroformylation.

4.4.3 Surface species fractions

Surface species fractions typically give strategic insight in the kinetically most relevant phenomena in the reaction mechanism according to the model simulations. On both investigated catalysts the MMO and MMMC surface species fractions were very low. This is in agreement with the employed ethylene hydroformylation reaction mechanism that

considers molecular CO chemisorption prior to its insertion in a metal alkyl species rather than undergoing dissociation. The most relevant surface species fractions as obtained with the SEMK model are MH, MMCO and the empty sites i.e., ME, as shown in Figure 4-8 for both catalysts.

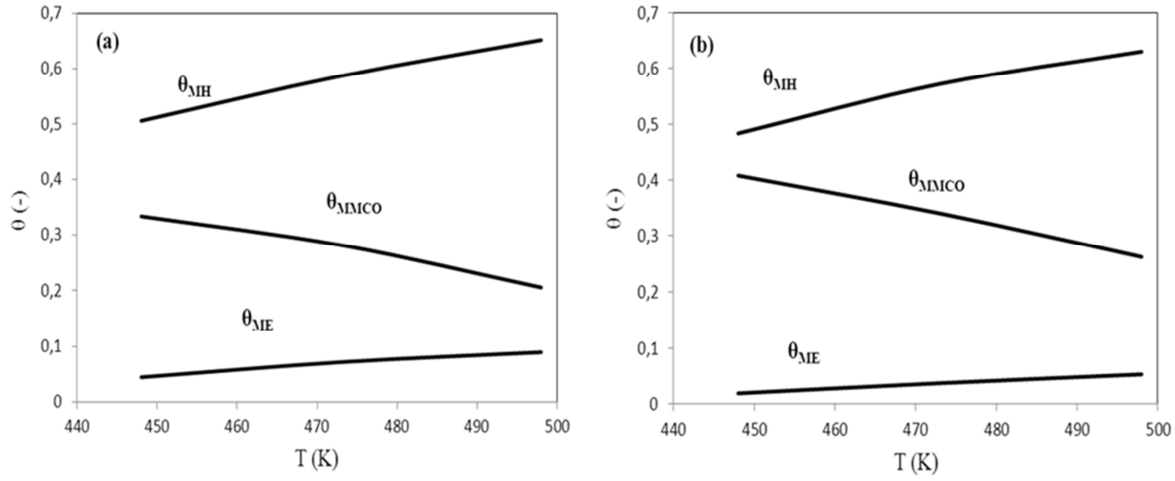

Figure 4- 8. Surface coverage of MH, MMCO and ME on (a) 5%Rh/Al_2O_3 and (b) 1%Co/Al_2O_3 catalysts at 2*MPa* pressure

A temperature increase has a very similar effect on the surface species fractions on both investigated catalysts. The surface H and free metal atom fractions increase with the temperature while that of CO decreases. CO has the most negative chemisorption enthalpy, i.e., -116 *kJ/mol*, such that its surface fraction indeed decreases with increasing temperature. The H_2 chemisorption enthalpy being less negative than that of CO, i.e., -58.34 *kJ/mol*, results in an increasing surface H fraction because the effect of the decreasing H_2 chemisorption equilibrium coefficient is overcompensated by the increase of the free site fraction due to the pronounced CO desorption with the temperature. The higher H concentration on the catalyst surface than expected from the experimental analysis, is believed to be due to the difference in adsorption entropy between hydrogen and carbon monoxide. CO is and remains adsorbed on 2 adjacent metal atoms and, hence, loses much more entropy than H_2 upon adsorption on catalyst surface, the latter also requiring two metal atoms, however, in the final state these atoms are no longer necessarily situated adjacent to each other. It is also observed that the CO surface coverage is more sensitive to a change in the partial pressure of the reactants.

Despite of the higher activation energy for CO insertion compared to metal alkyl hydrogenation, which leads to a more pronounced increase in the corresponding rate coefficient for the formation of the desired aldehyde compared to the hydrogenated side product, the ultimate selectivity to the desired product is decreasing with the temperature. This is a result of the decreasing respectively increasing surface species fractions of the critical species involved in both reactions, i.e., CO and H, which overcompensate the temperature effect on the rate coefficients.

According to the SEMK model, the higher activity of a Rh catalyst in hydroformylation can be attributed to the variation in C, O and H atomic chemisorption enthalpies which is favouring the adsorption of the relevant species, i.e., MH, MMCO and ME on a Rh compared to a Co catalyst.

4.5 Conclusions

In this work, a Single-Event MicroKinetic (SEMK) model has been developed for and applied to ethylene hydroformylation to propanal on 5%Rh/Al_2O_3 and 1%Co/Al_2O_3 catalysts. Activation energies of the considered elementary steps and atomic chemisorption enthalpies for carbon, hydrogen and oxygen were determined from regression and where physically and statistically significant, while preexponential factors were assessed from differences in mobility of the species involved. Molecular CO insertion in a metal alkyl and hydride addition were identified as the key elementary steps determining the overall observed behavior. The more pronounced ethane formation at higher temperatures was well reflected in the corresponding parameter estimates and surface species fractions. Parity diagrams for major and side products did not indicate any systematic deviation in the model simulations.

The Rh based catalyst exhibited a higher activity than the Co based on in the entire range of operating conditions that was investigated.

The incorporation of catalyst descriptors into the model allowed a simply extension of the model to other catalysts. As evidenced by all these results, this model is a useful tool that can be used for catalyst design and development. A further optimization of the propanal to ethane yield ratio within the investigated operating conditions is simulated to occur on catalysts which more strongly chemisorb carbon and less strongly chemisorb oxygen. Finely dispersed metals below Rh in the periodic table such as Ir or their alloys with Rh may bring this goal within reach.

4.6 References

[1] N. Navidi, J. W. Thybaut, G. B. Marin, Appl. Catal. A. 469 (2014) 357–366.

[2] T. A. Zeelie, Rhodium and cobalt catalysts in the heterogeneous hydroformylation of ethane, propene and 1-hexene. PhD thesis, Helsinki, 2007.

[3] U. J. Jauregui-Haza, O. Diaz-Abin, A. M. Wilhelm, H. Delmas, Ind. Eng. Chem. Res. 44 (2005) 9636-9641.

[4] K. Tomishige, I. Furikado, T. Yamagishi, S. Ito, K. Kunimori, Catal. Lett. 103 (2005) 15-21.

[5] V. I. Zapirtan, B. L. Mojet, J.G.V. Ommen. J. Spitzer, L. Lefferts, Catal. Lett. 101 (2005) 43-47.

[6] T. Hanaoka, H. Arakawa, T. Matsuzaki, Y. Sugi, K. Kanno, Y. Abe, Catal. Today. 58 (2000) 271-280.

[7] F.S. Xiao, M. Ichikawa, J. Catal. 147 (1994) 578-593.

[8] C. U. Pittman Jr, G. M. Wilemon, J. Org. Chem. 46 (1981) 1901–1905.

[9] W. Junfan, S. Juntan, L. Hong, H. Binglin, React. Polym. 12 (1990) 177–186.

[10] M.W. Balakos, S.S.C. Chuang, J. Catal. 151 (1994) 266-278.

[11] M. A. Brundage, S.S.C. Chaung, J. Catal. 164 (1996) 94-108.

[12] D. Y. Murzin, A. Bernas, T. Salmi, AIChE Journal. 58 (2012) 2192-2201.

[13] G.F. Froment, Catal. Today. 52 (1999) 153-163.

[14] J.W. Thybaut, G.B. Marin, J. Catal. 308 (2013) 352-362.

[15] C.S.L. Narasimhan, J.W. Thybaut, G.B. Marin, P.A. Jacobs, J.A. Martens, J.F. Denayer, G.V. Baron, J. Catal. 220 (2003) 399-413.

[16] J.W. Thybaut, I.R. Choudhury, J.F. Denayer, G.V. Baron, P.A. Jacobs, J.A. Martens, G.B. Marin, Top. Catal. 52 (2009) 1251-1260.

[17] J.M. Martinis, G.F. Froment, Ind. Eng. Chem. Res. 45 (2006) 954-967.

[18] R. Sotelo-Boyas, G.F. Froment, Ind. Eng. Chem. Res. 48 (2009) 1107-1119.

[19] G. Lozano-Blanco, J.W. Thybaut, K. Surla, P. Galtier, G.B. Marin, Ind. Eng. Chem. Res. 47 (2008) 5879-5891.

[20] T. Bera, J.W. Thybaut, G.B. Marin, Ind. Eng. Chem. Res. 50 (2011) 12933-12945.

[21] G. Lozano-Blanco, J. W. Thybaut, K. Surla, P. Galtier, G. B. Marin, Oil Gas Sci. Technol. 6I (2006) 489-496.

[22] G.D. Svoboda, E. Vynckier, B. Debrabandere, G.F. Froment, Ind. Eng. Chem. Res. 34 (1995) 3793-3800.

[23] J.W. Thybaut, G.B. Marin, Chem. Eng. Technol. 26 (2003) 509-514.

[24] M. Boudart, G. Djéga-Mariadassou. Kinetics of heterogeneous catalytic reactions, Princeton University Press. New Jersey, 1984.

[25] E. Kaxiras, Atomic and electronic structure of solids, Cambridge university press, 2003.

[26] V. P. Zhdanov, J. Pavlicek, Z. Knor, Catal. Rev. Sci. Eng. 30 (1988) 501.

[27] R. A. Van Santen, J. W. Niemantsverdriet, Chemical kinetics and catalysis, Plenum Press, New York, 1995.

[28] C, T. Campbell, Y. K. Sun, W. H. Weinberg, Chem. Phys. Lett. 179 (1991) 53-57.

[29] E. Schustorovich, H. Sellers, Surf. Sci. Rep. 31 (1998) 5-119.

[30] L. Dietz, S. Piccinin, M. Maestri, J. Phys. Chem. C. 119 (2015) 4959-4966.

[31] A. V. Zeigarnik, R. E. Valdes-Prez, O. N. Myatkovskaya, J. Phys. Chem. B. 104 (2000) 10578 – 10587.

[32] D. O. Hayward, J.R. Anderson (Ed.), Chemisorption and reactions on metallic surfaces, Academic Press, London, 1971.

[33] I. Toyoshima, G. A. Somorjai, Catal. Rev. Sci. Eng. 19 (1979) 105.

[34] J. B. Bezinger, E. Schustorovich (Ed.), Thermochemical methods for reaction energetics on metal surfaces. In Metal-surface reaction energetics, VCH, New York, 1991.

[35] G. Lozano-Blanco, single-event microkinetics for metal catalysis: Fischer-Tropsch synthesis. Ghent (PhD thesis), 2007.

[36] X. Q. Gong, R. Raval, Surf. Sci. 562 (2004) 247-256.

[37] D. J. K. Linke, L. J. Broadbelt, Chem. Eng. Sci. 54 (1999) 3379-3389.

[38] R. A. Van Santen, M. Neurock., Molecular Heterogeneous catalysis: A conceptual and computational approach, Wiley-VCH, 2006.

[39] M. L. Burke, R. J. Madix, JACS. 114 (1992) 2780-2783.

[40] M. Neurock, R. A, Van Santen, J. Phys. Chem. B. 104 (2000) 11127-11145.

[41] C. Egawa, S. Osawa, S. Oki, Serf. Sci. 529 (2003) 349-358.

[42] X. Q. Gong, R. Raval, P. Hu, J. Chem. Phys. 2 (2005) 122.

Chapter 5:

General conclusions and future work

Hydroformylation is an important catalytic reaction for the production of aldehydes and alcohols from alkenes. Since the homogenous variant, which is widely used industrially, leads to inherent problems such as difficulties in separation of the catalyst from the products and equipment corrosion, the research towards an active and stable heterogeneous hydroformylation catalyst is strongly motivated. This thesis aims at contributing towards the development of such a catalyst via a detailed experimental investigation of the reaction kinetics on heterogeneous Rh and Co based catalysts followed by explaining and interpreting the corresponding reaction mechanism in terms of the elementary steps and the development of a fundamental kinetic model.

Using the HTK-MI set up, different catalysts and a wide range of the operation conditions have been investigated. Gas phase hydroformylation on 5%Rh on Al_2O_3, 1%Co on Al_2O_3 and 0.5%Co-0.5%Rh on Al_2O_3 practically exclusively resulted in propanal, ethane and propanol formation. The Rh catalyst showed the highest hydroformylation and hydrogenation site time conversions in the investigated range of operating conditions. It was observed that smaller Rh and Co particles appear to enhance the CO insertion activity rather than the hydrogenation activity resulting in an increase in the oxo-selectivity.
Irrespective of the investigated catalyst, a temperature increase affects ethylene hydrogenation more strongly than hydroformylation. The highest oxygenate selectivity can, hence, be expected at temperatures below 483 K. The higher apparent activation energy for ethane formation compared to that for propanal, is a result of the higher heat of chemisorption for CO than for hydrogen. The hydroformylation rate increases with the ethylene inlet concentration whereas the CO inlet concentration has an inhibiting effect on hydroformylation. Hydroformylation and hydrogenation rates increase with the total pressure to a similar extent although the slightly increased oxygenates selectivity indicates that in particular the CO surface concentration increases with increasing total pressure.

The obtained experimental data have been used to extend a previously developed Single-Event MicroKinetic model for Fischer-Tropsch Synthesis towards ethylene hydroformylation. Mechanistically, heterogeneous hydroformylation is very closely related to FTS. The main distinctive features are the inherent presence of an alkene, c.q., ethylene as reactant in hydroformylation, and the high probability of CO insertion into the metal alkyl bond and acyl hydrogenation rather than its CO bond scission. The adjustable model parameters were the activation energies of the kinetically relevant reaction families and atomic chemisorption

enthalpies for carbon, hydrogen and oxygen. They were determined from regression and physically meaningful as well as statistically significant values were obtained. Pre-exponential factors were assessed from differences in mobility of the species involved. Molecular CO insertion in a metal alkyl and hydride addition were identified as the key elementary steps determining the overall observed behavior. The more pronounced ethane formation at higher temperatures was well reflected in the corresponding parameter estimates and surface species fractions. Parity diagrams for major and side products did not indicate any systematic deviation in the model simulations.

The incorporation of catalyst descriptors into the model allowed a simple extension of the model to other catalysts. Based on all these results, the SEMK hydroformylation model was proven to be a promising tool in the design and development of more performing catalysts. To identify an optimal catalyst based on the knowledge gathered within the framework of the present thesis, the values of the atomic chemisorption enthalpies leading to the highest possible propanal to ethane yield ratio were determined within the investigated operating conditions. It was found that the optimized values i.e., Q_C=597, Q_O= 494 and Q_H=250 kJ/mol, correspond with catalysts which more strongly chemisorb carbon and less strongly chemisorb oxygen. Hence, finely dispersed metals below Rh in the periodic table such as Ir, or their alloys with Rh, seem promising candidates.

The results of the present work constitute a basis for further work in several possible directions:

- On the experimental side, a powerful HTK-MI set up provides the possibility of catalyst screening as well as gathering a wide range of kinetics measurements. Extension towards the hydroformylation of heavier alkenes could be performed to validate the effectiveness of the proposed catalysts for such feeds. Also the selection of an adequate temperature and pressure range would be a significant challenge to increase the selectivity towards the oxygenates products. The effect of the fraction of exposed metal on the activity and, hence, the metal particle size, and desired selectivity can be also investigated in more detail.
- The aim of the SEMK methodology is to reduce the model complexity by using reaction families that lead to fewer model parameters. As the developed SEMK model for ethylene hydroformylation is the first of its kind, the experimentation with heavier

alkenes as suggested above, would constitute a nice validation basis for the SEMK principle of unique, single-event rate coefficients within a reaction family.

- The effect of catalyst supports in heterogeneous catalysis in general is discussed widely in literature. However, the effect of the different supports on the heterogeneous ethylene hydroformylation deserves more study and research. Catalyst stability, especially in industrial processes, is an essential aspect, both from the economical and operational point of view. It is directly related to the catalyst structure and to the applied reaction conditions. Hence, research about the appropriate reaction conditions besides the properties of the catalytic metal and the support matrix are very important to find a stable and active catalyst.
- Structure sensitivity effects are worth being explored more systematically in order to be incorporated in the Single-Event MicroKinetic model for ethylene hydroformylation as developed and applied in this thesis. It would provide a strategic opportunity to widen the scope of features that can be the subject of a rational catalyst design, aiming at optimizing product yields and selectivities.
- Experimental data obtained from more advanced experimental techniques such as Steady State Isotopic Transient Kinetic Analysis (SSITKA) and/or operando infrared surface quantitative description can be compared to model simulated values for surface concentrations to reinforce the validity of the mechanistic model considered in this work.

Appendix A

Results of X-ray diffraction (XRD)

X-ray diffraction (XRD)

To determine the particle size of the employed catalysts, XRD measurements have been performed. All XRD patterns mainly exhibited the alumina peaks and only minor evidence for the presence of metal clusters was obtained. The latter was explained either by the small size of the metal particles, i.e., their high dispersion, or by the low metal loading used.

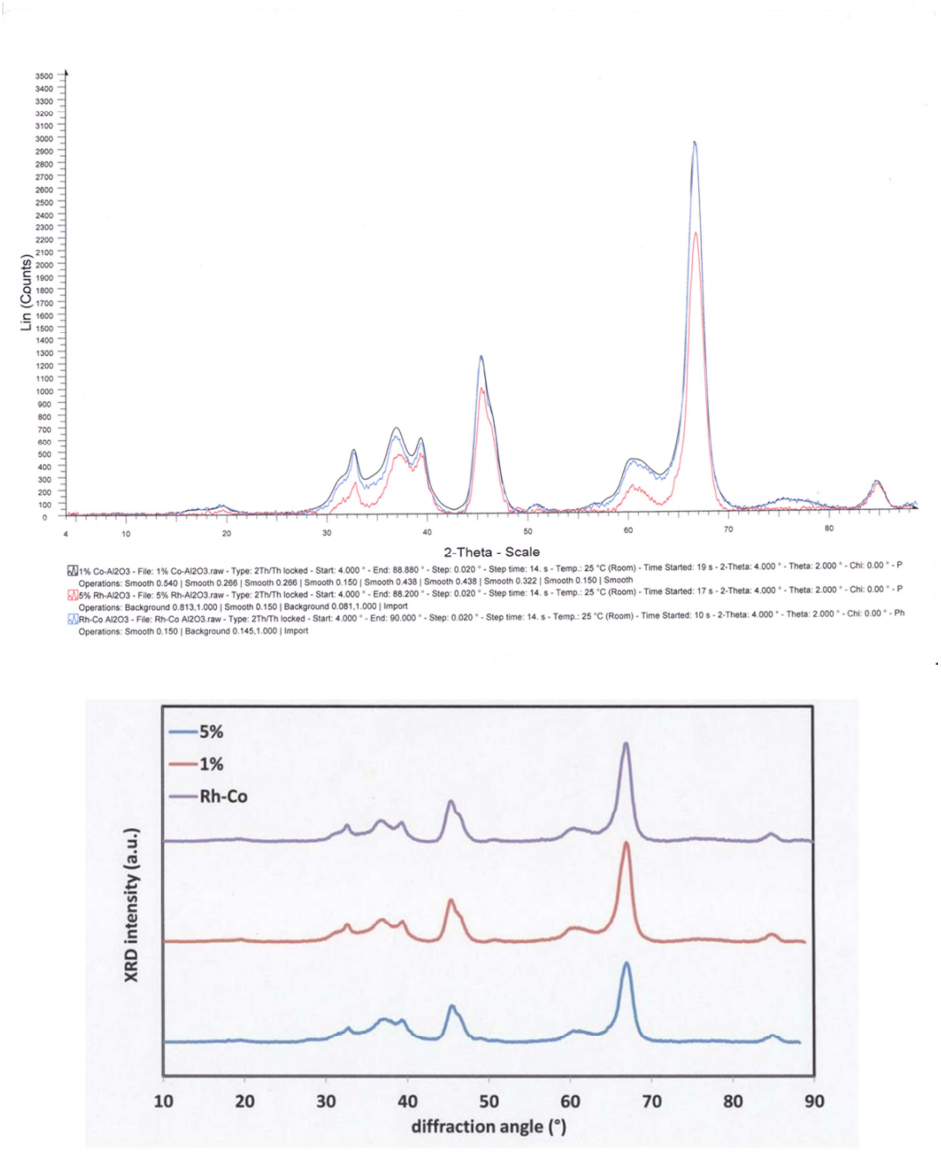

Figure A-1. XRD patterns of tested catalysts

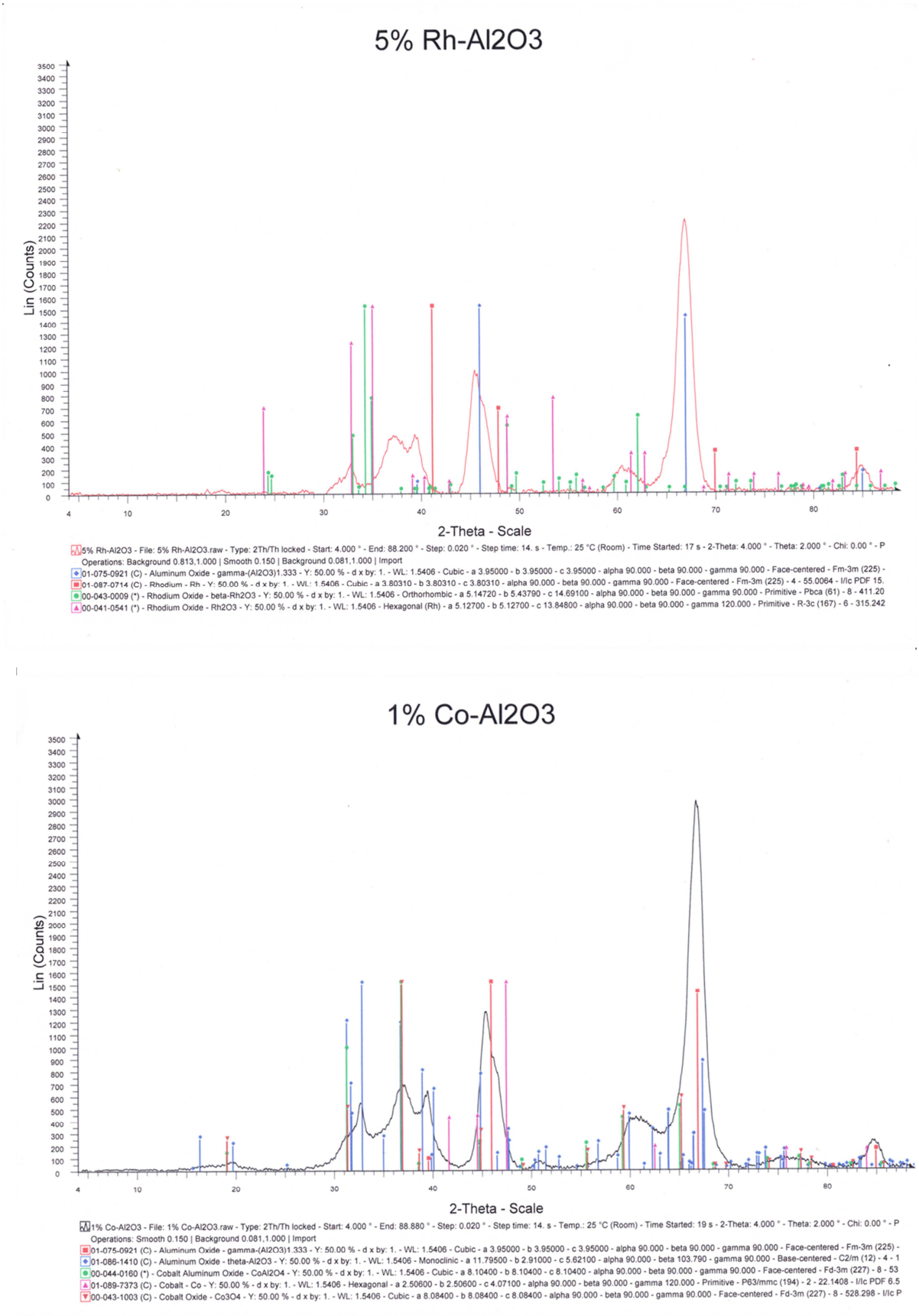

Figure A-2. XRD patterns for 5% Rh/Al_2O_3 and 1% Co/Al_2O_3 catalysts